DISCRETE ELEMENT MODELLING OF CPT USING SHAKING TABLE TESTS IN SANDS

A Thesis Submitted to the
the Graduate School of Engineering and Sciences of
İzmir Institute of Technology
in Partial Fulfillment of the Requirements for the Degree of

MASTER OF SCIENCE
in Civil Engineering

by
Paulina BAKUNOWICZ

July 2014
İZMİR

We approve the thesis of **Paulina BAKUNOWICZ**

Examining Committee Members:

Assist. Prof. Dr. Nurhan ECEMİŞ
Department of Civil Engineering, İzmir Institute of Technology

Assoc. Prof. Dr. İsfendiyar EGELİ
Department of Civil Engineering, İzmir Institute of Technology

Assist. Prof. Dr. Devrim Şüfa ERDOĞAN
Department of Civil Engineering, Ege University

10 July 2014

Assist. Prof.Dr. Nurhan ECEMİŞ
Supervisor,
Department of Civil Engineering
İzmir Institute of Technology

Prof. Dr. Gökmen TAYFUR
Head of the Department of
Civil Engineering

Prof. Dr. R.Tuğrul SENGER
Dean of the Graduate School of
Engineering and Sciences

ACKNOWLEDGMENTS

This research was accomplished in Izmir Institute of Technology during the period September 2012 to July 2014 with the help from many people.

First and foremost, I offer my sincerest gratitude to my supervisor Assist. Prof. Dr. Nurhan Ecemiş who supported me throughout my thesis with her knowledge and experience. Thanks to her support I was able to participate in the PFC training course that took place in Ecully, from 7th to 9th November, 2012. Her guidance, encouragement and supervision are gratefully acknowledged.

I would like to thank the members of my dissertation committee Assoc. Prof. Dr. İsfendiyar Egeli and Assist. Prof. Dr. Devrim Şüfa Erdoğan for providing useful suggestions for my dissertation. Dr. Egeli gave me a lot of advice about ongoing study as well as self-development paths. Dr. Erdoğan and her graduate students provided me an expert guidance and help during triaxial tests conducted at Ege University.

Big thanks go to Prof. Dr. Gokmen tayfur for his help in providing me with an expert knowledge about artificial intelligence methods, which fascinated me deeply and even more for being my academic mentor at IZTECH.

My heartfelt thanks go to my friends Mustafa Karaman, Hasan Emre Demirci and Irem Kahraman with whom I shared an office at IZTECH as well as work on CPTs from laminar box shaking table experiments. They were always on my side and I highly value their friendship, support and help.

I wish to acknowledge the funding I have received throughout my research. This work herein was supported financially by European Union 7th framework program Marie Curie fellowship (Grant number: PIRG05-GA-2009-248218), the Scientific and Technological Research Council of Turkey - TUBITAK (Grant number: 110M602) and Scientific Research Project - İYTE-BAP (2010İYTE14). These supports are gratefully acknowledged. I wish to gladly thank ITASCA for a loan of software within the Itasca Education Partnership (IEP).

Finally, my heartfelt thanks go to my family and friends for their support during the last few years. Especially my parents, Jolanta and Roman, and sister, Ania, receive my deepest gratitude and love for their dedication, neverending support and understanding. This thesis is dedicated to them.

ABSTRACT

DISCRETE ELEMENT MODELLING OF CPT USING SHAKING TABLE TESTS IN SANDS

This thesis contains an overview of the results obtained from detailed study exploring the ability of two-dimensional discrete element method (2D DEM) models to reproduce cone penetration tests in saturated sand deposits. The simulations of the cone penetration and triaxial tests are carried out under application of the commercially available numerical analysis software PFC2D (Itasca, 2008). This software is based on DEM with additional basic fluid analysis option.

The soil sample used in the laboratory experiments was uniform, river clean quartz sand, which was similar to Ottawa sand. The material properties that required calibration were normal stiffness, tangential stiffness and interparticle friction. These parameters were determined by trial and error from 2D DEM biaxial test simulations. Data from five laminar box shaking table tests of saturated sand was analysed with particular attention to the measured cone penetration resistance in assemblages deposited at various relative densities. Each shake table test was subjected to three series of shaking tests (at the same intensities) by using one-degree of freedom shaking table system, which allowed obtaining wide scope of different porosities. A new scaling factor was implemented in order to compare the data obtained from tests on real soil (3D) with numerical simulations by DEM (2D). Observations of the behaviour of discrete material at laminar box enabled us to make a correlation between porosity from large scale experiment and PFC2D model. To examine the effects of boundary conditions, porosity, particle diameter size, fluid grid dimensions, contacts, coordination number and others on the tip resistance value, multiple simulation tests were performed.

From the results presented we can deduce that 2D DEM CPT model can be powerful tool to enrich the conventional physical calibration tests. In this thesis it is also proven that CPT laminar box based correlations facilitate to overcome limitations of 2D simulation and can be widely and successfully applied for both scientific research and engineering practice purposes.

ÖZET

KUMLARDA SARSMA TABLASI DENEYLERİ KULLANILARAK CPT TESTİNİN AYRIK ELEMAN YÖNTEMİ İLE MODELLENMESİ

Bu tez, 2D DEM modellerinin doygun kumlarda koni penetrasyon deneyini modelleme kabiliyetini araştırmak için yapılan detaylı çalışmalardan elde edilen sonuçların genel değerlendirmesini içermektedir. Koni penetrasyon ve üç eksenli basınç deneylerinin simülasyonları nümerik analiz yazılımı olan PFC2D kullanılarak gerçekleştirilmiştir (Itasca, 2008). Bu yazılım ayrık elemanlar yöntemini kullanmakta olup, akışkan analizleri için temel analiz seçeneklerini de içermektedir.

Laboratuvar deneylerinde kullanılan zemin numuneleri Ottowa kumuna benzer olan üniform temiz kuvars kumudur. Kalibrasyon için gerekli malzeme özellikleri teğetsel rijitlik, normal rijitlik ve parçacıklar arası sürtünmedir. Kalibrasyon için gerekli parametreler deneme yanılma yöntemi kullanılarak 2D DEM simülasyonları yardımıyla belirlenmiştir. Doygun kumlar üzerinde yapılan beş adet farklı laminar kutu sarsma tablası deney verileri kullanılarak farklı relatif sıkılığa sahip zemin numunelerinin koni penetrasyon dirençleri dikkatli bir şekilde analiz edilmiştir. Farklı porozite değerleri için tek eksenli sarsma tablası sistemi kullanılarak her kum numunesi için 3 adet aynı ivmede sarsma deneyi gerçekleştirilmiştir. Zemin üzerinde yapılan 3 boyutlu deneylerden elde edilen verilerle 2 boyutlu DEM nümerik simülasyonları kullanılarak elde edilen verilerin karşılaştırabilmesi için yeni bir ölçekleme faktörü kullanılmıştır. Laminer kutu içindeki ayrık elemanların davranışları üzerine yapılan gözlemler bizlere büyük ölçekli deneylerden elde edilen porozite değerleri ile PFC2D modellerinden elde edilenler arasında korelasyon elde edilebilmesi imkanını sağlamaktadır. Sınır koşullarının, porozitenin, parçacık çap boyutunun, akışkan grid boyutunun, dane temaslarının, kordinasyon sayısının ve diğer faktörlerin koni uç direncine olan etkisini inceleyebilmek için birçok simülasyon gerçekleştirilmiştir.

Elde edilen sonuçlar yardımıyla 2D DEM CPT modelinin geleneksel fiziksel kalibrasyon testlerini zenginleştirmesi açısından güçlü bir araç olduğu sonucu çıkarılmıştır. Bu tez kapsamında; laminer kutu koni penetrasyon deneylerine bağlı korelasyonların, 2D simülasyonların sınırlamalarının üstesinden gelmesine olanak sağladığı ispatlanmıştır. Bu korelasyonların yaygın ve başarılı bir şekilde bilimsel araştırmalarda ve pratikte uygulanabileceği kanıtlanmıştır.

TABLE OF CONTENTS

LIST OF FIGURES x

LIST OF TABLES xv

LIST OF SYMBOLS xvii

CHAPTER 1. INTRODUCTION 1

1.1. General 1

1.2. Problem Statement and Scope of the Study 4

1.3. Organization of the Thesis 6

CHAPTER 2. LITERATURE SURVEY - CONE PENETRATION TEST 9

2.1. Introduction 9

2.2. Cone Penetration Test 9

2.3. Soil Disturbance Effects on Cone Penetration Test 12

2.4. Analytical Models of Cone Resistance 12

2.4.1. Bearing Capacity 13

2.4.2. Cavity Expansion Theory 14

2.4.3. Strain Path Method 16

2.4.4. Calibration Chamber Testing 18

2.5. Numerical Models of Cone Resistance 19

2.5.1. Finite Element Method (FEM) 19

2.5.1.1. Applications of the FEM in the CPT Analysis 20

2.5.2. Finite Difference Method (FDM) 22

2.5.2.1. Applications of the FDM in the CPT Analysis 23

2.5.3. Discrete Element Method (DEM) 24

2.5.3.1. Applications of the DEM in the CPT Analysis 25

CHAPTER 3. LABORATORY EXPERIMENTS - CPT and TRIAXIAL TESTS 27

3.1. Introduction 27

3.2. Scanning Electron Microscope View of Soil 27

3.3. Tested Soil Characteristic 29

3.3.1. Sieve Analysis and Hydrometer Test 29

3.3.2. Specific Gravity 31
3.3.3. Maximum and Minimum Void Ratio Tests 32
3.3.4. Constant Head Permeability Test 33
3.4. Triaxial Test 35
3.4.1. Triaxial Test Apparatus 36
3.4.2. Specimen Preparation for the Triaxial Test 38
3.4.3. Experimental Procedure 41
3.5. Cone Penetration Tests Inside the Laminar Box 45
3.5.1. Large Scale Laminar Box 46
3.5.2. Hydraulic Filling System 48
3.5.2.1. Relative Density 49
3.5.3. Cone Penetration System 52
3.5.3.1. Experimental Procedure of CPTs 53

CHAPTER 4. RESULTS OF TRIAXIAL AND CPT TESTS 55
4.1. Introduction 55
4.2. Triaxial Test Results 55
4.3. Cone Penetration Test Results 58
4.3.1 Cone Penetration Resistance 59
4.3.1.1 CPT Results Before and After Each Shaking Test 60
4.3.2. Relative Density 62
4.4. Correlation Between D_r and Limit q_c Values From Experiments 66
4.5. Validation of Relation Between D_r and Lim q_c with Fuzzy Logic 67
4.5.1. Membership Functions, Fuzzy Rules and Deffuzication Methods 68
4.5.2. Fuzzy Logic Implementation to CPT Study 69

CHAPTER 5. DISCRETE ELEMENT METHOD IN GEOMECHANICS 75
5.1. Introduction 75
5.2. Distinct Element Method 75
5.2.1. Key Problems in the 2-D DEM Modelling 77
5.2.2. Principles and Theory of Discrete Element Method 78
5.2.3 Use of the DEM within Geomechanics 79
5.2.4. DEM Software 80
5.3. Particle Flow Code in Two Dimensions 80

5.3.1. Basic Mechanics of PFC2D 81
5.3.2. Particle Generation 82
5.3.3. Contact Models 84
5.4. Basic Fluid Analysis Option 86
5.4.1. Theoretical Considerations 86

CHAPTER 6. CALIBRATION OF PHYSICAL PROPERTIES OF THE DISCRETE MATERIAL USING BIAXIAL TESTS 91
6.1. Introduction 91
6.2. Calibration Procedure 91
6.2.1. Sample Preparation for DEM Biaxial Tests 92
6.2.2. Computing and Controlling the Stress State 94
6.2.3. Monitoring the Test during the Loading Proccess 94
6.3. Results of the Biaxial Tests 94
6.4. Verification of Peak Friction Angle 96

CHAPTER 7. CALIBRATION OF DEM CPT MODEL 99
7.1. Introduction 99
7.2 Calibration of the CPT Model 99
7.2.1. Calculation Steps 100
7.2.2 Wall on Top of the Soil 103
7.2.3 Boundary Conditions 106
7.2.4. Computational Fluid Grids 108
7.2.4.1 Grid Size 109
7.2.4.2. Boundary Conditions of the Fluid 110
7.2.4.3. Fluid Properties 110
7.2.5. Particle Diameter 111
7.3. Scaling Factor 114
7.4. Validation of the Particle Size 115

CHAPTER 8. VALIDATION OF POROSITY IN THE 2D DEM CPT MODEL 117
8.1 Introduction 117
8.2. CPT Model 118
8.3. Calibration of Porosity in the 2D DEM CPT Model 120
8.4. The Other DEM CPT Simulations' Results 124

8.4.1. Measurement Circles 124
8.4.2. Porosity Before and After the CPTs 125
8.4.3. Coordination Number Before and After CPTs 127
8.4.4. Effects of Cone Penetration on Contact Forces and Displacement Vectors 128
8.4.5. Number of Particles in Model Assembly at Different Porosities . 132
8.5. Validation of the CPT model 133

CHAPTER 9. CONCLUSIONS 135
9.1 Summary of Findings 135
9.2. Suggestions for Future Research 136

REFERENCES.... 137

LIST OF FIGURES

Figure **Page**

Figure 1. 1. Construction mistakes related to geotechnical engineering: (a) Leaning Tower of Pisa, (b) liquefaction effects after the 1964 Niigata earthquake 2
Figure 2. 1. Terminology for cone penetrometers and location of pore water pressure measurements. 10
Figure 2. 2. Types of cone penetrometers: (a) mechanical, (b) electric and (c) piezocone penetrometer. 11
Figure 2. 3. Expansion of cavity 15
Figure 2. 4. Application of Strain Path Method in clays 16
Figure 2. 5. Deformation of square grid deep CPT (undrained conditions) for cone with apex of (a) 60° and (b) 18° 17
Figure 2. 6. LSU Calibration Chamber System 18
Figure 2. 7. Finite element mesh. 21
Figure 2. 8. FE model at initial configuration. 22
Figure 2. 9. Finite Difference mesh for CPT model. 23
Figure 2. 10. Finite Difference mesh for Cone Penetration. 24
Figure 2. 11. View of the DEM model components with indication of the main relevant dimensions: (a) calibration chamber; (b) cone penetrometer 25
Figure 2. 12. DEM model (a) before and (b) after penetration 26
Figure 3. 1. SEM images of sand tested in laboratory experiments (a) aggregate and (b) detail. 28
Figure 3. 2. SEM images of sand tested in laboratory experiments (a) aggregate and (b) detail. 28
Figure 3. 3. SEM images of sand tested in laboratory experiments (a) aggregate and (b) detail. 28
Figure 3. 4. SEM images of sand tested in laboratory experiments (a) detail and (b) aggregate. 29
Figure 3. 5. Sieves column on the mechanical shaker, (b) control hydraulic stem. 30
Figure 3. 6. Sieve analysis and hydrometer test results. 30
Figure 3. 7. (a) Desiccator and Vacuum Pump, (b) Pycnometer, Distilled Water and Weighting scale (Left to Right) 32

Figure 3. 8. (a) Mold and weight, (b) The mold attached to the vibrating table..... 33
Figure 3. 9. Coefficient of permeability (k) at different relative densities (D_r) for tested soil. 34
Figure 3. 10. (a) General set-up of a soil specimen inside a triaxial cell, (b) scheme of triaxial test apparatus. 38
Figure 3. 11. Saturation stage (a) increasing back pressure in the triaxial cell, (b) confirmation of specimen saturation by B-check. 42
Figure 3. 12. Saturation stage for the tested soil in the traixial test for both initial confining stress values. 43
Figure 3. 13. Consolidation results of the test specimen for both initial confining stress values used. 44
Figure 3. 14. Triaxial test apparatus uses at Ege University lab. 45
Figure 3. 15. Side View of the Laminar Box (N-S view), (b) Side View of Laminar Box (W-E view). 47
Figure 3. 16. Scheme of hydraulic filling of laminar box. 48
Figure 3. 17. Hydraulic filling process at IZTECH. 49
Figure 3. 18. Relative density measurements by buckets. 50
Figure 3. 19. Locations of Buckets. 51
Figure 3. 20. CPT components implemented in the study. 52
Figure 3. 21. CPTu Probe: 1)Point, 10 cm^2 , 2) O-ring, 3) Filter Ring, 4) X-ring, 5) Support Ring, 6) O-ring, 7) O-ring, 8) O-ring, 9) Friction Sleeve, 10) Cone Body, 11) O-ring 53
Figure 3. 22. Location of CPTs – general view. 54
Figure 3. 23. Location of CPTu Tests – Top View 54
Figure 4. 1. Triaxial test results confined at 100 and 200 kPa (D_r=30%). 56
Figure 4. 2. Failure plane of specimen sheared at initial confining stress of 100 kPa. 57
Figure 4. 3. Determination of the friction angle using the Mohr-Coulomb Circle. 58
Figure 4. 4. The procedure of chosing limit value of cone penetration resistance (lim q_c)… 59
Figure 4. 5. CPT results from laboratory experiments performed at IZTECH (a) before 1^{st} shake, (b) after 1^{st} shake, (c) after 2^{nd} shake and (d) after 3^{rd} shake. 61
Figure 4. 6. D_r results after the 1^{st}, 2^{nd} and 3^{rd} shake with calculated AVG. D_r values. . 63
Figure 4. 7. Change in relative density for succeeding shakings. 65
Figure 4. 8. Change in void ratio for succeeding shakings. 65

Figure 4. 9. Average values of D_r at each stage of experiments, where: 1 – ini_shake AVG. D_r, 2 – 1st_shake AVG. D_r, 3 – 2nd_shake AVG. D_r, 4 – 3rd_shake AVG. D_r. 66
Figure 4. 10. Relationship between relative density and limit cone penetration resistance from laboratory tests. 67
Figure 4. 11. Membership fucntions. 69
Figure 4. 12. A two-input single-output Mamdani fuzzy model for the FL CPT study. 70
Figure 4. 13. Membership functions for the FL CPT study. 71
Figure 4. 14. 3D surface graph illustrates our model govern by matrix of fuzzy rules. . 72
Figure 4. 15. Relationship between the relative density and the limit cone penetration resistance from the laboratory tests by the FL concept. 73
Figure 4. 16. Results of q_c with different deffuzzification methods, compared to the laboratory data. 73
Figure 5. 1. Annual rate of discrete element modeling publications identified by using the approach of Zhu et al. (2007) 79
Figure 5. 2. Flow chart for the general solution procedure in PF2D 82
Figure 5. 3. Basic contact model in PFC2D for (a) walls, and (b) particles. 84
Figure 5. 4. Contact forces and displacements in PFC2D. 85
Figure 5. 5. Flow chart in PFC2D 89
Figure 5.6. Flow chart of the fluid sheme. 90
Figure 6. 1. Qualitative relationship between porosity and initial stress for various contact stiffnesses. n = 0.16 is the porosity value adopted for all the calibration simulations. 93
Figure 6. 2. (a) Biaxial sample, (b) triaxial sample, (c) triaxial apparatus. 93
Figure 6. 3. Stress-strain curves of a laboratory triaxial and DEM biaxial tests for confining stress of 100 kPa. 95
Figure 6. 4. Volume change vs axial strain of laboratory triaxial and DEM biaxial tests for confining stress of 100 kPa. 95
Figure 6. 5. Comparison of friction angle from (a) Mohr-Coulomb envelope (b) DEM simulation. 97
Figure 7. 1. (a) Simplified CPT model by Arrayo et al., 2011, (b) simplified CPT model by Bakunowicz and Ecemis, 2014, (c) notation of walls. 101
Figure 7. 2. Influence of timesteps of history on wall 1. 101
Figure 7. 3. Influence of timesteps of history on wall 2. 102

Figure 7. 4. Forces accumulated on cone with 2 cm history interval for wall 1 and 2. 102
Figure 7. 5. The schematic view of the cone, box and wall on top in PFC2D. 103
Figure 7. 6. Measurement circle location. 104
Figure 7. 7. Cones used during calibration phase. 105
Figure 7. 8. Summary of results of the CPT simulations without moving wall on top. 105
Figure 7. 9. Summary of results of the CPT simulations with moving wall on top. 105
Figure 7. 10. Porosity change after the CPTs. 106
Figure 7. 11. Location of the CPT in the laboratory – top view. 107
Figure 7. 12. Ratio of chamber diameter, R_d. 107
Figure 7. 13. (a) DEM-SIMPLE model of CPT, (b) computational fluid grids. 109
Figure 7. 14. Fluid model of (a) boundary conditions, properties and pressure of fluid before the CPT, (b) porosity of fluid with recessed cone. 111
Figure 7. 15. Contact forces' chains in the assembly of the particle diameter of (a) 2cm; and (b) 1cm. 112
Figure 7. 16. Influence of the cone diam. on the number of cone-particles contacts ... 113
Figure 7. 17. Scaling logic for (a) 2D and (b) 3D simulations. 114
Figure 7. 18. Smoothing procedure and determination of limit qc for data obtained from DEM CPT simulations. 116
Figure 7. 19. Numerical experiment results from validation of particle size by DEM. 116
Figure 8. 1. Final CPT model (a) before and (b) after cone penetration. 118
Figure 8. 2. Relationship between the limit cone penetration resistance and the relative density from the CPT DEM simulations. 122
Figure 8. 3. Relationship between the limit cone penetration resistance and the void ratio from the CPT DEM simulations. 123
Figure 8. 4 Relationship between the limit cone penetration resistance and the porosity from the CPT DEM simulations. 123
Figure 8. 5. Relationship between the porosity in laboratory and in the DEM. 123
Figure 8. 6. Locationof measurement circles in the box. 124
Figure 8. 7. Porosity in the box before and after the cone penetration tests. 125
Figure 8. 8. (a) Model of the CPT in dense assembly (n = 0.09 in PFC2D); particles occur to penetrate (b) inside the cone, (c) outside the boundary conditions, due to penetration process. 126
Figure 8. 9. Discrete particles with diffrent amount of contacts. 127
Figure 8. 10. CN results (a) before and (b) after the CPTs. 128

Figure 8. 11. Average CN results before and after the cone penetration. 128
Figure 8. 12. Contact forces and dissplacement vectors near the cone at 1 m depth from assembly of porosity of 0.39 and particle diameter of (a) 2.0 cm, (b) 1.5 cm, (c) 1.0 cm and (d) 0.8cm 130
Figure 8. 13. Contact forces and dissplacement vectors near the cone at 1 m depth from assembly of porosity of 0.41 and particle diameter of (a) 2.0 cm, (b) 1.5 cm, (c) 1.0 cm and (d) 0.8cm 131
Figure 8. 14. Contact forces and dissplacement vectors near the cone at 1 m depth from assembly of porosity of 0.41 and particle diameter of (a) 2.0 cm, (b) 1.5 cm, (c) 1.0 cm and (d) 0.8cm 132
Figure 8. 15. Comparison of DEM and lab. results after validation of porosity (a) D_r=45%, (b) D_r=50%, (c) D_r=60% and (d) D_r=65%. 134

LIST OF TABLES

Table **Page**

Table 2. 1. Analysis methods used while CPT investigation..... 13
Table 3. 1. Results of the sievie analysis. 31
Table 3. 2. Maximum and minimum void ratio tests results. 33
Table 3. 3. Coefficient of permability in diffeernt soils. 34
Table 3. 4. Main components of conventional triaxial system 37
Table 3. 5. Steps to achieve a proper saturation degree for the triaxial test at 100 kPa and 200 kPa confinement. 43
Table 3. 6. Steps to achieve a proper consolidation level in the triaxial test at 100 kPa and 200 kPa confinement. 44
Table 3. 7. Summary of shake tables and CPT tests. 47
Table 3. 8. Results from buckets tests from TEST 1 51
Table 4. 1. Conditions at failure for 100 and 200 kPa initial confining stresses. 57
Table 4. 2. Calculation of the elasticity modulus from the stress-strain curve for the initial confining pressure of 100 and 200 kPa. 58
Table 4. 3. Limit q_c values for all CPTs conducted in this study. 60
Table 4. 4. Average relative density, void ratio and porosity obtained from CPTs. 64
Table 4. 5. Change in relative density and void ratio between each stage of experiments. 65
Table 4. 6. D_r - lim q_c pairs from CPTs. 66
Table 4. 7. Set of data obtained from CPT used in FL calculation. 70
Table 4. 8. Fuzzy rules for the FL CPT study. 71
Table 4. 9. Results of q_c with different deffuzzification methods. 73
Table 5. 1. Neccessary parameters to build a model in the DEM. 81
Table 6. 1. Calculation of elasticity modulus from stress-strain curve for initial confining pressure of 100 kPa using laboratory and DEM results. 96
Table 6. 2. Granular deposit simulation data. 98
Table 7. 1. Literature on geometric parameters of 2D DEM studies related to CPTs. . 108
Table 7. 2. The results of the cone diameter effects on the number of cone-particles conatcts with their ratio. 113
Table 8. 1. Input parameters for the discrete material, cone, walls and fluid. 120

Table 8. 2. Relationship of porosity from the DEM with the relative density, porosity and void ratio in the tested soil. 122

LIST OF SYMBOLS

A_c = Area of the cone

A_p = Sum of particle areas

A = Container area

a_{max} = Maximum acceleration amplitude of the applied ground acceleration

A_s = Surface area of the friction sleeve

B = Width or diameter of the foundation

B-value = Pore water pressure coefficient

c = Cohesion

C_c = Coefficient of gradation

c_u = Undrained cohesion

C_u = Uniformity coefficient

d = Diameter

D_{10} = Diameter through 10% of the total soil mass passed

D_{30} = Diameter through 30% of the total soil mass passed

D_{60} = Diameter through 60% of the total soil mass passed

d_c = Diameter of the cone

d^j = Diameter of the j-th particle

D_r = Relative density

e = Void ratio

e_{min} = Minimum void ratio

e_{max} = Maximum void ratio

$\vec{f_b}$ = Body force per unit volume

f_s = Sleeve friction

F_s = The total force acting on the friction sleeve

F^s = Shear contact force

g = Acceleration due to gravity

G = Shear modulus of the soil at shear strain level

G_s = Specific gravity

k = Permeability

k_1 = Stiffness of the spring

k_n = Normal stiffness

K^n = Normal stiffness at the contact

k_s = Tangent stiffness

K^s = Shear stiffness at the contact

m = Total mass of the particle

n_0 = 'Old' porosity before radius expansion

n = 'New' porosity after radius expansion

N = Total numer of particles in an element

N_c = Bearing capacity factor

N_q = Bearing capacity factor

N_r = Bearing capacity factor

p = Fluid pressure

q_0 = Surcharge load

q_b = Bearing capacity

q_c = Cone tip resistance

Q_c = Total force acting on the cone

R_d = Ratio of chamber diameter

S = Scaling factor

t_{crit} = Critical time-step for DEM

t_f = Fluid time step

t_m = Mechanical time step

u = Pore water pressure

u_1 = Pore pressure measured on the cone

u_2 = Pore pressure measured behind the cone

u_3 = Pore pressure measured behind the friction sleeve

U^n = Relative contact displacement

U^s = Relative contact displacement

v = Penetration velocity

V = Volume of a fluid element

Vp = Total volume of particles within the considered element

$v^{\rightarrow}$ = Fluid velocity

w = Water content

W_0 = weight of dry sample

W_A = weight of pycnometer with distilled water

W_B = weight of pycnometer, distilled water and soil sample

z = depth

α = k_s/k_n

β = Coefficient

γ = Unit weight of soil

γ_{sat} = Saturated unit weight

ΔP = Change in pressure

Δu = Excess pore pressure

$\Delta\sigma_3$ = Change in minor principal stress

$\in$ = Porosity

μ = Friction coefficient

μ_d = Dynamic viscosity

μ_c = Friction coefficient of cone

μ_p = Friction coefficient of particles

μ_w = Friction coefficient of walls

ν = Poisson's ratio

ρ = Density

ρ_f = Density of the fluid

ρ_{matrix} = Matrix density

σ_r = Component of stress tensor

σ_{vo} = Initial effective normal stress

σ_{vo}' = Effective vertical stress

σ_z = Component of stress tensor

σ_θ = Component of stress tensor

ϕ = Peak friction angle

CHAPTER 1

INTRODUCTION

1.1. General

Soil is a principal component of the Earth's ecosystem as well as it is known as the "skin of the earth" with interfaces between the lithosphere, hydrosphere, atmosphere, and biosphere (Chesworth, 2008). According to Charles E. Kellogg who said, “Essentially, all life depends upon the soil....There can be no life without soil and no soil without life; they have evolved together.” I could not agree more with that statement. Due to enormous significance of soil in our lives, multiple studies were conducted and soil was investigated from various points of view such as social, biological, agricultural, ecological and last but not least engineering. In this study, the focus is laid on the engineering perspective in understanding the nature of soil.

Hundreds years of research and tons of studies have isolated many key problems related to soil in the engineering discipline borders. Geotechnical engineering is a branch of civil engineering, which deals with soils and Earth materials. Geotechnical engineers use their expertise about soil and rocks to the evolution of foundations for a diversity of structures. In advance of any design or construction, the proper and complex soil investigation should be performed along with environmental site assessments. Site assessments are investigations of the soil under the planned building that take place before some other engineering is carried out. A proposed structure or development need to be evaluated based on soil properties determined in field, laboratory and by empirical relations.

The effects of the wrong assumption of soil properties can trigger tragic consequences for the existing structure. The most well recognized example of engineering mistake and inadequate design is Leaning Tower of Pisa in Italy which is depicted in Figure 1.1(a). Leaning Tower of Pisa has multiple causes for its out of verticality. However the main one is the subsoil profile which was not carefully recognized before starting the construction. It is a great incident to realize the

importance of the soil conditions which need to be known in advance in order to properly support structures during their entire lifespan.

However, the properties of soil might change during the lifetime of the structure which makes the proper design and construction a really challenging phase. Alterations of soil are usually triggered by factors such as stress, time, water, environment, and disturbance (Lambe, 1969). Figure 1.1(b) shows the severe consequences of liquefaction phenomenon which occurs in saturated or partially saturated soils when soil essentially loses strength and stiffness in response to monotonic or cycling loading, mainly due to earthquake shaking or other sudden change in stress condition. In the image below, Figure 1.1(b), some buildings toppled when the soil underwent liquefaction during the 1964 Niigata earthquake. The construction may even sink into the ground during liquefaction hazard. Although the phenomenon of liquefaction was recognized prior to the 1964 Niigata earthquake, there was not enough attention of engineers and researchers brought to its effects. As shown in Figure 1.1(b) buildings are intact; in the contrary the foundation which was designed inaccurately to the soil conditions and possibility of earthquakes.

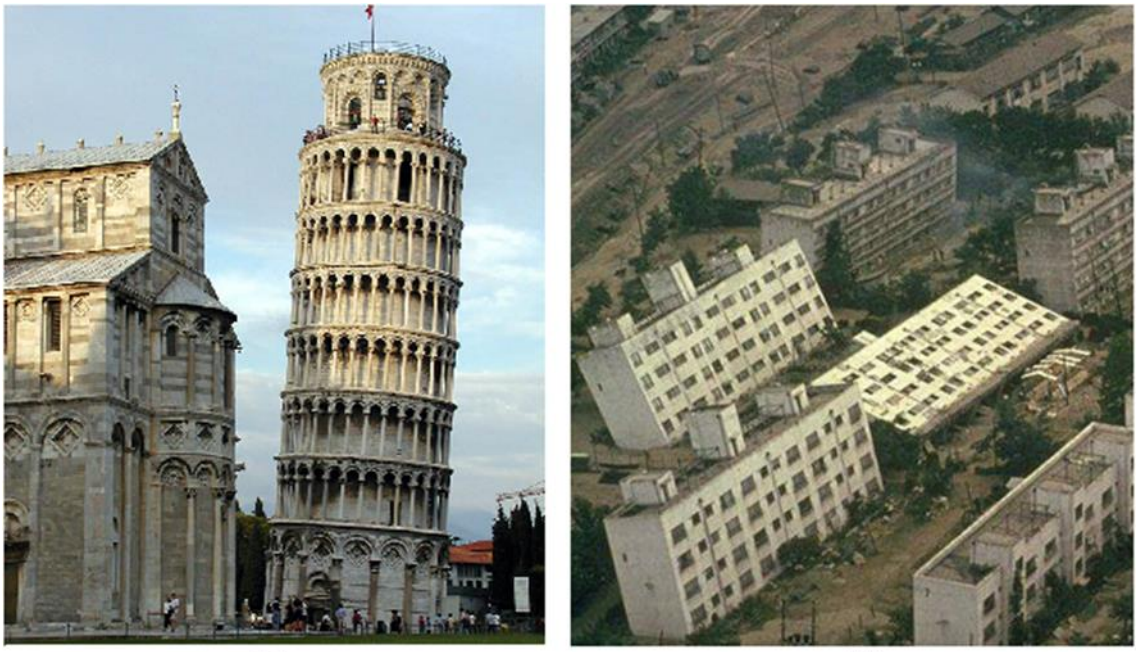

Figure 1. 1. Construction mistakes related to geotechnical engineering: (a) Leaning Tower of Pisa (b) liquefaction effects after the 1964 Niigata earthquake. (Source: (a) wikipedia.org, (b) www.ce.washington.edu).

In order to not repeat mistakes of past, soil investigation methods are improving constantly with the technology progress and experience of former engineers. Lambe (1969) has divided the methods of soil investigation into:

- Reconnaissance
    - Visual control
    - Air photos
    - Reports from past construction
    - Geologic reports and maps
- Exploration
    - Geophysical
    - Electrical
    - Sampling and testing by pits or borings
- Field tests
    - Penetration tests
        - Cone penetration tests (CPT)
        - Standard penetration tests (SPT)
        - Flat dilatometer (DMT)
    - Water table pressure tests
    - Vane tests
    - Load tests
    - Compaction tests

Reconnaissance techniques give a general picture of the entire site. Exploration tactics are also widely used in field. Geophysical and electrical methods enable us to detect various layers in soil profile. Sampling followed by laboratory tests is also very common procedure. This method has limitations like difficulty to obtain high quality undisturbed soil samples, especially at greater depths. Moreover, it is also complicated to mimic the field conditions of soil for laboratory testing. Therefore field tests are suitable for soils which are prone to soil disturbance as well in soils having multiple layers which vary laterally and/or vertically. Lunne et al. (1997) has summarized the applicability and usefulness of various in situ tests and concluded that the CPTs have the highest capacity among other in situ tests based on former authors' experience.

Cone penetration test has been used for decades and still is one of the most convenient methods of soil investigation. Essentially, it consists of a cone on the end of numerous rods and then the penetrometer is pushed into the soil at a constant rate while

measuring a number of quantities (Lunne et al., 1997). Despite CPT's multifunctionality and long-record use, rational methods for interpretation of CPT data remain vague. Aside from experiments, analytical and numerical techniques were developed in order to deeply understand the mechanics of the processes related to penetrometer insertion (Elsworth et al., 2008). There is a variety of approaches available to deal with CPT problems. The most commonly used are the following: bearing capacity theory (Terzaghi, 1943), cavity expansion methods (Salgado et al., 1997), strain paths methods (Baligh, 1985) finite element methods (Huang et al., 2004), chamber tests (Houlsby et al., 1988), wedge penetration tests (Durgunoglu and Mitchell, 1975), centrifuge tests (Bolton and Gui, 1993) and discrete element method (Cundall and Strack, 1979) which is gaining popularity over the past two decades.

1.2. Problem Statement and Scope of the Study

A discrete element method (DEM), which is also called a distinct element method, has particular advantages over other numerical approaches, such as finite element method (FEM) or finite difference method (FDM). The cone penetration experiments generate momentous deformations within surrounding soil. Much insight on these processes can be gained through model testing including, chamber tests, wedge penetration tests and centrifuge tests in combination with DEM simulations. The advantage of using DEM modelling to support experimental testing to study various aspects of penetration process is that modelling provides the possibility of investigating mechanical behaviour of materials at both micro and macro levels. Soil is a discontinuous medium, thus DEM techniques work more efficiently than FEM of FDM. Moreover, simulations by discrete element methods are very useful for purpose of parametric studies as DEM creates a virtual laboratory.

Experimental results presented in this thesis and those of distinctive research found in the literature show that real soil behaviour is neither ideal, nor predictable. Therefore, real soil as complex medium is difficult to mimic by means of numerical software. Simplifying assumptions are obligatory for the development of theory related to cone penetration applications. The purpose of this project is to gain deeper understanding in behaviour of sands, subjected to cone penetration tests. In the scope of this study, both laboratory CPTs and numerical DEM simulations of penetrometer

insertion were conducted. The numerical analyses have been performed using the commercially available software PFC2D which is specialized in geomechanics problems.

There are multiple problems related to two-dimensional modeling by means of distinct element method. For instance, typical (real) soil assembly contains billions of particles, but contemporary DEM assemblies must be usually scaled (magnification of particle diameter) in order to sustain the simulation for sufficiently long time. Moreover, there are particular limitations in using a two dimensional (2D) codes like PFC2D to mimic physical phenomena by distinct element method. The main restrictions of using PFC2D are: (1) the concept of stress and strain, (2) packing, (3) porosity and (4) mass properties. In this study we focused on:

- The accurate description of soil properties tested in laboratory tests that need to be mimicked by discrete material in PFC2D.
- Obtaining a correlation between D_r and limit q_c values from CPT experiments.
- The calibration of physical properties of discrete material using biaxial tests in PFC2D environment from triaxial tests performed in laboratory.
- Implementation of a new scaling factor in order to compare the data obtained from tests on real soil (3D) with numerical simulations by DEM (2D).
- Validation of porosity, based on physical experiments calibration.
- Investigation on behaviour of discrete material before and after CPTs.

For purpose of this study, multiple laboratory experiments were performed. The test program included:

- Scanning electron microscope analysis
- Laboratory tests to identify the soil properties
    - sieve analysis,
    - hydrometer tests,
    - specific gravity tests,
    - maximum and minimum void ratio tests,
    - relative density tests,
    - constant head permeability tests.
- Consolidated drained triaxial tests under 100 and 200 kPa initial confinement
- Cone penetration tests inside a large scale laminar box before and after shake table tests.

The numerical analysis by PFC2D included:

- Numerical simulations of biaxial tests.
- Simple slope modeling in order to validate the peak friction angle (ϕ) of the material assembly.
- Cone penetration in simplified conditions (calibration of CPT model in DEM).
- Cone penetration simulations in order to validate particle size and porosity. DEM test program was performed according to Table. 1.2.

During the work on this thesis, a paper that is related to the ongoing research was accepted for publishing and presentation in the 14th International Conference of the International Association for Computer Methods and Advances in Geomechanics (14IACMAG), which will be held in Kyoto during September 22-25, 2014 (Bakunowicz and Ecemis, 2014).

1.3. Organization of the Thesis

In this thesis the numerical simulation of the cone penetration tests in saturated sands is attempted. It involves the simulation of triaxial compression and cone penetration tests by discrete element method. All numerical analyses presented in this thesis have been conducted by use of the commercially available software Particle Flow Code in 2 Dimensions – PFC2D (Itasca, 2008). Experiments performed in laboratory to calibrate stiffness parameters and validate porosity in 2D DEM simulations are explained. The thesis consists of nine chapters:

Chapter 2 presents a brief review of the variety of approaches available to deal with CPT problems. Literature on current analytical methods, numerical models and empirical correlations relating CPT results with soil properties is summarized.

Chapter 3 is an attempt to describe the laboratory equipment and the experimental procedures followed during the laboratory experiments - CPT and triaxial tests used in this thesis. The first part gives the basic view on soil characteristics like size and shape. The second part focuses on the tested soil characteristic determined by laboratory tests, which include sieve analysis, hydrometer, specific gravity, maximum and minimum void ratio, relative density and constant head permeability tests. In the third part, the triaxial test is explained. Triaxial test apparatus, specimen preparation methods for triaxial tests and experimental procedure are summarized. Finally, the

fourth part describes the cone penetration tests inside the large scale laminar box. Equipment and experimental procedure of the CPTs are concisely portrayed.

Chapter 4 presents results of triaxial and cone penetration tests. In the first section, results from shearing stage of a series of consolidated drained (CD) triaxial tests are given. These results are necessary to calibrate the stiffness parameters of numerical model in PFC2D. In the second part, the CPTs results are presented. Cone penetration resistance and relative density obtained from the performed laboratory CPTs are analysed in order to derive a correlation between relative density (D_r) and limit cone penetration resistance (q_c) values from experiments, which are described in the third part. Moreover, the CPT results are analysed by means of fuzzy logic and the relationship between Dr and limit qc is validated.

Chapter 5 consists of literature review of discrete element method in geomechanics. In the first part, the principals of distinct element method are presented. Special focus is put on key problems in 2-D DEM modeling, theoretical considerations, use of DEM within Geomechanics and DEM Software. In the second part, the most important features of PFC2D software are explained. The final part of the chapter describes basic fluid analysis option by Itasca that allows us to simulate saturated conditions from laboratory cone penetration experiments.

Chapter 6 contains the calibration of physical properties of discrete material using biaxial tests in PFC2D environment. In the first part the calibration procedure is briefly explained. In the second part, the results of biaxial DEM simulations are presented and discussed. At the end, the third part presents the verification of peak friction angle by means of simple slope tests. Thus by using the best set of parameters, it was possible to match the DEM biaxial test results with the laboratory triaxial test outcome.

Chapter 7 presents the numerical calibration of the CPT model using PFC2D. In the first part, the CPT model is simplified and calibration of calculation steps, wall on top of the soil, boundary conditions, computational fluid grids and particle size are performed. In the second part, a scaling factor is implemented into the cone penetration resistance equation in order to validate the particle diameter and subsequently to be used in analysis of DEM CPT results after deciding on final CPT model characteristics.

Chapter 8 consists of validation of porosity in the 2D DEM CPT model. First, the CPT model generation is described. In the second part of this chapter, the calibration of porosity in 2D DEM from the laboratory experiments is presented. After validation of

porosity in PFC2D, further DEM simulation results are given in the fourth part of the chapter. Effects of multiple quantities such as porosity, contact forces, displacement vectors, coordination number and the number of particles are carefully investigated. Finally, the results from laboratory and DEM CPT tests are compared.

Chapter 9 gives a summary of the work carried out in this thesis and the major conclusions reached. Moreover, it gives recommendations for further research.

CHAPTER 2

LITERATURE SURVEY - CONE PENETRATION TEST

2.1. Introduction

In this chapter, literature on current analytical methods and empirical correlations relating cone penetration results with soil properties is summarized. The focus is on literature concerning:

1. Cone penetration test;
2. Soil disturbance effects in CPT analysis;
3. Analytical models of cone resistance;
4. Numerical models of cone resistance;

Moreover, finite element, finite difference and discrete element methods are explained. Examples of previous models of CPT developed using numerical methods are presented.

2.2. Cone Penetration Test

The cone penetration test (CPT) is an in-situ test in geotechnical engineering, in which a cone at the end of series of rods is pushed into the ground at a constant rate (v=2 cm/s, ASTM D3441). The independent measured parameters are cone penetration resistance (q_c), friction resistance (f_s) and pore water pressure (u) (Lunne et al., 1997). The total vertical force acting on the cone (Q_c) is divided by projected area of cone (A_c) to obtain cone resistance. Sleeve friction (f_s) is obtained similarly by dividing total force acting on the sleeve (F_s) by the surface area of the friction sleeve, (A_s). It is also possible to measure pore water pressure by filters on the cone. First attempts to construct CPT equipment were done in the 1950s at the Dutch Laboratory for Soil Mechanics in Delft to investigate soft soils. The test method was constantly developed since then. Nowadays the role of CPT in site investigation is huge and demand for this commonly used subsurface exploration method is rapidly growing.

We can distinguish three main groups of CPT systems as: mechanical cone penetrometers, electric cone penetrometers and piezocone penetrometers. The photos of these CPT systems are given in Figure 2.2. The most popular penetrometer has tip area of 10 cm^2 with an apex angle of 60° and has been accepted as a reference. More details are available in the International Reference Test Procedure (ISSMFE, 1989). The CPT test has been mainly used for three applications: 1) to estimate soil properties based on an appropriate correlation, 2) to provide results for direct geotechnical design, and 3) to determine subsurface stratigraphy. To investigate soil for geotechnical design, engineers strongly rely on in-situ tests, due to difficulty in obtaining undisturbed, intact granular samples.

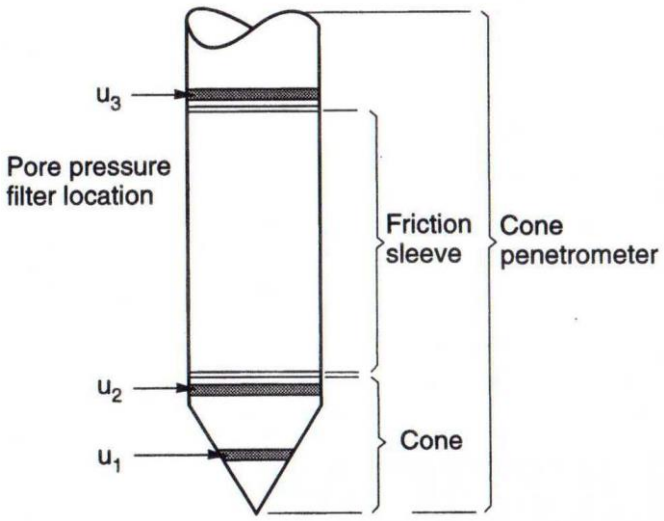

Figure 2. 1. Terminology for cone penetrometers and location of pore water pressure measurements. (Source: Lunne et al. 1997)

Pore water pressure is one of the quantities that can be measured during cone penetration test. It is typically measured at one, two or three locations, as it is depicted in Figure 2.1. Over the years, sensors has been incorporated into the cone to measure the arrival of a seismic shear wave, thanks to which the shear wave velocity can be estimated (Mitchell, 1988).

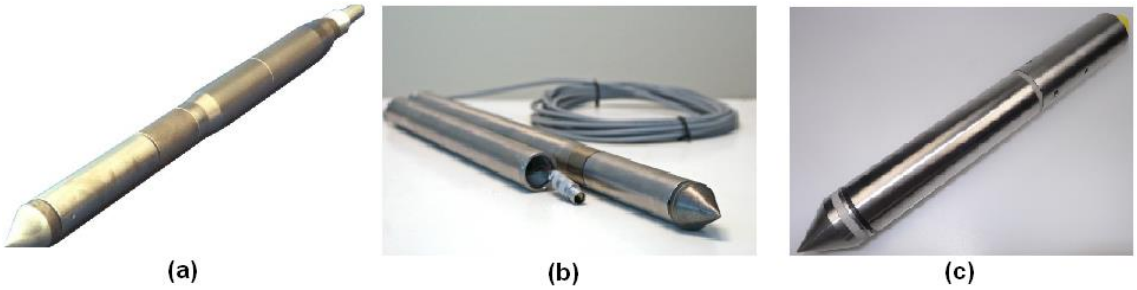

Figure 2. 2. Types of cone penetrometers: (a) mechanical (b) electric and (c) piezocone penetrometer. (Source: (a) www.geomil.com, (b) www.envi.se and (c) www.gauda-geo.com)

With recent technological development, special cones can be run concurrently with the standard cone test to evaluate the natural foundation material properties, which include: shear wave velocity, in-situ water content, shear modulus, shear strength and other quantities. Furthermore, CPT platform can be used for deploying high quality push fixed piston samplers. Multifunctionality of CPT has promoted the use of this test. Moreover, the ability of the CPT to collect multiple and simultaneous readings with depth, is a valuable feature. Thus greater delineation of strata can be achieved. Further advantages are elimination of operator error, reliable, repeatable penetration details, minimal soil disturbance and high productivity (new models are able to penetrate up to 150m soil tested per day). More manageable data handling is an underutilized advantage of the CPT. The penetration process is vulnerable to theoretical modeling. Based on CPT results, numerous empirical correlations and numerical simulations can be done.

Various attempts have been made over the years to develop reliable analytical models for simulating cone penetration process as well as to derive proper correlations with soil properties from empirical CPT results. During CPT penetration, soil around the penetrometer may be pushed in all directions, which makes a complex boundary problem. Moreover, analysis of the problem is difficult, due to large stresses and strains imposed during penetration and complicated soil behaviour induced by complex initial soil conditions. Uncertainties associated with own creep of soil, aging effects and other specific characteristic of soil also make the problem more complicated. Thus, it has great importance to validate the penetration process with proper continuum models for granular soils, in order to analyze and interpret this popular, widely used in-situ test.

2.3. Soil Disturbance Effects on Cone Penetration Test

For the past many years it is vivid to understand soil disturbances caused by installation CPT into soil, which was similar to a deep foundation installation. The improvement of a sound understanding and reliable predictive techniques for distortion effects are complex, due to following factors gathered by Baligh (1985):

- Field variables like displacements, strains, stresses and pore water pressures depend on the radial and vertical positions which is a key problem in especially 2D analysis,
- Large deformations and strains are observed in the soil both in laboratory and in situ testing,
- Because of presence of water and air in the soil profile, soil need to be treated as a multiphase medium,
- Complex behaviour of soil, which includes nonlinearities, anisotropy, inelasticity, time-dependant and frictional response,
- Characteristics of the soil interface cannot be mimicked by linear model for instance Coulomb friction.

With the aid of expansion of numerical methods and constant development of technology, some aforementioned limitations were overcome and realistic solutions to nature of soil deformations while performing CPT were formulated. Numerical techniques such a finite, finite difference and discrete element methods have been sufficiently developed to overcome the above stated difficulties.

2.4. Analytical Models of Cone Resistance

In this section, an overview of some analytical model is presented. As it was mentioned before, complex soil behaviour accompanied by large stresses and strains imposed during penetration cause difficulty for developing a rigorous model of cone penetration. Some assumptions to simplify soil response, penetration process and boundary effects are necessary, as for any analytical model, which has to mimic the reality. However, limitations are obvious when applying these methods to penetration analyses in granulates, mainly due to the shear-dilatant characteristics of granular materials. Various scientists have been investigating the CPT related problems. The

general approaches are gathered in Table 2.1. Analytical and numerical approaches investigating CPT related problems.

In this chapter, an attempt has been made to present four general theoretical approaches commonly used to estimate cone penetration resistance are: (1) Bearing capacity analysis; (2) Cavity expansion theory; (3) Strain path methods; and (4) Calibration chamber testing. A brief summary and comparison of these methods are given in the following sections.

Table 2. 1. Analysis methods used while CPT investigation.

No.	Analysis method	Investigator	Year
1	Bearing capacity theory	Terzaghi	1943
		Durgonoglu and Mitchell	1975
2	Cavity expansion method	Vesic	1972
		Yu and Houlsby	1991
		Salgado et al.	1997
3	Strain paths methods	Baligh	1985
		Sagaseta et al.	1995
4	Finite element method (FEM)	De Borst & Vermeer	1984
		Abu-Faraskh et al.	1998
		Huang et al.	2004
5	Chamber test	Parkin & Lunne	1982
		Houlsby & Hitchman	1988
6	Wedge penetration tests	Durgonoglu and Mitchell	1975
7	Centrifuge test	Phillips & Valsangkar	1987
		Bolton et al.	1993
8	Discrete element method (DEM)	Cundall & Strack	1979

2.4.1. Bearing Capacity

Pushing a cone into a soil is very similar to installing a pile. This is the reason why bearing capacity theory has often been used to illustrate the cone penetration mechanism (Meyerhof, 1951). Bearing capacity analysis of the CPT is based on the fundamental solution for a strip footing on the surface of an elastic-plastic solid developed by Prandtl (1921). However, it requires to determine both a shape and depth factor while the most demand is about the use of shape factors for circular cone penetration. The basic bearing capacity formula developed by Terzagi (1943) consists of following terms;

$$q_b = c \cdot N_c + q_0 \cdot N_q + 0.5 \cdot \gamma \cdot B \cdot N_\gamma \quad (2.1)$$

where,

q_b = bearing capacity;

c = cohesion;

q_0 = surcharge load;

N_c, N_q, N_r = bearing capacity factors;

B = width or diameter of the foundation;

γ = unit weight of soil.

As sands in the failure state are modelled as a material with c = 0 with φ different than 0, the Equation 2.1 can be simplified to the following equation:

$$q_b = q_0 \cdot N_q + 0.5 \cdot \gamma \cdot B \cdot N_\gamma \quad (2.2)$$

Seeing that this method was originated for strip footings accommodated on the territory, shape and depth corrections to N_c are obligatory. Meyerhof (1951) has used empirical data or approximate analyses to derive the depth and shape factors. Cone factor, N_k values was derived for piles from the method of bearing capacity theory by Salgado et al. (2004). Shape and depth factors ware defined using a rigorous analysis based on finite-element limit analysis. They computed bearing capacities for strip, circular and square shape footings at various depths and computed shape and depth factors from these values. According to their findings, the scope of N_c values for circular footings at large depths between 11 ~ 14. It was done according to lower and upper bound analysis. The limitation of this method is that the bearing capacity solution neglects soils compressibility.

2.4.2. Cavity Expansion Theory

The main assumption of the cavity expansion method is that the mobilized cone tip resistance is linked to the pressure required to expand a cavity in soil. Expansion takes place from a radius equal to zero to a radius equal to that of the cone

penetrometer. Bishop et al. (1945) were the first contributors to the theory for the expansion of a cylindrical cavity in an elastic, perfectly plastic material. The theory has been extended by Vesic (1972). The study has lead to approximate solutions for spherical and cylindrical cavity limit pressures and used these solutions to propose bearing capacity factors for deep foundations. He assumed the soil as a linear elastic perfectly plastic material to simplify cavity expansion analysis, and followed the Mohr-Coulomb failure criterion. Expansion of a cavity in soil is shown in Figure 2.3. In this illustration, the initial cavity radius, R_i is expanded to R_u, when a uniformly distributed internal cavity pressure reached its limit value. Vesic's model doesn't take into account the effects of dilatancy. Salgado (1993) criticized it stating that it has a potential for underpredicting limit pressure and, thus, penetration resistance. The cavity expansion method may be capable of modeling the CPT in loose to medium granulates of slight dilation, but is unsuitable for medium-dense and very dense granulates of significant dilation. After Vesic, significant progress was observed in developing cavity expansion solutions by adapting improved soil stress-strain models and yield criteria in both sand and clay (Cater et al. 1986, Yu and Houlsby 1991, Salgado et al. 1997, Salgado and Randolph 2001). More precisely, many investigators have related limit pressure solutions to practical values, such as; pile end bearing or cone resistances (e.g. Randolph et al. 1979, Salgado 1993).

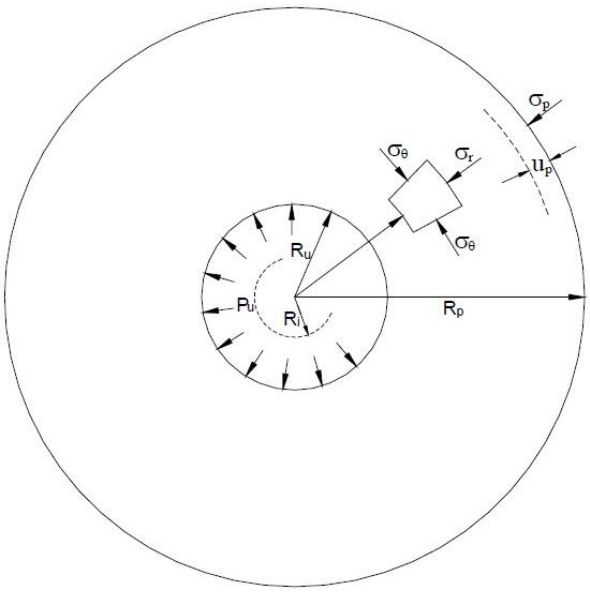

Figure 2. 3. Expansion of cavity.
(Source: Vesic, 1972)

2.4.3. Strain Path Method

The concept of strain path theory was initiated by Baligh (1975). He ensured that the nature of soil deformations caused by the installation of a rigid object in the ground is essentially strain-controlled. Based on this concept, Baligh (1985) developed the strain path method to solve problems of deep quasi-static penetration of axisymmetric rigid bodies in saturated clays (e.g., piles, cone penetrometers, samplers, etc.) and drained penetration in sands. Application of strain path method to deep penetration is shown in Figure 2.4 by example of clay (Baligh, 1975).

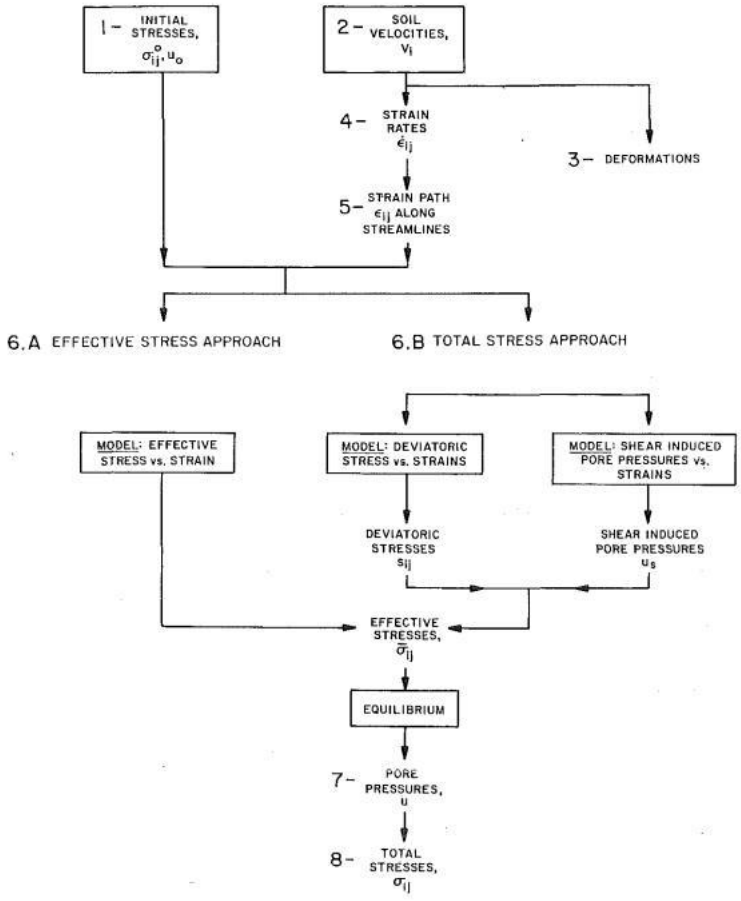

Figure 2. 4. Application of Strain Path Method in clays.
(Source: Blaigh, 1985)

The flowing chart for the basic concept of this method is shown in Figure 2.5. This method is an approximate tool to predict soil disturbances caused by the installation of multiple rigid objects in the soil. The proposed solution was the first step

in understanding, modeling and predicting the behaviour of structures like piles, penetrometers etc. The big advantage of this method is that its comprehensive framework aid to understand the significant shearing and distortion of the surrounding soil while conducting CPT in the method as in the field. Approach is in a realistic and rational manner. Continuous penetration of the cone mechanism is assumed to be in a steady-state condition. Moreover a steady state of flow passing along a fixed cone penetrometer in soil around a cone is also considered. This means that the stress and strain fields in soil do not change with time from the point of view of the cone tip if homogeneous soil conditions are present. The used soil model is simplified as a rigid, perfectly plastic material under isotropic conditions. The strain field is obtained by integrating the velocity field along streamlines. Deviatoric stresses were determined by integrating the appropriate constitutive laws along the streamlines. The difficulty of using the finite element method for cone penetration problems is how to simulate the whole expansion on an initially prepared soil mesh. Teh and Houlsby (1991) combined the merits of strain path method, which correctly accounts for the steady state flow, with the FEM, which enables to compute force equilibrium. The expression for N_k derived from the strain-path finite element analysis also includes the effect of rigidity index, I_r, cone roughness, and in-situ stress.

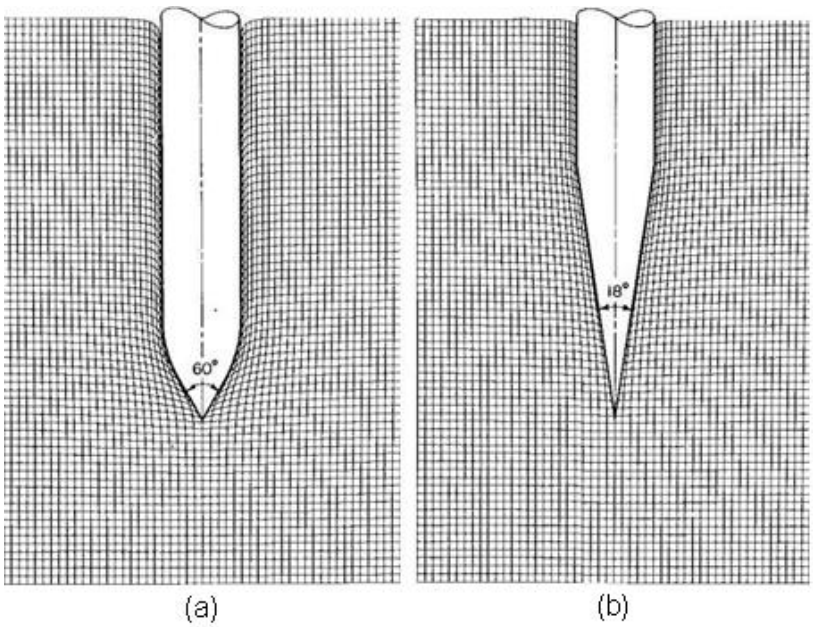

Figure 2. 5. Deformation of square grid deep CPT (undrained conditions) for cone with apex of (a) 60° and (b) 18°. (Source: Baligh, 1985)

2.4.4. Calibration Chamber Testing

Relationship between cone resistance and soil properties can be established by means large calibration chambers. The first complex chamber with measurements of boundary stress and strains was invented in Australia in 1969. Decades later, the chambers are developed in particular areas like dimensions, controlling and simulating the boundary conditions, material deposition method and capability to prepare saturated specimens. Most of them aim to investigate the cohesionless soils (sand chambers). The calibration chamber tests for cohesive soils has difficulties with instrumentation for measuring pore water pressure, achieving saturation and the preparation of large specimens. It is highly time and labour consuming process, so there are just a few calibration chamber tests for large cohesive specimens. Fig. 2.6 shows an example of the Calibration Chamber System used in the Civil and Environmental Engineering Department of Louisiana State University, USA.

Figure 2. 6. LSU Calibration Chamber System.
(Source: cee.lsu.edu)

Cone resistance obtained from the calibration chamber test may vary from the in-situ one. The reason lies in its inability to represent field boundary conditions in the calibration chamber. There can be a noticeable difference between the CPT results measured in field and chamber, depending on the dimensions of the chamber and the type of applied boundary conditions to the model. Correction factors are used to overcome this limitation. Many researchers (Parkin and Lunne, 1982, Renzi et al., 1994) have explored the influence of boundary conditions on CPT data and have determined a

diameter ratio, R_d, defined as the ratio of the chamber diameter to cone diameter. Outcome of these studies indicate that the side boundary effects depend on the relative density of the sand. For loose sand (D_r order of 30%) the side boundary effects are negligible and for denser assemblies are more rigorously described (Sharp and Dobry, 2010). However the chamber correlation obtained for one soil cannot be applied to another material.

2.5. Numerical Models of Cone Resistance

In order to understand the CPT process and its mechanism to determine soil properties from the measured cone data, it is necessary to model CPT by computer programs which can help to establish some relations among them. As mentioned before, the difficulties lie in the complicated deformation of the soil, which results from the punching of the penetrometer, as well as the complex micro behaviour. Rigorous closed form solutions are not available for penetration problems, and analyses are often based on simplified theories.

Various numerical methods have also been employed to model cone-penetration analyses. However, it is not possible to always provide straightforward correlations. Advanced numerical methods provide a better insight into penetration process. Thanks to later ones it is possible to check the factors affecting the cone resistance, and to verify empirical relations. Because cone penetration involves finite deformation of the soil and large-scale sliding at the penetrometer–soil interface, rigorous numerical modeling of it is rather difficult and various approximations are often adapted, similarly to analytical methods. Three general numerical approaches are commonly used to estimate cone penetration resistance: (1) Finite Element Method (FEM), (2) Finite Difference Method (FDM), and (3) Discrete Element Method (DEM).

2.5.1. Finite Element Method (FEM)

Many researchers applied finite element method in the analysis of cone penetration test. Nowadays, with the development of computer science, higher computational speeds and greater memory have been achieved, which led to reduced

cost of complicated analyses of penetration tests. The ability to easily implement to find any type of constitutive model, solving problems with difficult geometries, and solutions with a high degree of accuracy are valuable profits of the FEM. Moreover, soil stiffness and compressibility can be easily moulded, initial stresses may be applied, increases in stress, including pore water pressure, during the penetration can be accurately determined, failure modes do not need to be adopted, both equilibrium equations and yield criterion are satisfied, and variety of constitutive models can be utilized. In granular materials, cone penetration test can be modelled by pre-placing a penetrometer in the soil model with a borehole (De Borst and Vermeer, 1984), or by using contact elements to capture large-scale slipping at the penetrometer-soil interface (Huang et al., 2004).

However, CPT modeling by the finite elements has so far been plagued by very large mesh distortion in zones of high strain concentration around the cone tip. In contrary to the bearing capacity theory or the cavity expansion theory, the cone resistance is affected by deformation properties, such as; shear modulus, G and angle of dilation, ξ. It demonstrates a difference in actual deformation pattern around a cone from the previously mentioned methods. When penetration distances are large, mesh distortion leads to a severe loss of accuracy, a reduction in the stable time increment and numerical divergence. Furthermore, the inherent CPT geometry and the boundary condition along the center line below the CPT makes modeling more complicated.

2.5.1.1. Applications of the FEM in the CPT Analysis

The finite element analysis of the cone penetration in cohesionless soil by Huang et al. (2004) is a good example of attempt of using finite element method in the penetration tests in granular soils. By means of modeling finite strain in the soil material and large scale sliding at the CPT–soil interface, enabled them to achieve realistic results. The study was carried out using commercial software ABAQUS, which uses the concept of master and slave surface. Soil was assumes to be a perfect elasto-plastic medium obeying the Mohr–Coulomb criterion. Mesh of the FEM model designed by Huang et al. is shown in Fig 2.7. The grids are so designed that the items potentially in contact with the penetrometer which has the size of about 1/3 of the penetrometer radius. It was observed that there is no significant influence on the numerical results

with increase in the element sizes, both horizontally and vertically from the penetrometer. As a result of this analysis, the deformation pattern of the soil around the cone, as well as the plastic zone has indicated that it was similar to that caused by cavity expansion and it can be comparable with empirical correlations based on cavity-expansion.

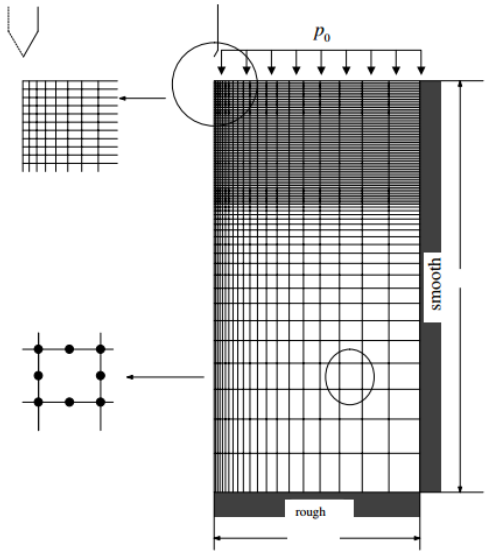

Figure 2. 7. Finite element mesh.
(Source: Huang et al., 2004)

Kumar et al. (2010) has improved the Huang et al. model of CPT in dried cohesionless soil by adapting a software package, which enables both automatic re-meshing and relatively coarse mesh. They have investigated the influence of friction and dilation angles on cone tip resistance and sleeve friction in dry sand using ABAQUS software too. The non-associative isotropic elastic perfectly plastic sand behaviour and rigid-plastic frictional cone-sand interaction was assumed in the model. In this study, extreme distortion of granular material around the cone was solved with auto-adaptive remeshing. In Figure 2.8 this is depicted how the FEM model was built.

Axisymmetric rigid line elements were used to model the rigid surface of the cone and further field conditions were constructed by constraining the displacements normal to the boundary to be zero. At the beginning, the cone was placed within a conical notch at the top surface of the soil (detail A in Fig. 2.8). Analytical results have revealed that friction and dilation angles highly influenced normalized cone tip

resistance and the relationships depend on lateral earth pressure. From the other hand, friction ratio was only strongly influenced by friction, but weakly by dilation angle.

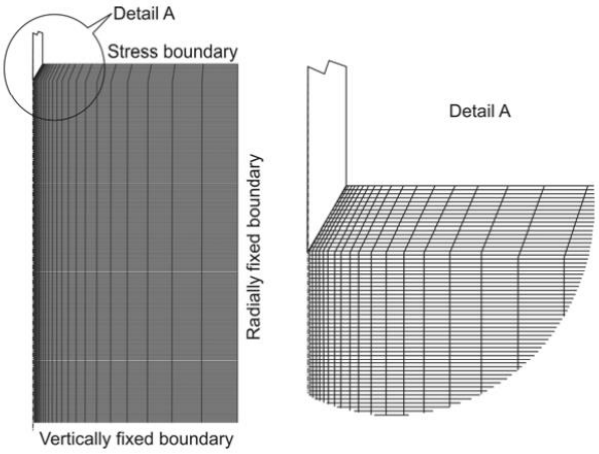

Figure 2. 8. FE model at initial configuration.
(Source: Kumar et al., 2010)

2.5.2. Finite Difference Method (FDM)

Finite difference method is also used to solve problems related to cone penetration tests. Numerical solution method is based on solving governing differential equations, including the Navier-Stockes flow equations (Roache, 1976). During the research study of Cee-Ing (1987), the overall solution algorithm of solving the particular forms of finite difference equations was presented. Similarly to FEM, choice of proper mesh for calculation was crucial dilemma. In order to obtain meaningful results, it is fundamental to look for various aspects of the numerical analysis. The modeller need to take into account the infinite extent of the fluid medium and it requires sufficiently large boundary, so that mesh can be in greater distance from the cone. Usually non-uniform mesh is chosen as shown in Figure 2.9.

For case of correct solution for the numerical algorithm, the finite difference equations must be in agreement with the partial differential equations. Usually numerical scientists make use of two methods: second upwind differencing and the Dufort-Franke's substitution to arrive to correct solution. Moreover, as those equations are determined primarily by boundary conditions, the proper choice of them is necessary to obtain a satisfactory solution.

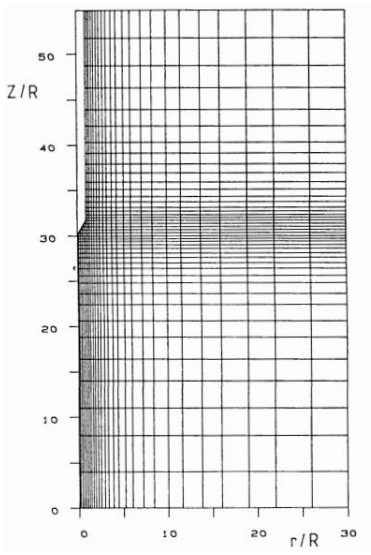

Figure 2. 9. Finite Difference mesh for CPT model.
(Source: Cee-Ing, 1987)

2.5.2.1. Applications of the FDM in the CPT Analysis

Finite difference analysis by Palla et al. (2012) is a proper example of work on the CPT. They have analyzed interaction between cone and surrounding soil using FLAC2D (Fast Lagrangian Analysis of Continua in two-dimensions by Itasca, 2009). Figure 2.10 shows a mesh of the soil-cone system used in the analysis. In this study, five different soil conditions ranging from very stiff to very soft were investigated for selected three cone positions. As result, cone displacements were obtained for each case condition. Simultaneously, graphical relations of undrained cohesion (c_u) vs. blow count (NTCP) were developed and showed that those parameters were depth dependent.

Ahmadi et al. (2005) also have performed the numerical analysis by FLAC. They proved that with the capability of the FDM program, CPT can give realistic solutions also in layered soils. The Mohr-Coulomb elasto- plastic model was assumed in this problem. Shear and bulk modulus were used in analysis and they were determined from the calibration chamber tests on the Ticino sand. For the numerical model, the axisymmetric configuration was used for simulating the penetrating process realistically. Because of existing large strain, the proper option for this phenomenon was used as well as the soil elements (grids) were suitably located. As a result of the study of Ahmadi et al. (2005), the numerical prediction of q_c obtained by suggested by them approach was in good agreement with the experimental values in the calibration

chamber with assigned boundary condition and a wide range of relative densities, vertical as well as horizontal stresses, and OCR ratios. Their analysis proved that FDM can be used for characterization of soil stratigraphy, evaluation of engineering properties and for estimating the cone penetration resistance.

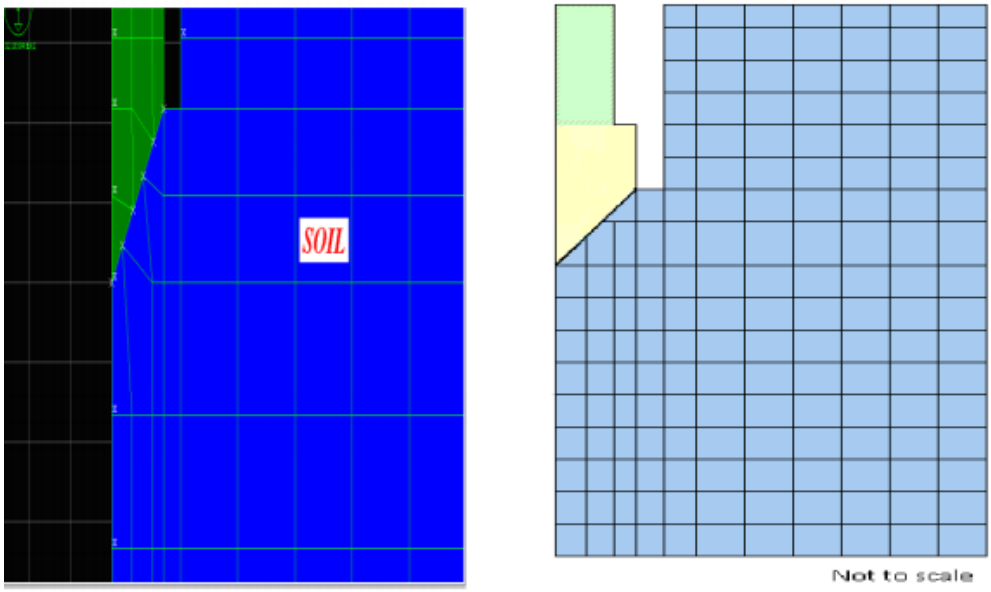

Figure 2. 10. Finite Difference mesh for Cone Penetration.
(Source: Palla et al., 2012)

2.5.3. Discrete Element Method (DEM)

Discrete element method, which isalso so called distinct element method, is recently becoming more and more popular for the cone penetration analysis. It is proven to have numerous advantages over other numerical approaches like FEM or FDM. For instance, the DEM offers a particle-to-particle interaction mechanism which enables more microscopic analysis of soil material to be done. Moreover, the DEM can be coupled with other numerical methods to solve various application problems including flow in ground, liquefaction (only 3D analysis), permeability etc. The fundamentals of the method, as well as its applications in geomechanics, pros and cons, key problems in 2D modeling, available DEM software with a detailed description of the PFC2D – a DEM software which is used in this thesis.

2.5.3.1. Applications of the DEM in the CPT Analysis

Arrayo et al. (2011) have created a three-dimensional model based on the discrete-element method. Commercial software PFC3D was implemented in this study. The model of CPT is depicted in Figure 2.11. They have used some physical experiments to calibrate and validate their DEM model. Triaxial tests were conducted to find material properties fitting to Ticino sand which was used in the laboratory CPT tests. Cone/chamber size effects were found to have a substantially significant influence on the cone penetration resistance. They have found factors which enable to correct the CPT results. The corrected q_c, obtained from the so called virtual calibration chamber CPTs showed good quantitative agreement with the correlations that recapitulate previous physical results.

Bultanska et al. (2013) has investigated homogeneity and symmetry in DEM models of the CPT. PFC3D was chosen to simulate the discrete analysis. The 3D model was used to examine effects of symmetry on the CPT results. The model was calibrated by laboratory experiments on the Ticino sand. The full, half and quarter calibration chambers were used for those simulations. Observations of homogeneity were done by two methods. First one was visual observation of the network of contact forces between particles. Second method for examination of homogeneity was done by examination of porosity, d_{50} and c_u distributions inside the samples by means of representative elementary volume (REV).

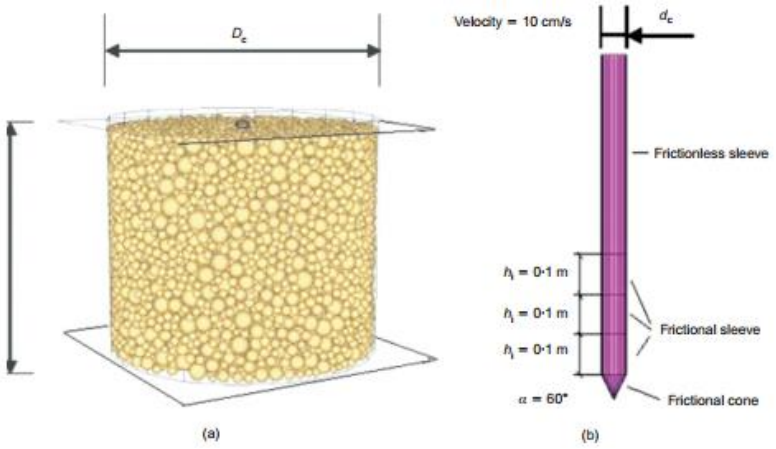

Figure 2. 11. View of the DEM model components with indication of the main relevant dimensions: (a) calibration chamber; (b) cone penetrometer. (Source: Arrayo et al., 2011).

Jiang et al. (2006) presented a numerical study on deep penetration mechanisms in granular materials with the focus on the effect of soil–cone interface friction. A 2D DEM model has been developed to carry out the CPT simulations under an amplified gravity with a K_0 lateral stress boundary conditions. Mohr–Coulomb friction law was also incorporated. In Figure 2.12 penetration process and modelled assembly is depicted. Colourful 'grids' helped to investigated displacement paths. A complex displacement path in the soil near penetrometer was detected after deep penetration using numerical software. What is more, the soil sustains an evident loading and unloading process and a rotation of principal stresses are as large as 180^o. It was also observed that the penetration leads to significant changes in displacement and velocity fields, as well as the value and direction of stresses. Soil–penetrometer interface friction had significant effects on the actual various penetration mechanisms. Several kinds of failure mechanisms were found. In conclusion, researchers have found that the soil of large deformation may reach a stress state slightly over the strength envelope obtained from conventional compression tests.

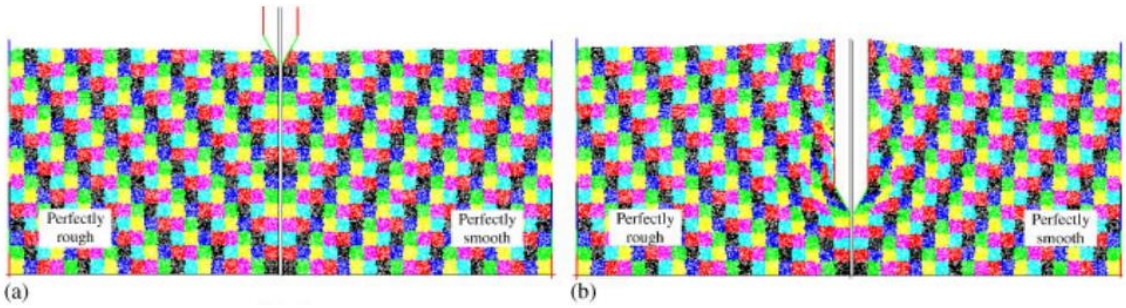

Figure 2. 12. DEM model (a) before and (b) after penetration.
(Source: Jiang et al., 2006)

CHAPTER 3

LABORATORY EXPERIMENTS - CPT and TRIAXIAL TESTS

3.1. Introduction

Laboratory tests were conducted in order to determine the basic index properties of the soil. Tested soil was used in the consolidated drained triaxial and cone penetration tests to calibrate a 2D distinct element model (DEM). Calibration includes both physical parameters as well as porosity which is one of the biggest limitations of two-dimensional DEM modeling.

In this chapter, first, the basic soil properties were determined by means of various laboratory experiments. Tests were briefly described and the basic properties of the soil were presented. Next, triaxial test is explained, including the test procedure and influence of sample's preparation method on specimen's uniformity. Finally, cone penetration test (CPT) conducted at Civil Engineering Laboratory at IZTECH were described. CPTs were conducted inside the laminar box which was subjected to subsequent shakings as well as at the initial state after filling process. Moreover, special attention was given to the laminar box dimensions, specimen preparation and boundary conditions.

3.2. Scanning Electron Microscope View of Soil

A scanning electron microscope (SEM) is a type of electron microscope that produces images of a sample by scanning it with a focused beam of electrons. The basic concept is that the electrons interact with atoms in the sample, producing various signals that can be detected and that contain information about the sample's 3D surface topography and composition.

SEM was performed at the Material Research Center (MAM) at IZTECH. Soil samples were magnified at different pressures to obtain pictures with scales: 1 mm, 500 μm and 200 μm. These images are illustrated in Figures 3.1-3.4. In general, the soil that

was used in the triaxial and shaking table tests had sub-rounded particles however some particles were angular as it is visible at 3.1-3.3(b) .

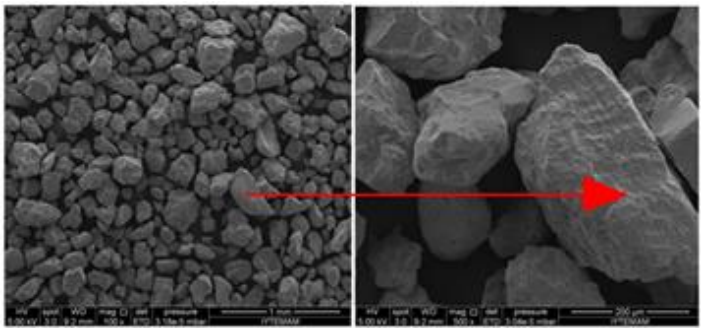

(a) (b)

Figure 3. 1. SEM images of sand tested in laboratory experiments (a) aggregate and (b) detail.

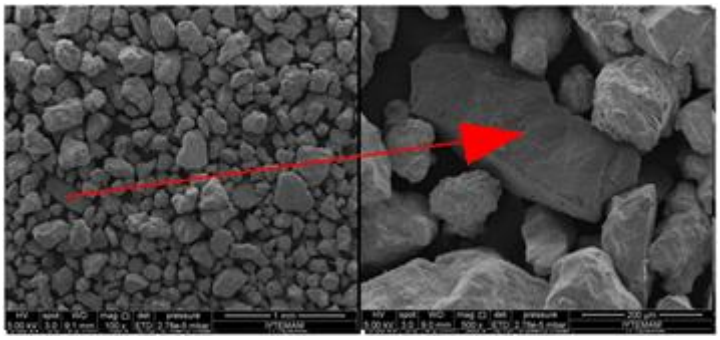

(a) (b)

Figure 3. 2. SEM images of sand tested in laboratory experiments (a) aggregate and (b) detail.

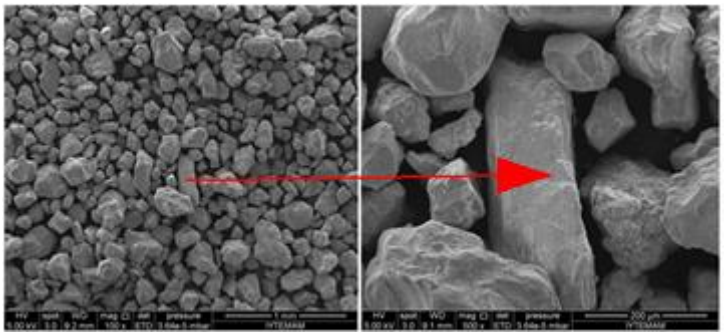

(a) (b)

Figure 3. 3. SEM images of sand tested in laboratory experiments (a) aggregate and (b) detail.

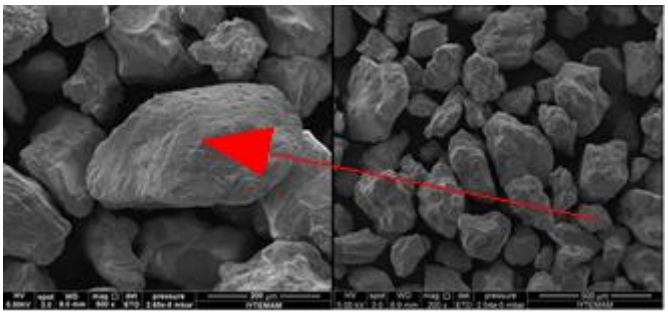

(a) (b)

Figure 3. 4. SEM images of sand tested in laboratory experiments (a) detail and (b) aggregate.

3.3. Tested Soil Characteristic

In general, the soil sample used in the laboratory experiments was uniform, river clean quartz sand, which was similar to Ottawa sand. It is very common to adapt this soil in experimental and numerical research, because individual sand particles are very uniform in size. Therefore, the behavior of this material can be modelled as a group of uniformly sized spheres and considered theoretically. As tested sand has properties close to well known reference material – Ottawa sand, it offers very useful advantage to simplify numerical DEM simulations and shortens computation time.

Laboratory tests were conducted in order to determine the main properties of soil which was used in the CPT and triaxial tests. Laboratory tests, which were conducted in the scope of this research objective were:

1. sieve analysis,
2. hydrometer tests,
3. specific gravity tests (G_s),
4. maximum and minimum void ratio tests (e_{max} and e_{min}),
6. constant head permeability tests (k).

3.3.1. Sieve Analysis and Hydrometer Test

In order to identify the basic index properties and gradation of investigated in laboratory soil, which is going to be reproduced in numerical simulations, a sieve analysis was performed. Hydrometer test was also done in order to determine the

distribution of the fine particles. Both tests were conducted according to ASTM D422. Sieves column on the mechanical shaker used in the experiment is shown at Figure 3.5 (a) and control cylinder and hydraulic stem is depicted in Figure 3.5(b). Results of the sieve analysis are presented at Figure 3.6.

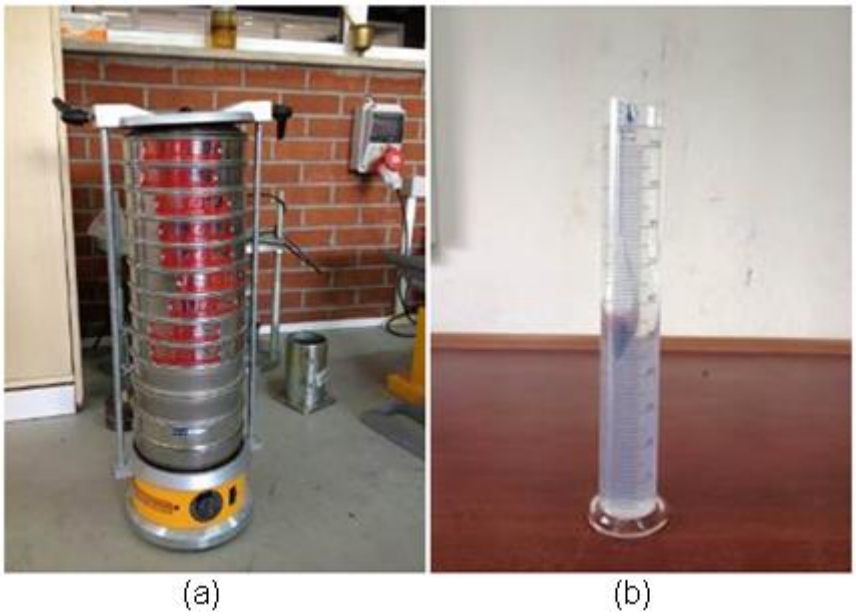

Figure 3. 5. Sieves column on the mechanical shaker, (b) control hydraulic stem.

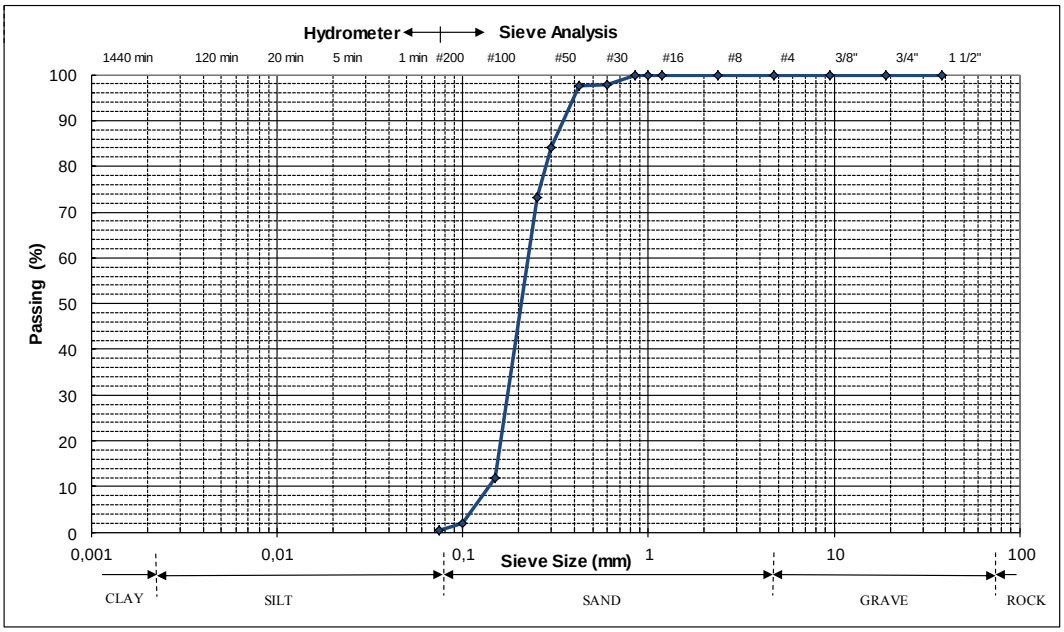

Figure 3. 6. Sieve analysis and hydrometer test results.

Besides obtaining a grain distribution, the effective size, the uniformity coefficient and the coefficient of gradation were determined. Uniformity coefficient (C_u) and coefficient of curvature (C_c) were computed as follows:

$$C_u = \frac{D_{60}}{D_{10}} \tag{3.1}$$

$$C_c = \frac{(D_{30})^2}{D_{60} x D_{10}} \tag{3.2}$$

where,

D_{10} = diameter through which 10% of the total soil mass has passed (the effective grain size);

D_{30} = diameter through which 30% of the total soil mass has passed;

D_{60} = diameter through which 60% of the total soil mass has passed.

Table 3. 1. Results of the sievie analysis.

D_{10} [mm]	**D_{30}** [mm]	**D_{60}** [mm]	**C_u** [-]	**C_c** [-]
0.15	**0.17**	**0.23**	**1.53**	**0.84**

Table 3.1 summarizes the outcomes. The results are found as follows: C_u = 1.53 and C_c = 0.84. In accordance with the Unified Soil Classification System (USCS) tested soil is poorly graded sand (SP) because it didn't meet both of the criteria for well graded sand which are as follows:

1. $C_u \geq 6$
2. $1 < C_c < 3$

3.3.2. Specific Gravity

The ASTM D 854-00 standard test method was used to determine the specific gravity. Specific gravity is the ratio of the mass of unit volume of soil at a stated temperature to the mass of the same volume of gas-free distilled water at a stated temperature. For this test, equipment included pycnometer, balance, vacuum pump,

funnel and spoon are shown in Figure 3.7 and the testing procedure is explained in ASTM D 854-00. The pycnometer with distilled water was filled and weighted (W_A). Weight of the empty pycnometer was called (W_P). Next, in pycnometer of 100ml, 10gr dry soil sample (W_0) which passed through the #200 sieve was placed inside and filled with distilled water up to 1/3 height. Then the entrapped air was vacuumed by placing a pycnometer inside the desiccator. After pycnometer was taken from desiccator, they are filled with distilled water and weighted again (W_B). Specific gravity is computed as follows:

$$G_S = \frac{W_0}{W_0 + (W_A - W_B)} \tag{3.3}$$

where,

W_0 = weight of dry sample;

W_A = weight of pycnometer with distilled water;

W_B = weight of pycnometer, distilled water and soil sample.

Figure 3. 7. (a) Desiccator and Vacuum Pump, (b) Pycnometer, Distilled Water and Weighting scale (Left to Right).

G_s was found to be equal to 2.65 in all five samples which were tested.

3.3.3. Maximum and Minimum Void Ratio Tests

The ASTM D 4253 test procedure was used to determine the maximum void ratio (e_{max}) and the ASTM D 4254 standard test method was used to determine the minimum void ratio (e_{min}).

(a) (b)

Figure 3. 8. (a) Mold and weight, (b) The mold attached to the vibrating table.

Procedures for both the maximum and the minimum void ratio tests start with the calibration of the mould and with the preparation of the sample. For e_{min}, the mould was weighted accurately and dry material was poured into the mould through a funnel in a steady stream. The free fall height of soil particles was always 25 mm, due to adjustment of spout. The procedure was continued to fill up the mould with soil up to about 25mm above the top. Then it was levelled, with the soil and weight was recorded. For e_{max}, the mould was filled with the oven dried soil sample till ½ or 2/3 of the collar. Then, the mould was placed on the vibrating deck as in Fig. 3.8(b), and the mould was fixed to the table with nuts and bolts check. Next, the surcharge weight was placed on the mould and the table was allowed to run under vibrations for 8 minutes. After this process, the mould was weighted again with soil. Results are gathered in Table 3.2.

Table 3. 2. Maximum and minimum void ratio tests results.

maximum void ratio [-]	minimum void ratio [-]
0.8	0.6
Corresponding porosity [-]	Corresponding porosity [-]
0.440	0.375

3.3.4. Constant Head Permeability Test

The constant head permeability test is used to determine the coefficient of permeability (k) of coarse sands (ASTM D2434 – 68) This test is performed since the pore openings are large and hence high permeability occurs ($k > 10^{-4}$ cm/s).

A total of 14 constant head permeability tests at different relative density were taken into acount, while creating the relationship for this particular sand. Relative density considered in these tests ranged from 0% to 85%. As shown in the Figure 3.9, it is observed that the coefficient of permeability is decreasing with increasing D_r. The function which accurately approximate the relationship of k and D_r is $k=0.0289e^{-0.027Dr}$ [cm/s]. R-squared value was found as 0.94.

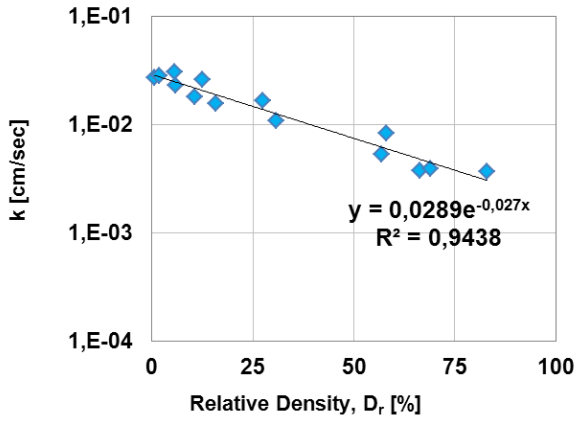

Figure 3. 9. Coefficient of permeability (k) at different relative densities (D_r) for tested soil.

The coefficient of permeability was found between $4x10^{-3}$ cm/s – $3x10^{-2}$ cm/s for investigated range of relative density. According to Kulhawy and Mayne (1990), the tested soil falled within the framework of medium degree of permeabilty which charatcterize soils including sandy gravel, clean snd fine sand as shown in Table 3.3.

Table 3. 3. Coefficient of permability in diffeernt soils.
(Source: Kulhawy and Mayne, 1990)

Soil	Coefficient of permeability k (cm/s)	Degree of permeability
Gravel	Over 10^{-1}	High
Sandy gravel, clean sand, fine sand	10^{-1} to 10^{-3}	Medium
Sand, dirty sand, silty sand	10^{-3} to 10^{-5}	Low
Silt, silty clay	10^{-5} to 10^{-7}	Very low
Clay	Less than 10^{-7}	Practically impermeable

3.4. Triaxial Test

The triaxial test (TX) is one of the most universal and commonly performed geotechnical laboratory tests, allowing the shear strength and stiffness of soil and rock to be determined for geotechnical design practice (ASTM D7181- 11). It is described more precisely by Bishop and Henkel (1962) in their specific book on measurement of soil properties in triaxial tests.

Its main benefit is that, it is relatively simple to perform and what is more, large strain levels can be obtained. On the other hand, the triaxial cell can also be used for the measurement of very minor strains by using specified gauges, and the investigation of the non-linear characteristic of soil materials can be studied. Further advantages over more facile procedures, such as the direct shear test, include the ability to control specimen drainage and take measurements of pore water pressures. The main disadvantage is due to the fact that the mean effective stress can be consider either vertically (α=0°, which depicts compression) or horizontally (α =90°, which leads to extension). Thus, it is impossible to obtain the angle α value between 0° and 90° and the intermediate mean stress is always simplified and assumed to be equal to the triaxial cell pressure. Haythornthwaite (1970) claimed that although in literature is generally assumed that homogenous state of stress is produced in the TX specimen, the reality is more complex and influenced by many factors. He was perhaps the first contributor, who noticed the boundary conditions' limitations in the TX. Pressure distribution is not given as a boundary condition, but only the total thrust on the end of platens. Even assuming circular symmetry and similarity of conditions on each normal cross-section, there are still three unknown stresses b_r b_θ and b_z with only two equilibrium equations:

$$\frac{d\sigma_r}{dr} + \frac{\sigma_r - \sigma_\theta}{r} = 0 \tag{3.4}$$

$$\frac{d\sigma_z}{dz} = 0 \tag{3.5}$$

However, with the constant and rapid development of technology, there are already available triaxial testing systems which can simulate desired soil conditions more realistic. For instance, the GDS True Triaxial Apparatus can control all three principal stresses independently, rather than just two in a conventional triaxial system.

Thanks to this amelioration it is possible to obtain wider scope of complex stress paths to be performed.

Primary parameters obtained from the TX test may include the angle of shearing resistance φ, cohesion c, and undrained shear strength C_u, although other parameters such as the shear stiffness G, compression index C_c, and permeability k, may also be determined indirectly.

Overall, triaxial apparatus is perhaps the most widely used geotechnical laboratory equipment to extract fundamental material parameters for a variety of soil types under drained or undrained conditions.

3.4.1. Triaxial Test Apparatus

This review is focused on the triaxial apparatus for the strain-controlled monotonic tests of the cylindrical shape of specimens (50 mm in diameter and 100 mm in height). This apparatus basically consists of a cell, loading devices, and measurement devices. The lucid acrylic or transparent Plexiglas cell is preferably used, so that the behaviour of specimen during the test can be observed from outside of the cell. Servomotor is a loading device of the conventional triaxial apparatus for monotonic shear. The vertical load, total and small displacements, cell pressure, pore water pressure, and drainage water volume are constantly measured during experiments. The general set-up of a soil specimen inside a triaxial cell is shown at Fig. 3.10(a). Main functions of the most important components of conventional triaxial test apparatus are gathered in Table 3.4 (www.gdsinstruments.com).

A cross section of a conventional triaxial apparatus is schematically shown in Figure 3.12. It incorporates a cylindrical soil sample which has a diameter of 50 mm. The sample is enclosed within a thin rubber membrane and mounted between rings end platens. For better sealing of the membrane, rubber O-ring seals are placed at the top and bottom platens. It enables to radial deformation of the cell pressure sample. Besides, further function is to separate pore pressures generated inside the sample from total radial stresses opposed to the outside of the sample by means of hydrostatic Pressure which is applied by means of an enveloping fluid. The sealed sample is placed on a pedestal in a water-filled cell. An all-around cell pressure (σ_c) applies radial total stress (σ_r) to the vertical sides of the sample and a uniform

vertical stress to the top rigid platen, as shown on Figure 3.10(b). An additional axial force, F_a, is applied to the top platen via a loading frame. There is two commonly used ways of measuring pore pressure. By using the first method, it can be measured in the end platens adjacent to the bottom and/or top end of the sample, or by a probe placed at approximately mid-height of the sample.

Table 3. 4. Main components of conventional triaxial system.
(Source: www.gdsinstruments.com)

Component	Main function
Triaxial cell	House the specimen and cell fluid
Pedestal & top-cap	Provide specimen seating and drainage ports
Rubber membrane, O-rings & porous discs	Seal the specimen from the cell fluid, allowing control over the effective stress and drainage
Cell pressure / volume controller	Apply confining stress to the specimen ($\sigma_c = \sigma_3$) by pressurising the cell fluid
Back pressure / volume controller	Apply back / pore pressure u to the specimen and measure volume change ΔV
Velocity–controlled load frame	Shear the specimen through axial movement of a loading platen at a constant rate
Internal submersible load cell	Measure the change in axial load F applied to the specimen during shear
Pore water pressure (PWP) transducer	Measure the change in pore water pressure u within the specimen
Axial displacement transducer	Measure the change in height (and hence axial strain ε_a) of the specimen
Data acquisition unit	Convert analogue readings from the load cell, PWP and axial displacement transducers to digital data
GDSLab control & acquisition software	Control test hardware and record digital readings taken from the data acquisition unit

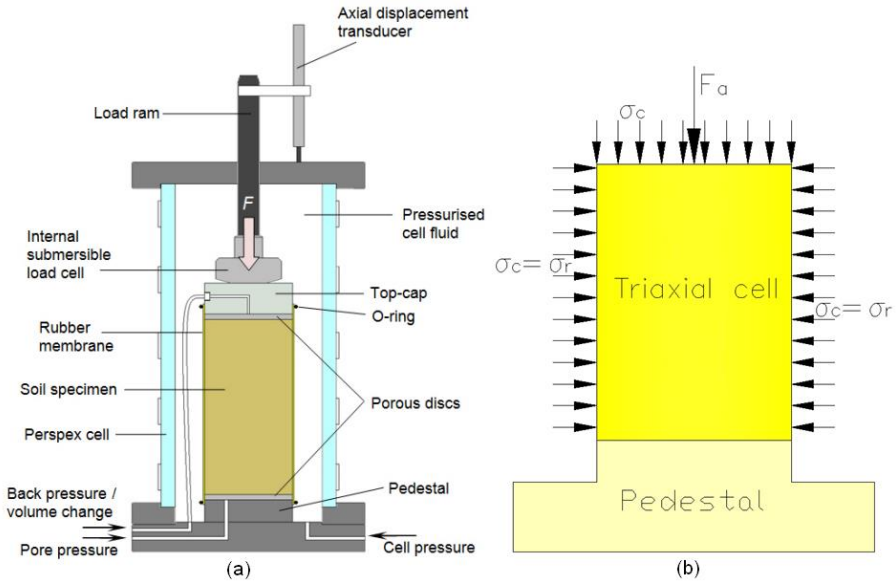

Figure 3. 10. (a) General set-up of a soil specimen inside a triaxial cell (b) scheme of triaxial test apparatus. (Source: (a) www.gdsinstruments.com)

This apparatus still occupies one of central positions among the devices constructed to measure the strength of soil, because of its multifunctionality. It allows performing several different tests by making use of the triaxial apparatus, the most common of which are as follows;

- one-dimensional compression (similar to oedometer conditions)
- isotropic compression
- drained or undrained shearing

depending on the stress scenario and the conditions desirable to be applied.

3.4.2. Specimen Preparation for the Triaxial Test

Many researchers throughout the history have noticed the importance of specimen preparation techniques (Juneja and Raghunandan, 2010; Monkul, 2010). In this thesis, an overview of specimen preparation methods for silty sands and sands is in general presented.

Moist tamping, dry funnel deposition, slurry deposition, dry air pluviation are one of the most often employed deposition methods for sands and silty sands in the engineering practice. We can observe a huge influence of those various methods on the tested soil behaviour, which either needs to simulate in-situ soil conditions or will be

used for the numerical analysis and in the calibration of the model. Own creep of coil, aging effects and other specific characteristic of soil deposit are beyond of the scope of this study, while reconstituting samples is the main objective.

a) Moist Tamping (MT)

Moist tamping is a commonly used method for granular soil preparation. Various critically assessed researchers explained details of this method, including Ladd (1978) and Frost and Park, (2003). Among other methods, moist tamping has the advantage that it is relatively easy to control the global specimen density to be achieved, even for loose specimens, and it is possible to achieve a wide range of densities. However using moist tamping for silty sands and sands has been subjected to some criticism, because it yields less uniform specimens (Ishihara, 1993, Vaid et al., 1999). Frost and Park (2003) critically assessed MT by measuring the forces applied during the tamping process and investigated the homogeneity of the samples prepared using quantitative analysis by both X-ray and optical image methods. Generally, densification (obtaining greater density) of the specimens is achieved by adjusting the moist weight of the soil required for each layer. As the name of the method implies, layers are formed by tamping. Dennis (1988) has distinguished two methods: equal-volume and equal-energy methods. He concluded that samples prepared using equal-volume method were more resistant to any volume change when subjected to a confining vacuum, prior to removal of the mold than those prepared by using equal-energy technique. Specimen deposition method influenced the slope of the steady state line for stressed controlled loading, though its effects for strain-controlled loading were minor.

b) Slurry Deposition (SD)

Slurry deposition (SD) is another common specimen preparation method for granular suggest materials. Kuerbis and Vaid (1988) presented a SD method of preparing homogeneous samples of well graded and silty sands and found that the method yields homogeneous saturated samples that are easy to replicate and possess fabric similar to that of hydraulic fills, compared to moist tamping. Since water pluviation results in segregation of well graded and silty sand, the proposed method provides a practical method of fundamental study to see undrained behaviour of these

liquefaction prone materials. Recently, Polito and Martin II (2003) confronted the moist tamping method with slurry deposition method through a limited number of tests. Although the specimens prepared by the slurry deposition method had relative densities two times greater than specimens prepared by moist tamping, the cyclic resistance of the samples prepared by the slurry deposition was close to the half of that prepared by moist tamping method. Murthy et al. (2007) reported that moist tamped specimens had considerably larger initial peak principal stress difference (q_{peak}) than slurry deposited specimens.

Densification of the specimens is performed via mechanical vibrator or soft hammer. Details of the densification method are well explained in the studies of Kuerbis and Vaid, 1988.

c) Water Sedimentation (WS)

Different water sedimentation (WS) procedures for sands and silty sands have been mentioned in the literature with two main behviour. Vaid at al., 1999 preferred to involve depositing dry soil through water, while others (Yamamuro and Wood, 2004) used methods of depositing pre-saturated soil through water. As a method of densification of the specimens Vaid et. al. (1999) suggested tapping the base in contrary to Huang and Huang (2007) who adviced tapping the side of the mould by a soft hammer.

d) Air Pluviation (AP)

Multiple air pluviation techniques have been proposed in the literature for sands Vaid et al. (1999), Wood et al. (2008), Monkul and Yamamuro (2010) discussed them in detail. Thevanayagam (1998) prepared soil samples by the dry air pluviation method. First, one-fourth of the mold was filled with the material and it was approachable compacted by tamping, until reaching a desired target void ratio. The most approachable method is to rain the soil through a dispersing screen down a tube with an equivalent inside diameter as the split mold. Densification of the specimens can be performed either by tapping (Vaid et. al., 1999) or tamping of multiple deposition layers (Thevanayagam, 1998) or decreasing the deposition rate (Monkul and Yamamuro, 2010).

e) Dry Funnel Deposition (DFD)

Dry funnel deposition is also a common specimen preparation method for silty sands (Ishihara, 1993). Densification of the specimens was essentially achieved by tapping. After the funnel containing silty sand was carefully raised along the axis of symmetry, the split mold was gently tapped in a symmetrical pattern (Lade and Yamamuro, 1997). Later, Wood et al. (2008) named this technique as tapped funnel deposition (TFD) and started to prepare specimens by raising the funnel faster, which require less tapping and named as fast funnel deposition (FFD) method. Sitharam and Dash (2008) used multi layer deposition with different densities and tapped the mold for each layer, separately to achieve a uniform density at the end.

3.4.3. Experimental Procedure

Triaxial tests were performed in geotechnical laboratory at Ege University. A sample size of 50 mm x 100 mm was tested in digital triaxial apparatus under drained conditions. Laboratory tests were conducted in accordance with the ASTM D7181-11 Standard Method for Consolidated Drained Triaxial Compression Test for Soils. For the initial confining stress of 100 kPa and 200 kPa and formed with relative density of 30%. The general procedure typically consists of four main steps: (1) specimen and system preparation, (2) saturation, (3) consolidation, and (4) shearing. These stages are explained below.

(1) Specimen and System Preparation

The specimen was prepared from the soil which was used in all CPT tests and was investigated before through many laboratory tests to learn the basic index properties of the tested soil. Then the specimen, prepared from a sample of soil was placed into the triaxial cell. The moist tamping method was chosen as a most suitable technique for tested soil. For granular soils it was necessary to prepare the specimen directly on the pedestal using a split-part mould. Disturbance to the specimen was kept to a minimum during preparation. Next, the triaxial cell and other system components are assembled.

Following the assemblage of triaxial test components, the cell was filled with fluid. Pressure-volume controllers were connected and transducer readings set as required.

(2) Saturation

The saturation process was obligatory to ensure all voids within the test sample were filled with water. Also it was checked if the pore pressure transducer and drainage lines were properly de-aired. Specimen saturation was obtained by increasing back pressure in the triaxial cell. During the process depicted in Figure 3.11(a), a constant effective pressure should be achieved. Skempton's pore pressure parameter, B-value was utilized to ensure of the degree of specimen saturation. Skempton (1954) proposed the following equation to describe B-value:

$$\mathrm{B-value} = \frac{\Delta u}{\Delta \sigma_3} \tag{3.6}$$

where,

Δu = change in pore water pressure;

$\Delta \sigma_3$ = change in minor principal stress.

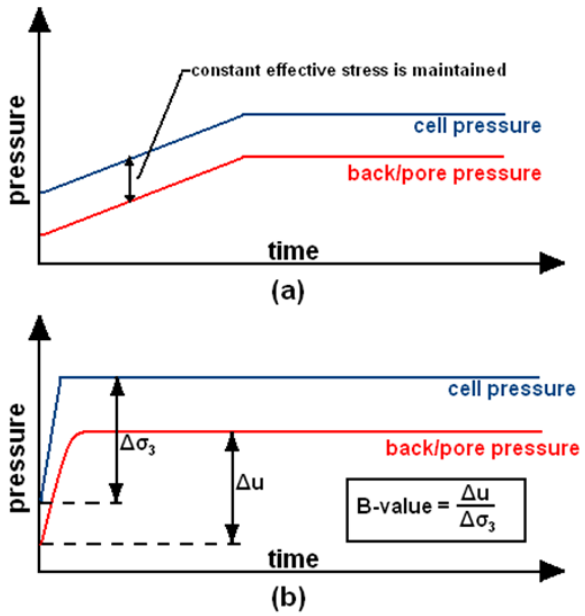

Figure 3. 11. Saturation stage (a) increasing back pressure in the triaxial cell, (b) confirmation of specimen saturation by B-check.

Determination of the B-value is necessary. B-check requires specimen drainage to be closed and at the same time the cell pressure is increased by approximately 50 kPa. It is shown in Figure 3.11(b). Pore-pressure coefficient B needs to be sufficiently high before moving to consolidation stage. It is commonly accepted to keep the value of B bigger or equal to 0.95. B is a soil dependent parameter and some soils are in the fully saturated state although B-value is around 0.91, like in the case of very dense sand and stiff clay. Figure 3.12 shows the B-check process for tested soil for both initial confining stress values used. In Table 3.5 cell and back pressure increments which allowed achieving the final B-value are gathered.

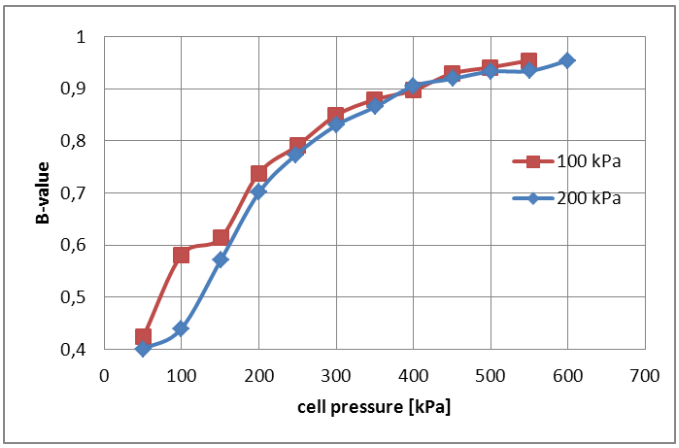

Figure 3. 12. Saturation stage for the tested soil in the traixial test for both initial confining stress values.

Table 3. 5. Steps to achieve a proper saturation degree for the triaxial test at 100 kPa and 200 kPa confinement.

100 kpa			
Saturation Method	Back Pressure Increments	**Cell Increments**	39.6,58.6,52.0,50.2,49.3,50.0,50.1,49.8,50.7,46.4,25.5,kPa
Final Cell Pressure	549.9kPa	**Back Increments**	31.3,48.4,51.1,48.0,52.0,48.3,49.8,49.8,51.3,49.6,kPa
Final Pore Pressure	528.2kPa	**Final B-Value**	0.954
200 kPa			
Saturation Method	Back Pressure Increments	**Cell Increments**	50.5,48.7,51.1,50.2,49.8,50.3,49.8,49.8,50.9,49.0,50.2,50.3,kPa
Final Cell Pressure	600.3kPa	**Back Increments**	28.8,48.3,53.7,48.4,49.8,50.9,50.1,50.0,50.6,49.4,50.6,kPa
Final Pore Pressure	571.9kPa	**Final B-Value**	0.954

(3) Consolidation:

The consolidation stage was performed to bring the specimen to the effective stress state required for shearing. It was conducted by increasing the cell pressure, whilst maintaining a constant back pressure as shown in Figure 3.13. This process is continued until the volume change ΔV has stabilized, and at least 95% of the excess pore pressure has dissipated. In Table 3.6, the final specimen properties before shearing are shown, including the final pore water pressure and the final effective pressure.

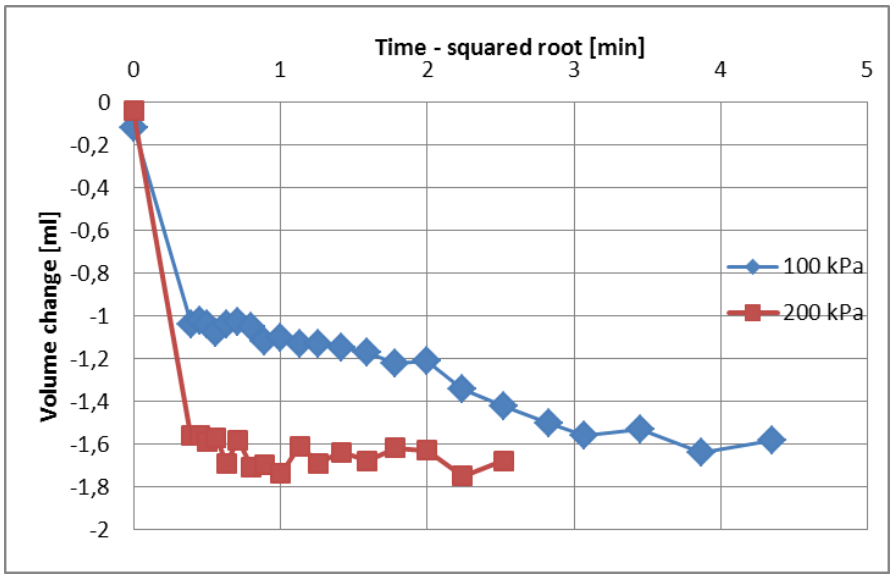

Figure 3. 13. Consolidation results of the test specimen for both initial confining stress values used.

Table 3. 6. Steps to achieve a proper consolidation level in the triaxial test at 100 kPa and 200 kPa confinement.

100 kPa			
Cell Pressure	579.7kPa	**Back Pressure**	479.8kPa
Effective Pressure	99.9kPa	**Final Pore Pressure Dissipation**	99.60%
Final Pore Pressure	480.1kPa	**Time to 50% Primary Consolidation**	0.00 Min
Dry Unit Weight	14.35 kN/m3	**Cross sectional Area after consolidation (Method A)**	1953.71 mm2
Void Ratio	0.78	**Saturation**	134.2%
200 kPa			
Cell Pressure	730.4kPa	**Back Pressure**	530.6kPa
Effective Pressure	199.8kPa	**Final Pore Pressure Dissipation**	104.19%

Final Pore Pressure	523.6kPa	**Time to 50% Primary Consolidation**	0.00 Min
Dry Unit Weight	14.12 kN/m3	**Cross sectional Area after consolidation (Method A)**	1974.37 mm2
Void Ratio	0.78	**Saturation**	129.5%

(4) Shearing:

The soil was sheared by applying an axial strain (ε_a) to the test specimen at a constant rate through upward (compression) movement of the load frame platen. This rate, along with the specimen's drainage condition, is dependent on the type of triaxial test being performed. For the consolidated drained tests, which were performed for this study, the rate of axial strain need to be slow enough to allow proper equalization of excess pore water pressure. Drainage needs to be closed and pore water pressure need to be recorded. Triaxial apparatus during the shearing process is shown in Figure 3.14.

Figure 3. 14. Triaxial test apparatus uses at Ege University lab. (ELE International).

3.5. Cone Penetration Tests Inside the Laminar Box

In order to perform calibration and validation of porosity in the DEM model, CPT tests were performed inside the large scale laminar box (Ecemis, 2013). Thanks to those large scale laboratory experiments wide range of porosity was obtained and

multiple cone penetration tests were performed. Tests were carried out at the Civil Engineering - structural laboratory of the Izmir Institute of Technology (IZTECH).

The large scale system is consisted of:

1. A longitudinal laminar box;
2. Cone penetration system;
3. Hydraulic filling system;
4. Strong floor;
5. 1-D shake table;
6. A hydraulic actuator;
7. Computer controlled system (to give shaking motion for the 1-D shake table);
8. Instrumentation;
9. Data acquisition system.

In this thesis, we explained only (1) longitudinal laminar box, (2) Cone penetration system and (3) hydraulic filling system. The more detail about the design and specifications of the laminar box system can be found at Ecemis (2013) and Kahraman (2013).

3.5.1. Large Scale Laminar Box

Laminar box was composed of 24 laminates to simulate the field conditions. Laminar box which was used in this study was made of aluminium laminates to fullfill one of Whitman and Lambe (1986) criteria that preffers less mass. It had a perfectly flexible shear beam at the same time, thoughr it was perfectly rigid in any horizontal plane. Consequently, some rollers were placed between two laminates. Laminar box size was limited by the size of the one-dimensional shake table, which was developed by Turan in 2008 and is available at IZTECH, Izmir, Turkey. The dimension of the box is as follows:

- Height = 1.4m
- Width = 0.5m
- Length = 1.8m

The schematic view of the laminar box is depicted at Figure 3.15 from N-S and W-E side view.

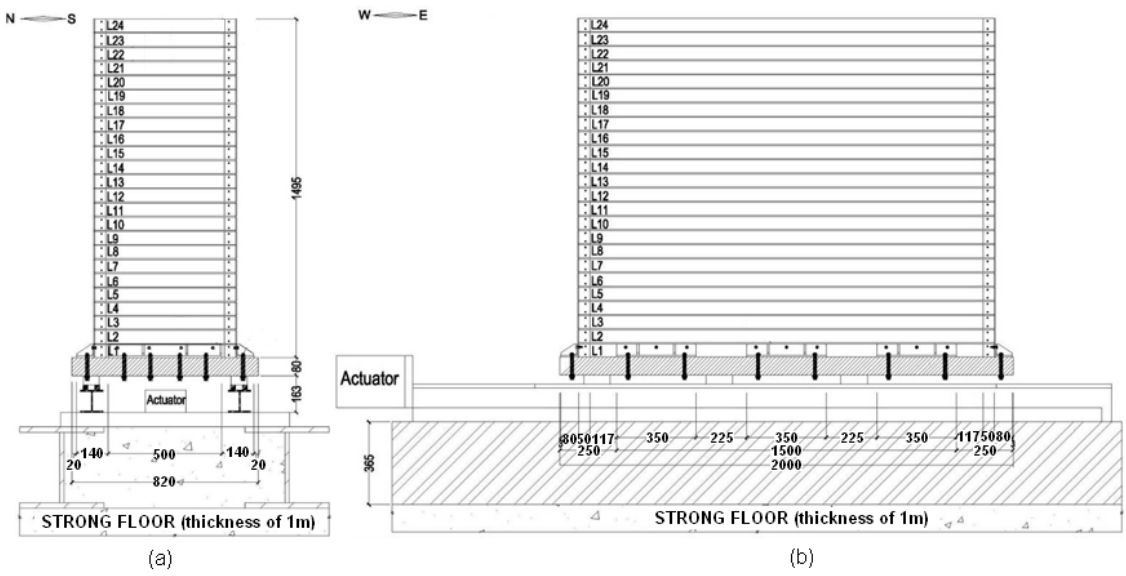

Figure 3. 15. Side View of the Laminar Box (N-S view), (b) Side View of Laminar Box (W-E view). (Source: Kahraman, 2013)

Five different (large scale) laminar box shaking table tests were performed for the purpose of this study. Sand deposits were prepared inside the laminar box and subjected to individual sinusoidal motions for duration of 12 seconds with different peak ground accelerations (PGA) under the undrained conditions. The CPTs were performed after filling process and after each of three subsequent shakings. Maximum input accelerations, frequency and duration is summarized in Table 3.7.

Table 3. 7. Summary of shake tables and CPT tests.

Test No.	Shake no.	max. input acceleration of shake	frequency	duration	CPT Test no
	[-]	[g]	[Hz]	[s]	[-]
TEST 1	Before 1st Shake	-	-	-	CPT 0
	1st Shake	0.05	2	12	CPT 1
TEST 2	Before 1st Shake	-	-	-	CPT 0
	1st Shake	0.35	2	12	CPT 1
	2nd Shake	0.35	2	12	CPT 2
	3rd Shake	0.35	2	12	CPT 3
TEST 3	Before 1st Shake	-	-	-	CPT 0
	1st Shake	0.22	2	12	CPT 1
	2nd Shake	0.22	2	12	CPT 2
	3rd Shake	0.22	2	12	CPT 3

TEST 4	Before 1st Shake	-	-	-	CPT 0
	1st Shake	0.11	2	12	CPT 1
	2nd Shake	0.11	2	12	CPT 2
	3rd Shake	0.11	2	12	CPT 3
TEST 5	Before 1st Shake	-	-	-	CPT 0
	1st Shake	0.46	2	12	CPT 1
	2nd Shake	0.46	2	12	CPT 2
	3rd Shake	0.46	2	12	CPT 3

3.5.2. Hydraulic Filling System

A robust hydraulic filling method (Whitman, 1985) was chosen in this research to fill the laminar box. This method has a great advantage because it is the most suitable for sensitive electronic equipment, actuators, instrumentations and computer systems. An EBARA CMR 1.00M slurry pump was used having the maximum solid particles' permeability of the slurry pump of 10 mm. Each of the sand models was prepared in the 0.42m^3 sample preparation box by mixing the soil with water before each test. The slurry pump was used to transfer the mixture of sand and water from preparation basins. It was a 20 mm diameter slurry hose that was attached to a 1-phase 50 Hz slurry pump. After sand grains settled naturally under gravity, excess water above sand was pumped out and process was repeated till the complete fulfilment of a box. At the end of the hydraulic filling method, sand grains were settled down through water, like natural alluvial deposition of sands in natural reservoirs or manmade islands. The top 30 cm of the soil inside the box was found to be slightly denser than the soil at the bottom, due to the limitation of maintaining the 30 cm water near the top of the box. During the pumping process, the water level above the sand was kept around 25 mm. The specimen preparation process is shown in Figures 3.16 - 3.17.

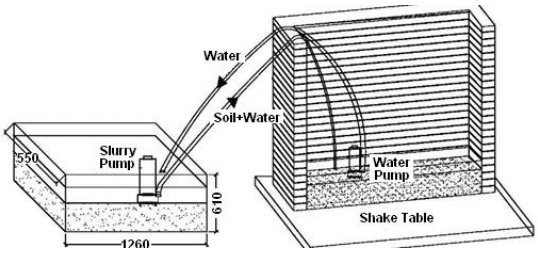

Figure 3. 16. Scheme of hydraulic filling of laminar box.
(Source: Kahraman, 2013)

Figure 3. 17. Hydraulic filling process at IZTECH.

3.5.2.1. Relative Density

Besides CPTs, bucket density tests were the method chosen to measure the relative density of the sand poured into the laminar box before shaking table tests. The relative density measured from CPTs will be explained in following chapters. The relative density depends on following factors:

- filling velocity,
- filling direction,
- discharge velocity,
- discharge direction,
- waiting time of the settlement of the soil grains.

The method is depicted in Figure 3.18.

Diameter of cylindrical bucket was 5 cm and the height of the bucket was 7 cm. Two buckets were placed on the soil surface at different depths during the filling process in the same vertical direction as CPT tests were performed (Figure 3.19). Buckets were pulled upwards with a rope from the laminar box when they were completely filled with soil and then its full weight was measured to estimate the saturated unit weight of the soil (Figure 3.19). Moreover two samples were taken from each bucket to determine the water contents (Table 3.8). Collecting undisturbed soil samples were difficult. Some samples were discharged from tests because of possible

disturbance. The summary of the saturated unit weight and water content results from the first shaking table test – TEST 1 with their location (depth) is displayed in Table 3.8.

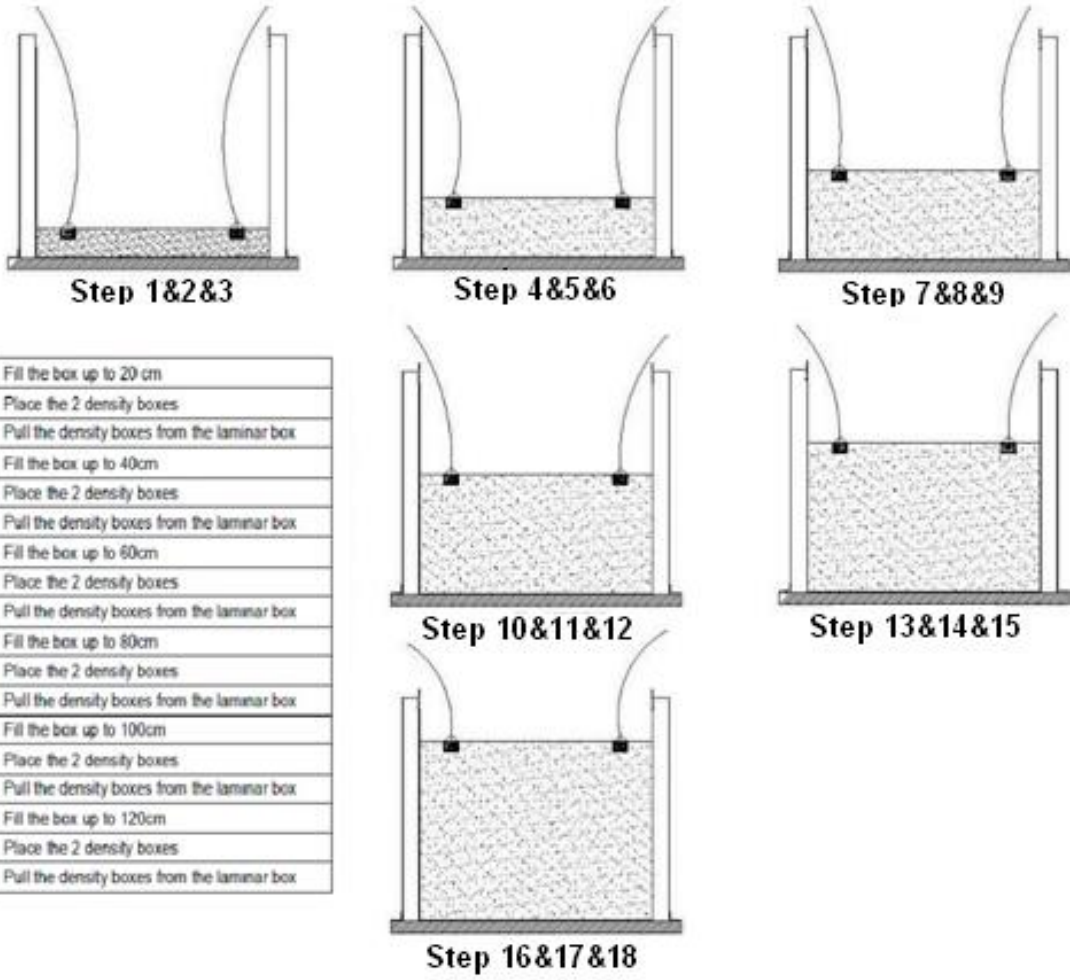

Step1	Fill the box up to 20 cm
Step2	Place the 2 density boxes
Step3	Pull the density boxes from the laminar box
Step4	Fill the box up to 40cm
Step5	Place the 2 density boxes
Step6	Pull the density boxes from the laminar box
Step7	Fill the box up to 60cm
Step8	Place the 2 density boxes
Step9	Pull the density boxes from the laminar box
Step10	Fill the box up to 80cm
Step11	Place the 2 density boxes
Step12	Pull the density boxes from the laminar box
Step13	Fill the box up to 100cm
Step14	Place the 2 density boxes
Step15	Pull the density boxes from the laminar box
Step16	Fill the box up to 120cm
Step17	Place the 2 density boxes
Step18	Pull the density boxes from the laminar box

Figure 3. 18. Relative density measurements by buckets.
(Source: Kahraman, 2013).

As we can observe from Table 3.8, it is fairly difficult to obtain uniform relative density throughout the whole depth however CPT tests done after filling process revealed that it was enough uniform. The average unit weight of the prepared sample ranged from 17-19 kN/m^3 throughout the depth, with an average for the entire deposit close to 18 kN/m^3. The time needed to the 1.4m deep soil model inside the box was approximately 9 hours. The D_r results obtained from the CPT tests will be discussed in Chapter 4.

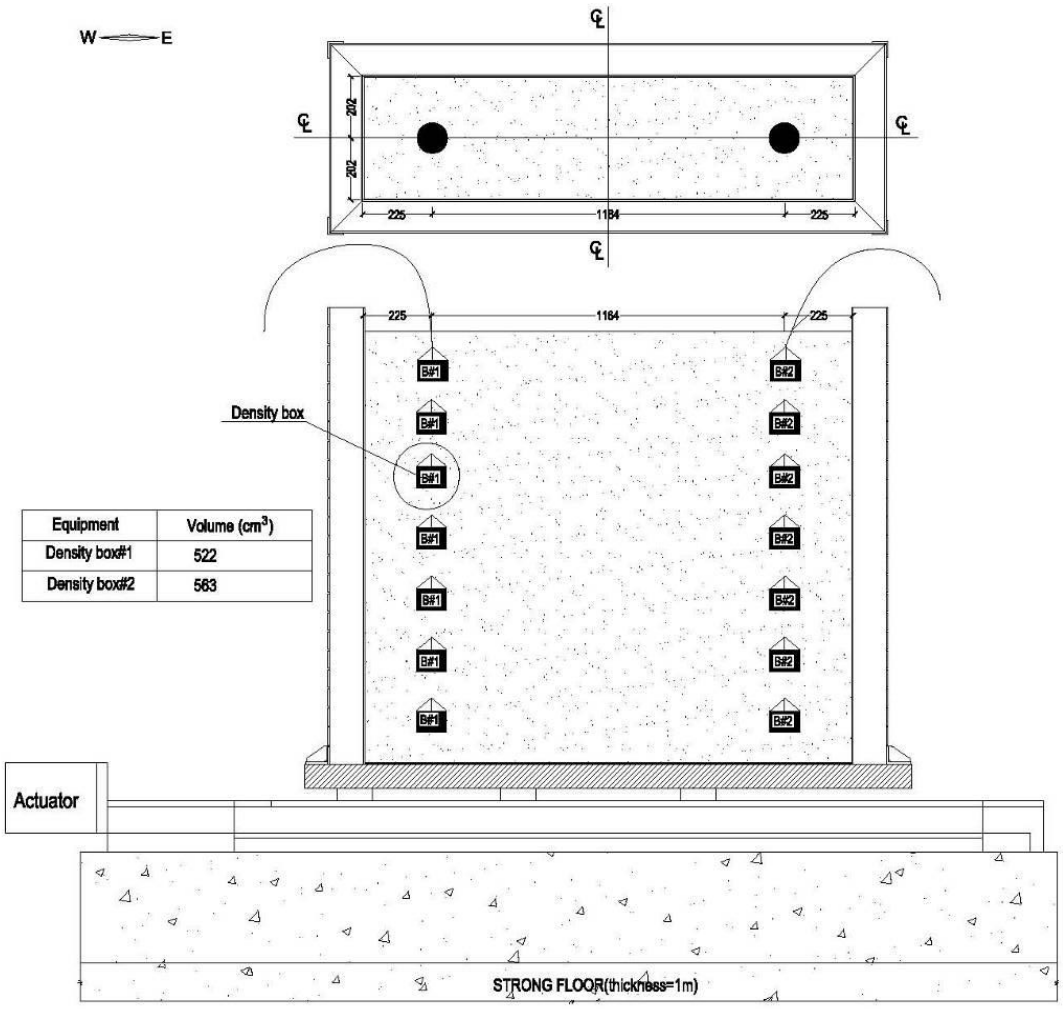

Figure 3. 19. Locations of Buckets.
(Source: Kahraman, 2013)

Table 3. 8. Results from buckets tests from TEST 1.
(Source: Kahraman, 2013)

TEST 1		
Depth [m]	Saturated Unit Weight [kN/m^3]	Water content [%]
0.38	17.68	36.00
0.56	18.71	28.00
0.70	17.11	29.70
0.85	19.08	28.10
1.00	16.02	28.90
1.13	19.24	31.40
1.30	16.90	30.35

3.5.3. Cone Penetration System

In this study, Geotech Co's cordless CPTu system was implemented. The CPTu system is illustrated in Figure 3.20 and it was consisted of:

1) CPT probe,
2) Rod,
3) Microphone,
4) Depth encoder,
5) Computer interface box.

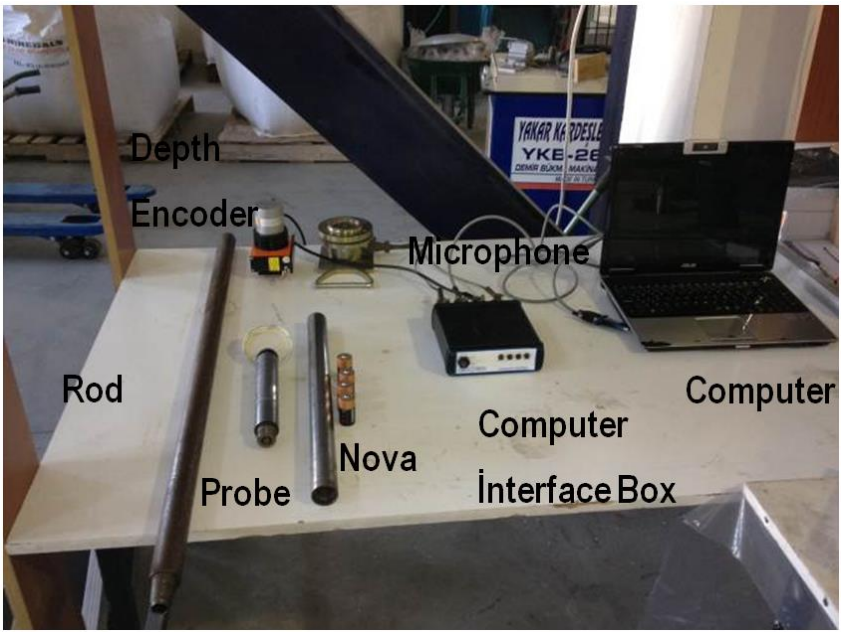

Figure 3. 20. CPT components implemented in the study.
(Source: Kahraman, 2013)

A cone penetrometer probe with 10 cm^2 base area cone and an apex angle of 60° was used during the CPTu tests. The details of the CPTu probe are given in Figure 3.21. During the CPTu tests, probe should be pushed into the soil at a constant penetration velocity. In all performed CPTu tests, the velocity was equal to 1.2 cm/s which is close to the standard velocity in cone penetration tests (2 cm/s). CPT tests were performed according to ASTM D3441- 05. Detailed description of the CPT procedure can be also found at Lunne et al (1997). The independently measured parameters are cone penetration resistance (q_c), friction resistance (f_s), and pore water pressure (u).

According to Lunne et al. (1997), to obtain reliable CPT results, fulfilment of the below specified factors is required:

1. Qualified operator,
2. Good technical facilities for calibration,
3. Proper maintaince of the equipment.

Test procedure requires careful attitude about aspects like:

1. Pre-drilling,
2. Verticality,
3. Reference measurements,
4. Rate of penetration,
5. Interval of readings,
6. Depth of measurements,
7. Saturation of piezocones (if there is a need for measurement of pore water pressure),
8. Dissipation tests (if there is a need for measurement of pore water pressure).

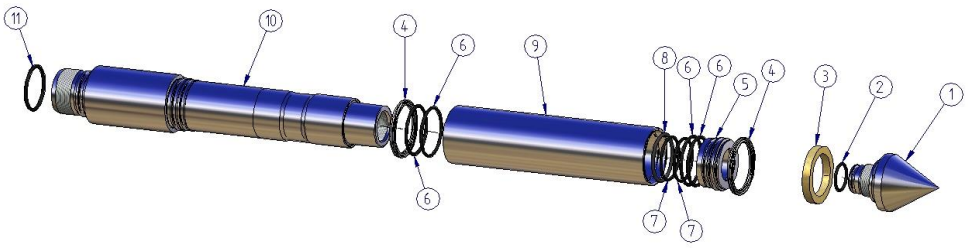

Figure 3. 21. CPTu Probe: 1)Point, 10 cm^2 , 2) O-ring, 3) Filter Ring, 4) X-ring, 5) Support Ring, 6) O-ring, 7) O-ring, 8) O-ring, 9) Friction Sleeve, 10) Cone Body, 11) O-ring. (Source: Geotech Nova CPT Acoustic Manual)

3.5.3.1. Experimental Procedure of CPTs

CPTu tests were conducted according to ASTM D 3441 test standard. All the components of the CPT shown in Figure 3.21 were placed accurately. Point and filters need to be kept in glycerine in order to provide valid pore water pressure measurements. The series of rods had a length of 150 cm. The microphone was mounted between the pushing system and a Nova CPTu probe. Depth of measurements was assured by

means of depth encoder which was placed to a laminar box wall. It was assured that all the cables are connected to the computer. The rods with cone at the end were pushed into the ground by means of hydraulic pump. The probe was pushed at a constant rate of approximately 1.2 cm/s. After 70 cm penetration, a pause occurred, due to limited length of the probe and a next rod was added to the system.

The location of the cone penetration tests in the laminar box is shown in Figure 3.22 from the top view. Top view is depicted in Figure 3.23. It is very crucial for investigation of boundary conditions to make realistic distinct element method modeling.

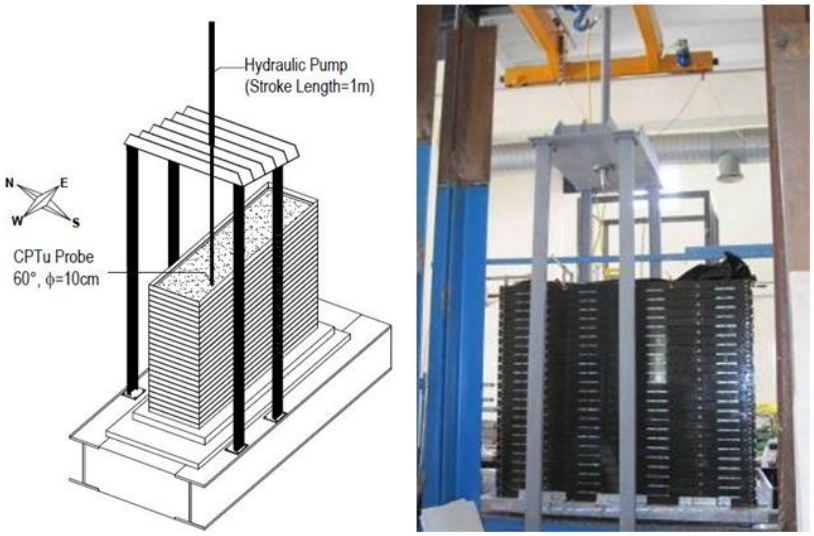

Figure 3. 22. Location of CPTs – general view.

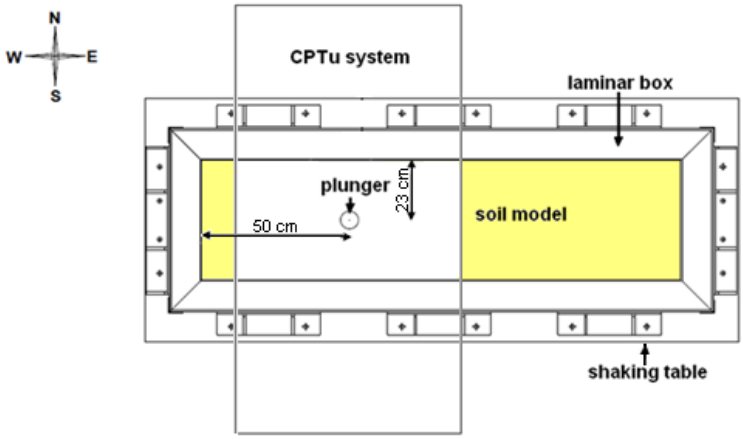

Figure 3. 23. Location of CPTu Tests – Top View.

CHAPTER 4

RESULTS OF TRIAXIAL AND CPT TESTS

4.1. Introduction

In this chapter, first, the results from the triaxial and cone penetration tests are presented. The focus is put on the results of the physical experiments which are essential to built a realistic two-dimensional distinct element method model. Next, analytical analysis is made to obtain a relationship between the limit cone penetration resistance and the relative density estimated from the CPT tests conducted inside the laminar box before and after each subsequent shaking. Afterwards, the measured data was analysed by using the fuzzy logic approach. The basic theoretical considerations upon which fuzzy logic was implemented in this study are presented to better understand this relative new and innovative concept.

Finally, both results from the analytical and fuzzy logic approaches led us to have a converged solution. A correlation between the D_r and the limit q_c values from experiments was successfully determined.

4.2. Triaxial Test Results

A series of consolidated drained (CD) triaxial tests were performed on sand samples, prepared using wet tamping techniques under moist conditions to assess a stress-strain behaviour of the soil used in the laboratory experiments and after to calibrate the stiffness parameters of numerical model in PFC2D. The model parameters are derived from laboratory test data performed in the Ege University, Turkey.

In order to propose the stiffness parameters of the numerical DEM model, a series of conventional consolidated drained (CD) triaxial tests were performed in the laboratory. Triaxial test procedure was explained in the previous chapter. The effects of depositional methods on the undrained behavior and on microstructure of sand were examined. Samples prepared by using moist tamping technique, usually demonstrates

strain softening behavior, because of their integral high void ratios (DeGregorio, 1990, Vaid and Sivathayalan, 2000). Yamamuro and Woods (2004) concluded that wet deposition methods seem to point out a more volumetrically dilatant or stable response, while dry methods appeared to signal a more contractive or unstable behavior. Therefore, a moist tamping procedure was applied to prepare the specimen used in triaxial testing. A sample size of 50 mm x 100 mm was tested in digital triaxial apparatus under undrained condition. Laboratory tests were conducted in accordance with the ASTM D7181-11 standard for initial vertical stress of 100 kPa and 200 kPa and formed with relative density (D_r) of 30%. Figure 4.1 shows the stress-strain curve for both initial vertical stress values. As shwon in the figure for 100 kPa and 200 kPa, axial strain increased with increase in deviatoric stress up to 7-8% and then started to decrease. For each drained triaxial etst, the point of failure was determined. Failure criterion was to reach to a maximum deviatoric stress. Failure occured at the axial strain of 7.98 and 8.02%, for 100 and 200 kPa initial confining stress values, respectively. Conditions at failure for both tests are showed in Table 4.1.

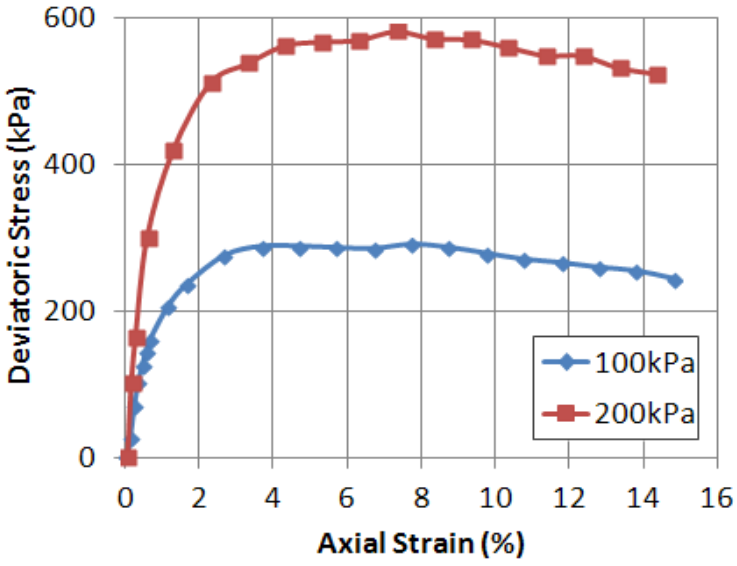

Figure 4. 1. Triaxial test results confined at 100 and 200 kPa (D_r=30%).

Table 4. 1. Conditions at failure for 100 and 200 kPa initial confining stresses.

Conditions at Failure for 100 kPa			
Failure Criterion	Maximum Deviator Stress		
Pore Pressure	522.5kPa	**Minor Effective Principal Stress**	207.6kPa
Deviator Stress	582.7kPa	**Major Effective Principal Stress**	790.2kPa
Axial Strain	7.98%	**Final Moisture Content**	40.4 %
Deviator Stress Correction	0.0kPa		
Conditions at Failure for 200 kPa			
Failure Criterion	Maximum Deviator Stress		
Pore Pressure	478.9kPa	**Minor Effective Principal Stress**	100.4kPa
Deviator Stress	290.9kPa	**Major Effective Principal Stress**	391.4kPa
Axial Strain	8.02%	**Final Moisture Content**	40.4 %
Deviator Stress Correction	0.0kPa		

Figure 4.2 shows an observed failure plane of a sample sheared at 100 kPa confining stress.

Figure 4. 2. Failure plane of specimen sheared at initial confining stress of 100 kPa.

The modulus of elasticity also called elasticity modulus was obtained from deviator stress versus axial strain curve (Fig. 4.1). Elasticity modulus was calculated based on triaxial test results under drained loading conditions. The method which was chosen for determining the elasticity modulus was through tangent and secant modulus. The curves were non-linear for most of their part. Modulus of elasticity is not constant for each soil as well is varies over stress ranges. There are many suggestions for selection of elasticity modulus of soil. Bowles (1982) favours the use of initial tangent

modulus (E_{init}), however Lambe and Withman (1963) prefers to use the secant modulus from zero deviator stress up to ½ ($E'_{1/2}$) or 1/3 ($E'_{1/3}$) of peak deviatoric stress, σ_d at which a failure has occurred. Calculation of elasticity modulus from stress-strain curve for initial confining pressure of 100 and 200 kPa is presented in Table 4.2.

Table 4. 2. Calculation of the elasticity modulus from the stress-strain curve for the initial confining pressure of 100 and 200 kPa.

Initial confining pressure	E'_{init}	ε_a at ½ of peak σ_d	½ of peak σ_d	$E'_{1/2}$	ε_a at 1/3 of peak σ_d	1/3 of peak σ_d	$E'_{1/3}$
[kPa]	[MPa]	[%]	[kPa]	[MPa]	[%]	[kPa]	[MPa]
100	**18.19**	3.99	288.4	**7.23**	2.66	275.8	**10.37**
200	**60.61**	4.01	559.1	**13.94**	2.67	517.2	**19.37**

The Mohr-Coulomb friction angle based on the laboratory triaxial test chamber results of the soil for initial confining stress of 100 kPa and 200 kPa was of 36°. For poorly graded sands, gravelly sands, with little or no fines the range of friction angle varies from 30° to 39° (Kolowski et al., 1989). Friction angle determined during triaxial experiments is coherent with literature.

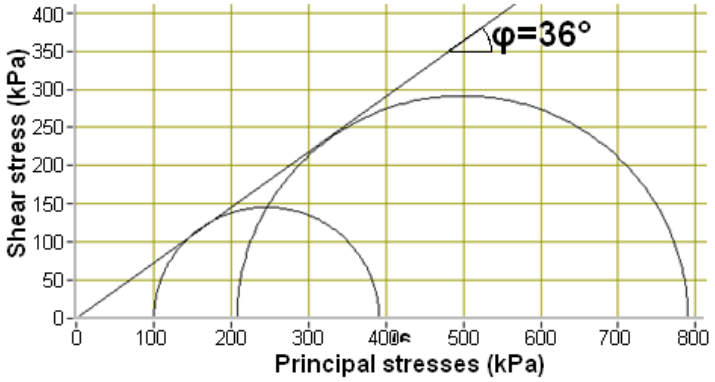

Figure 4. 3. Determination of the friction angle using the Mohr-Coulomb Circle.

4.3. Cone Penetration Test Results

Cone penetration test procedure was explained in previous chapter. For numerical analysis measured cone penetration resistance and estimated relative density

from CPT tests were required. Therefore, sleeve friction resistance and pore water pressure was omitted in the summary of the CPT results given in this study.

4.3.1 Cone Penetration Resistance

The cone penetration resistance was measured throughout the depth at every 2 cm. The limit cone penetration resistance values were assigned intuitively. The boundary effects were taken into account, as well as a neccessity for adding the additional rod during the penetration process at approximatly 1 m depth. The limit value was chosen considering the depth of 1 m of 1.4 m saturated loose assembly. Firstly, a trend line was chosen (red line in Fig. 4.4) and then the limit value of q_c (green line in Fig. 4.4) as the magnitute of q_c at the depth of 1m. The decrease in q_c from 0.7 to 1.0 m was likely caused by inserting the second rod to penetrate deeper depths. Thanks to intuition and experience, lim q_c was selected to be greater than the measured one at the depth of around 1m, which was less then the measured data close to the bottom of box.

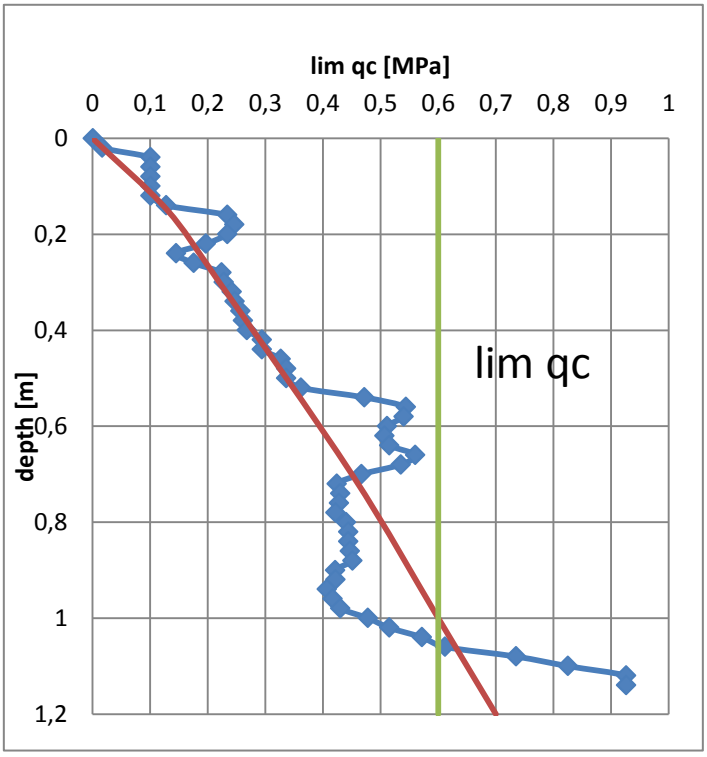

Figure 4. 4. The procedure of chosing limit value of cone penetration resistance (lim q_c).

4.3.1.1 CPT Results Before and After Each Shaking Test

Figure 4.5 show the q_c-depth graphs. As shown in the figure, the results after the 2nd and the 3rd shakings are very similar along the depth at each of five conducted tests. The CPT results just before the first shaking (so called ini_shake) were the most different from eachother . It may be caused by preparation method of the model. Filling proccess can be affected by many factors and it is rather random. At shallow depth we observed higher relative cone resistance q_c, due to the fact that the water table was just slightly above the soil assembly.

The CPT results after 1st shake were increasing with depth. The loose saturated material could be liquefied and at shallow depths soil lost its strenght. At the same time at depths, we observed some increase in q_c, due to increase in the relative density (D_r).

The data obtained from the cone penetration tests after the 2nd shake shows that CPT results are closer to eachother at the same depths. Along the depth, q_c was constantly increasing. Closer to the box bottom, the soil was much stiffer, though it was also influenced by the boundary conditions.

Tests 6,7 and 8 till the deph of 0.7 m were very close to eachother, with respect to q_c values. Boundary effects were clearly marked.

Table 4. 3. Limit q_c values for all CPTs conducted in this study.

Before 1st shake – ini_shake						
	TEST_1	TEST_2	TEST_3	TEST_4	TEST_5	TREND_ ini_shake
At depth 1m	trend_line	trend_line	trend_line	trend_line	trend_line	AVG. trend
lim q_c	0.27	0.29	0.2	0.26	0.22	**0.248**
After 1st shake						
	TEST_2	TEST_3	TEST_4	TEST_5	TEND_3rd _shake	
At depth 1m	trend_line	trend_line	trend_line	trend_line	AVG. trend	
lim q_c [MPa]	0.6	0.55	0.45	0.6	**0.62**	
After 2nd shake						
	TEST_2	TEST_3	TEST_4	TEST_5	TREND_2nd- _shake	
At depth 1m	trend_line	trend_line	trend_line	trend_line	AVG. trend	
lim q_c	0.6	0.55	0.58	0.6	**0.78**	
After 3rd shake						
	TEST_2	TEST_3	TEST_4	TEST_5	TEND_3rd _shake	
At depth 1m	trend_line	trend_line	trend_line	trend_line	AVG. trend	
lim q_c [MPa]	0.9	0.75	0.8	1	**1.613**	

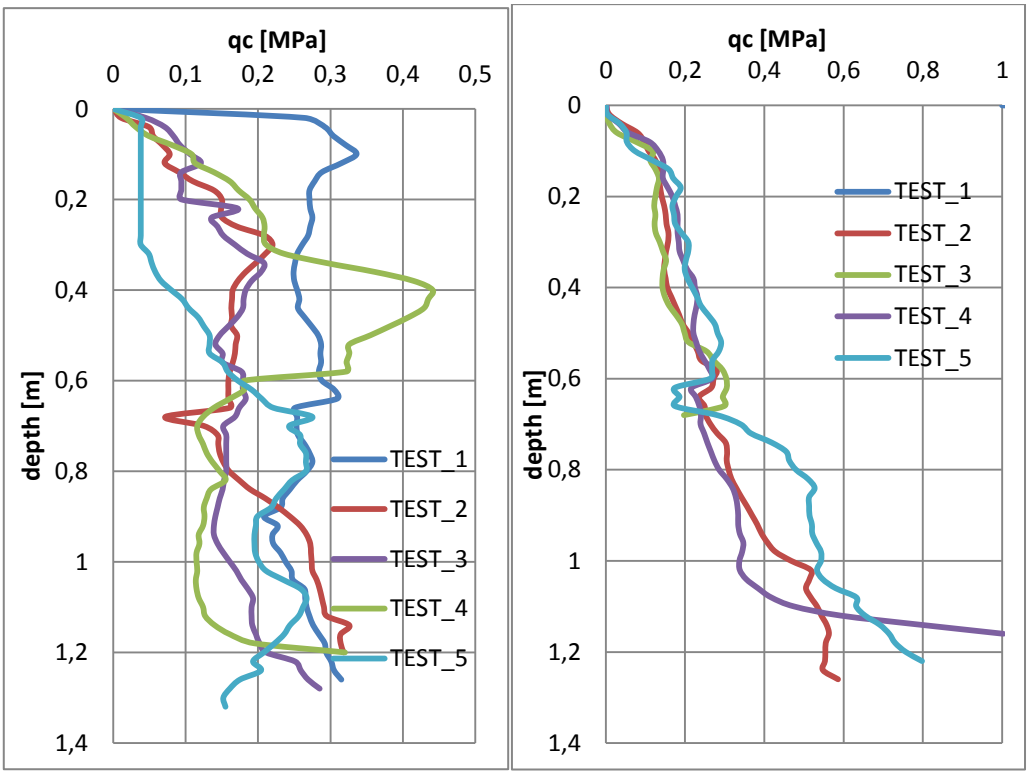

(a) (b)

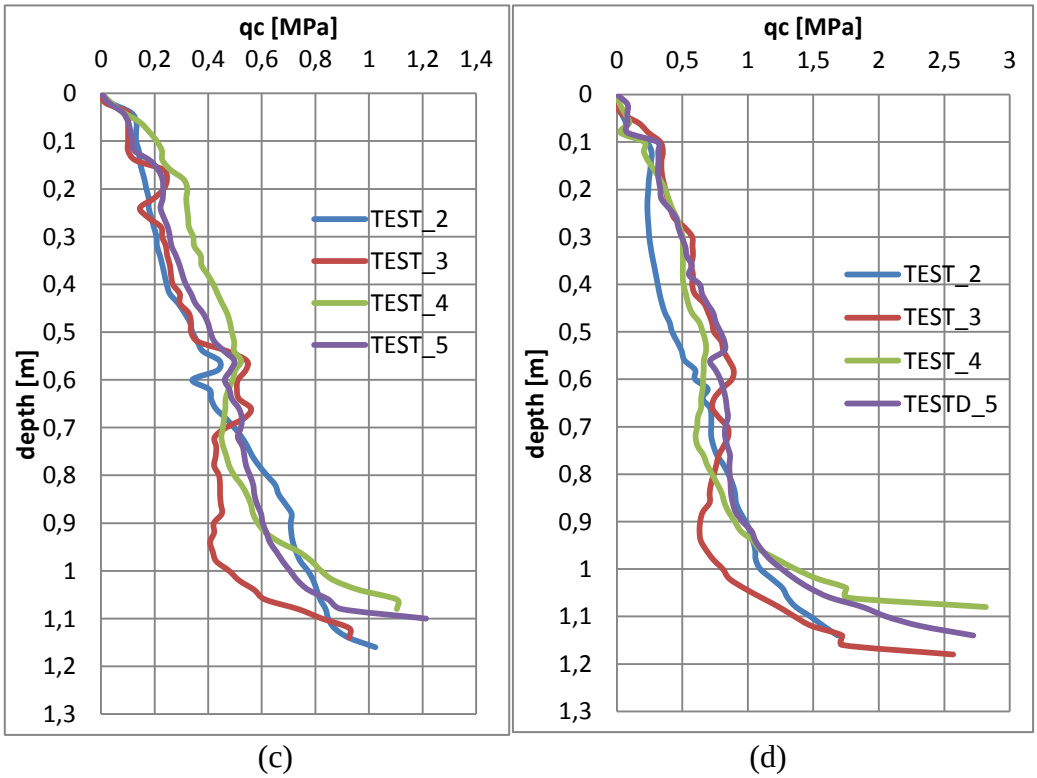

(c) (d)

Figure 4. 5. CPT results from laboratory experiments performed at IZTECH (a) before 1st shake, (b) after 1st shake, (c) after 2nd shake and (d) after 3rd shake.

In Table 4.3 the limit q_c values at the depth of 1m are gathered. The procedure described in section 5.3.2 was implemented.

4.3.2. Relative Density

Relative density, D_r was obtained, based on the equation derived by Jamiolkowski et al. (1958):

$$D_r = -98 + 66 \cdot \log_{10}\left(\frac{q_c}{\sqrt{\sigma_{vo}'}}\right) \tag{4.1}$$

where,

q_c = cone penetration resistanc;

σ_{vo} = initial effective normal stress.

Before each shaking, the average D_r value was calculated throughout the depth. First 4 cm of measurements were ommited because of the layer of water surging on sand after filling process. Average D_r (AVG. D_r) value was calculated by the arithmetic mean of all D_r measurements along the depth without first 4 cm according to given equation:

$$AVG.\ D_r = \sum_{i>0,04}^{n} D_{ri} \tag{4.2}$$

The average D_r values estimated from the CPT tests after each shaking was neccessary to assign the limit q_c value to specific relative density. As summarized in Table 4.3, total of five series of CPTs were investigated to define an average value of the desired relative density. For each CPT the 'AVG. D_r' was calculated along with the corresponding void ratio (e) and porosity (n). The formula derived from basic soil mechanis equation was used to obtain the void ratio from each CPT:

$$e = e_{max} - \frac{D_r(e_{max} - e_{min})}{100} \tag{4.3}$$

where,

e = void ratio;

e_{max} = maximum void ratio;

e_{min} = minimum viod ratio;

D_r = relative density.

Results of the maximum and minimum void ratio for the tested sand were 0.8 and 0.6, respectively. Next, porosity was calculated by means of equation:

$$n = \frac{e}{e+1} \tag{4.4}$$

Finally, the average values of the relative density, void ratio and porosity were derived for:

- initial conditions at laminar box,
- After 1st shaking,
- After 2nd shaking and,
- After 3rd shaking.

Summary of results is shown in the Table 4.4. The relative density measurements indicate that the uniformity of the deposit is achieved fairly good by the preparation method used in this study. D_r results after the 1st, 2nd and 3rd shakings for Test 4 are showed at Figure 4.6. Average lines are result of equation x and they prove that used procedure gives accurate averaged values of D_r. As shown in the figure the range of D_r for all tests varies from 19 to 69%.

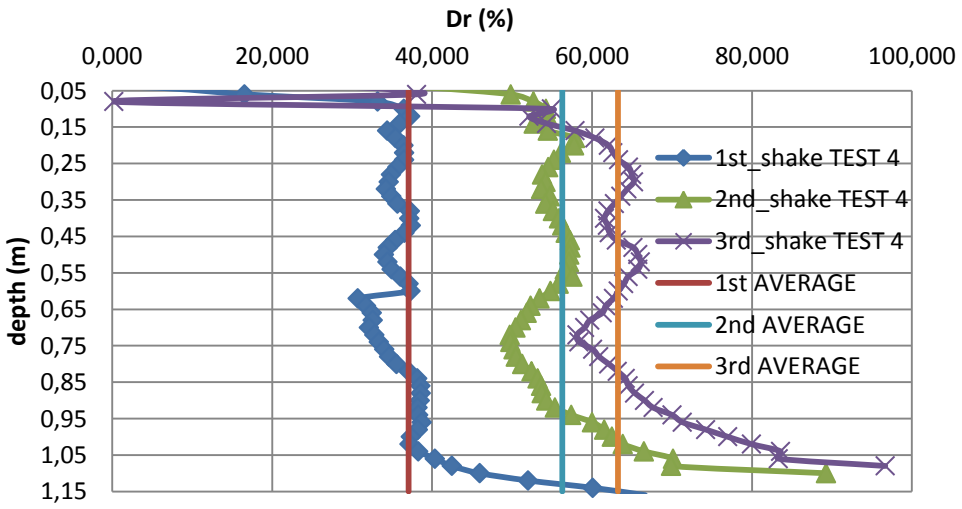

Figure 4. 6. D_r results after the 1st, 2nd and 3rd shake with calculated AVG. D_r values.

Table 4. 4. Average relative density, void ratio and porosity obtained from CPTs.

Initial conditions before shaking tests					
Test name	**TEST 1**	**TEST 2**	**TEST 3**	**TEST 4**	**TEST 5**
AVG. Dr [%]	40,45196	26,988	25,391	28,123	19,091
corresponding e [-]	0,71	0,74	0,74	0,740	0,750
corresponding n [-]	0,415	0,425	0,425	0,425	0,429
AVG. Dr [%] for all tests	28,01				
AVG. e [-] for all tests	0,74				
AVG. n [-] for all tests	0,425				
After 1st shaking					
Test name	**TEST 1**	**TEST 2**	**TEST 3**	**TEST 4**	**TEST 5**
AVG. Dr [%]	48,27731	39,704	33,787	37,066	45,067
corresponding e [-]	0,7	0,71	0,730	0,720	0,7
corresponding n [-]	0,411	0,415	0,422	0,419	0,412
AVG. Dr [%] for all tests	40,78				
AVG. e [-] for all tests	0,71				
AVG. n [-] for all tests	0,415				
After 2nd shaking					
Test name	**TEST 1**	**TEST 2**	**TEST 3**	**TEST 4**	**TEST 5**
AVG. Dr [%]	-	50,163	46,627	56,286	53,770
corresponding e [-]	-	0,7	0,700	0,680	0,69
corresponding n [-]	-	0,412	0,412	0,405	0,408
AVG. Dr [%] for all tests	51,72				
AVG. e [-] for all tests	0,69				
AVG. n [-] for all tests	0,408				
After 3rd shaking					
Test name	**TEST 1**	**TEST 2**	**TEST 3**	**TEST 4**	**TEST 5**
AVG. Dr [%]	-	54,773	63,128	63,241	68,794
corresponding e [-]	-	0,69	0,670	0,670	0,66
corresponding n [-]	-	0,408	0,401	0,401	0,397
AVG. Dr [%] for all tests	62,48				
AVG. e [-] for all tests	0,67				
AVG. n [-] for all tests	0,401				

Figures 4.5 and 4.6 present the change in relative density and void ratio for succeding shakings. After every test, the soil became more dense. Relative density increased significantly after each shake. From Table 4.4, we can conclude that relative density was increasing by 26% the most, and 5% at least between the succeeding shakings. As shown in Tab. 4.5, these results correspond to the change in void ratio from 0.05 to 0.01, respectively. In Figure 4.9 the average values of D_r at each stage of experiments are depicted. Between initial conditions in the laminar box and after the 1st shake the AVG. change in D_r was 13% and in other cases 11%.

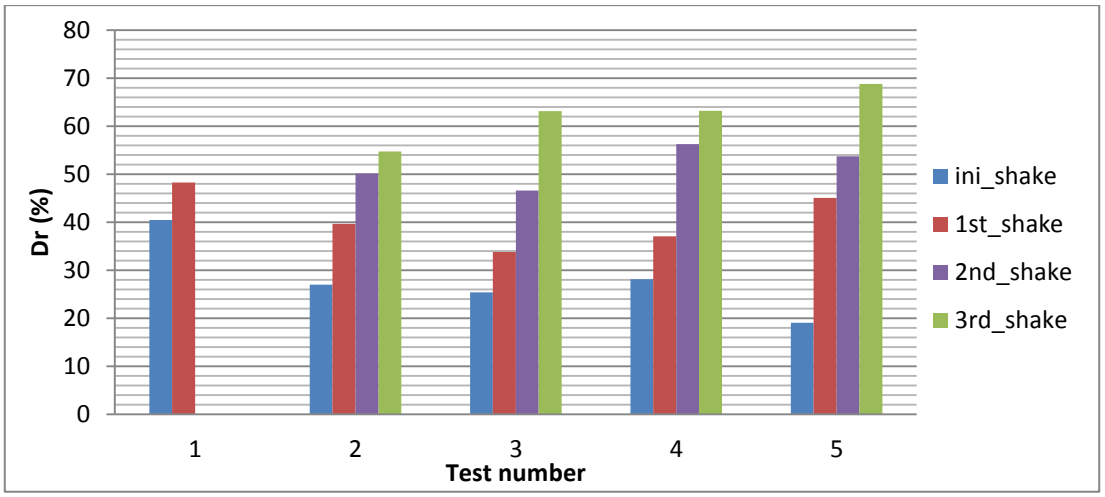

Figure 4. 7. Change in relative density for succeeding shakings.

Table 4. 5. Change in relative density and void ratio between each stage of experiments.

	Change in relative density [%]				
Between	**Test 1**	**Test 2**	**Test 3**	**Test 4**	**Test 5**
ini-1st	7.82	12.71	8.39	8.94	25.97
1st-2nd		10.45	12.83	19.21	8.70
2nd-3rd		4.61	16.50	6.95	15.02
	Change in void ratio [%]				
Between	**Test 1**	**Test 2**	**Test 3**	**Test 4**	**Test 5**
ini-1st	0.01	0.03	0.01	0.02	0.05
1st-2nd		0.01	0.03	0.04	0.01
2nd-3rd		0.01	0.03	0.01	0.03

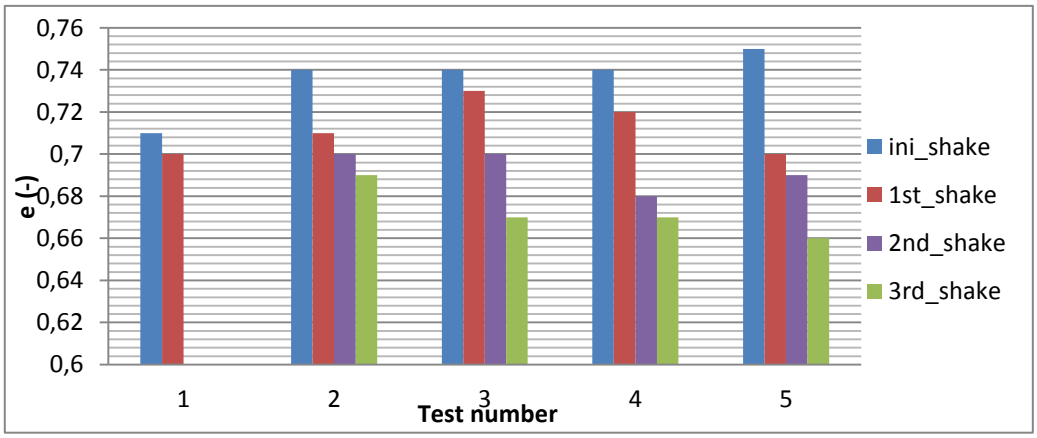

Figure 4. 8. Change in void ratio for succeeding shakings.

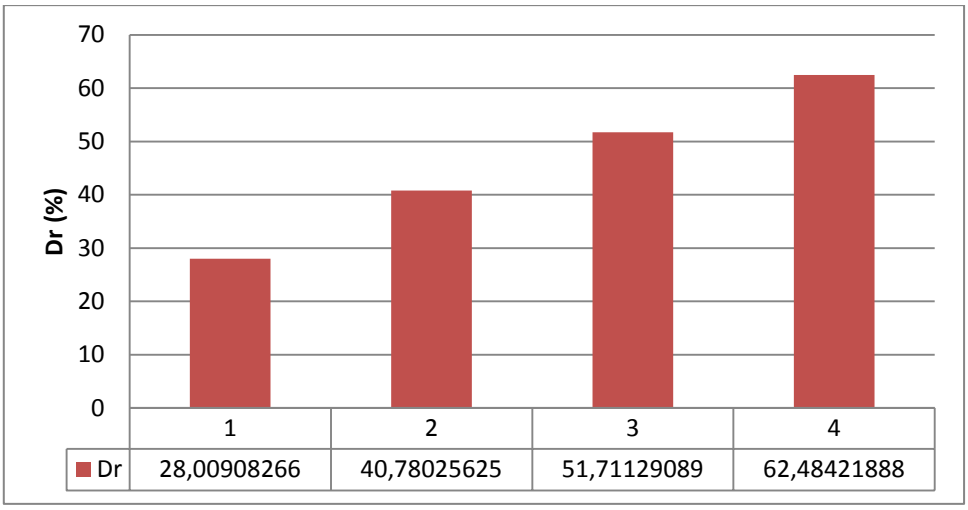

Figure 4. 9. Average values of D_r at each stage of experiments, where: 1 – ini_shake AVG. D_r, 2 – 1st_shake AVG. D_r, 3 – 2nd_shake AVG. D_r, 4 – 3rd_shake AVG. D_r.

4.4. Correlation Between D_r and Limit q_c Values From Experiments

The next part of calibration of the porosity was finding a correlation between the D_r and the limit q_c values from the CPTs. A total of 17 pairs of D_r - lim q_c were chosen. There are listed in Table 4.6. The closest approximation of the given set of data was a natural logarythm ic function. As a result, we have obtained an equation where the D_r is dependant on the lim q_c, as presented below:

$$D_r = 28{,}805 \ln(\lim q_c) + 66{,}534 \tag{4.5}$$

Table 4. 6. D_r - lim q_c pairs from CPTs.

Dr [%]	**Dr=19**	**Dr=25**	**Dr=27**	**Dr=28**	**Dr=34**	**Dr=37**	**Dr=40**	**Dr=41**	**Dr=45**
lim q_c [Mpa]	0,2	0,22	0,27	0,28	0,3	0,33	0,37	0,44	0,47
Dr [%]	**Dr=47**	**Dr=48**	**Dr=50**	**Dr=54**	**Dr=55%**	**Dr=56**	**Dr=64**	**Dr=69**	
lim q_c [Mpa]	0,5	0,54	0,6	0,68	0,75	0,77	0,85	0,9	

The realation is depicted at Figure 4.10.

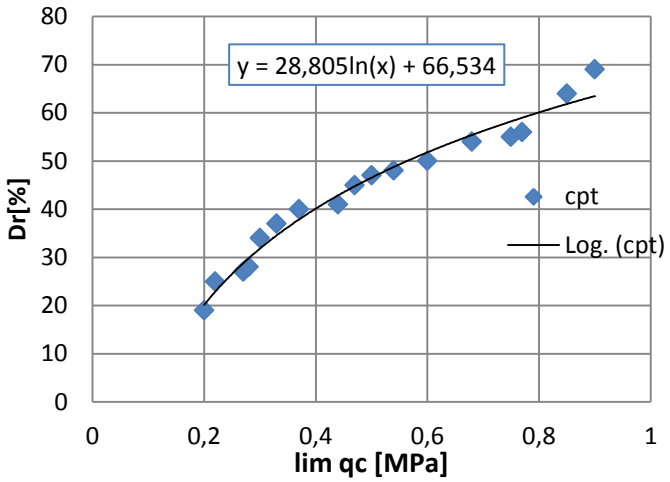

Figure 4. 10. Relationship between relative density and limit cone penetration resistance from laboratory tests.

The founded correlation will be used in the calibration of the DEM model, which is described in Chapter 7 in detail.

4.5. Validation of Relation Between D_r and Lim q_c with Fuzzy Logic

Fuzzy logic (FL) is a problem-solving control system methodology. It can be implemented in systems, ranging from simple and small to large data acquisition and control systems as well as in artificial intelligence methods. During the last decade, the application of fuzzy concepts is becoming increasingly popular within the engineering field, including geomechanics (Amin et al., 2001; Santamarina, 1987). It is mainly due to the fast that FL concepts provide a relatively easy way of dealing with complicated problems as they can be built with fuzzy models which are full of impreciseness. The ability to model a design problem realistically in precise mathematical form is more difficult, because it is based on usually intuitive approach. Fuzzy logic makes it simpler to find a definite conclusion with limited sometimes imprecise and ambiguous input data. Thanks to the FL approach, it is possible to mimic a person intuitive decision, but much faster.

It is a specified area which fundamentally differs from the other disciplines with its complexity and usual large scale usage. Due to these circumstances, there is uncertainty in its application of theoretical solutions. Furthermore, engineering

problems are constraint satisfaction problems. Fuzzy logic can be also applied to sort and handle data either from laboratory, field or numerical experiments. So, there has been a growing interest in the application of these concepts to engineering problems. Theoretical background can be found in ‘An Introduction to Fuzzy Logic’ written by S. D. Kaehler.

4.5.1. Membership Functions, Fuzzy Rules and Deffuzication Methods

In fuzzy logic, the most widely used are linguistic or "fuzzy" variables. The concept of linguistic variables was proposed by Lotfi Zadeh in 1973. The input is usually a noun like "displacement", "velocity", "flow", etc. The fuzzy variables themselves are adjectives like "small", "medium", "large", etc. Those adjectives modify the variable and divide the input on few groups like "small displacement", "medium displacement", "large displacement ", etc. The rule matrix is created from input, output and logical linkers. The simplest practical implementation is a 3-by-3 matrix. The most popular linking commands are “AND” and “OR”. It can be implemented in hardware, software or in a combination of both.

The membership function is a generalization of the indicator function – usually a graphical representation of the magnitude of participation of each input. There are different shapes, but the triangular is the most common. But bell, trapezoidal, haversine and, exponential types have been also used. Membership function connects a weighting with each of the input data that are taken into account during FL analysis, determine the functional overlay between the inputs, and ultimately defines an output response. The rules take advantage of the input membership values. They are treated as the weighting factors to determine their impact on the FL output sets of the final output response. Once the functions are deduced, scaled, and combined, next they are defuzzified into a new output, which drives the system. Deffucication methods are various, such as; centroid, bisector, the largest of maximum (LOM), the middle of maximum (MOM) and the smallest of maximum (SOM). The choice of methods is intuitive and unique for every application.

Summarizing, there is a unique membership function associated with each input parameter. These weighting factors determine the degree of influence or degree of

membership (DOM) each active rule has. By computing the logical product of the membership weights for each active rule, a set of fuzzy output response magnitudes are produced. All that remains is to combine and defuzzify these output responses. Figure 4.11 shows random membership functions with its properties like width, degree of membership and centres.

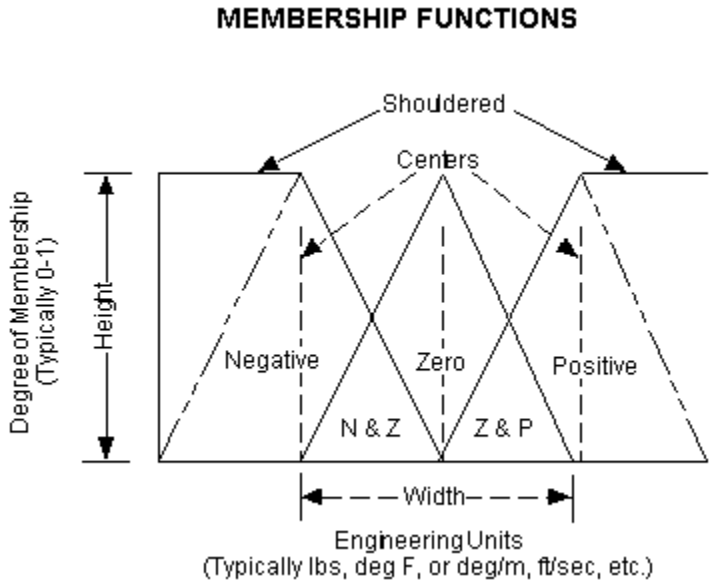

Figure 4. 11. Membership fucntions.
(Source: www.seattlerobotics.org)

4.5.2. Fuzzy Logic Implementation to CPT Study

Fuzzy logic was used to sort and handle data obtained from the laboratory experiments. It allowed us to check if the logarythmic approximation was close to the fuzzy logic solution. Fuzzy calculation was handled by MATLAB computer programing. The fuzzy calculation is based on a set of data obtained from the CPT done in the laminar box during the shaking table experiments. Data are compiled in Table 4.7. In this table σ_{v0}' is an initial effective stress.

A two-input single-output Mamdani fuzzy model with eight rules was generated. Mamdani's fuzzy inference method is the most commonly used fuzzy methodology. The input variables are: Mean stress at the depth of 1 m (kPa) and relative density-D_r (%) which lead to the q_c (MPa) output. It is presented in Figure 4.12. Exact segregation is illustrated in Figure 4.13. Membership functions were created intuitively.

Table 4. 7. Set of data obtained from CPT used in FL calculation.

D_r [%]	**19**	**25**	**27**	**28**	**30**	**34**	**37**	**40**	**41**
σ_{v0}' [kPa]	8,25	8,43	8,71	8,71	8,51	8,51	8,8	8,59	8,69
q_c [Mpa]	0,2	0,22	0,27	0,28	0,29	0,3	0,33	0,37	0,44
D_r [%]	**45**	**47**	**48**	**50**	**54**	**55**	**56**	**64**	**69**
σv_0' [kPa]	8,74	8,94	9,1	9,37	9,07	9,37	9,22	9,28	9,29
q_c [Mpa]	0,47	0,5	0,54	0,6	0,68	0,75	0,77	0,85	0,9

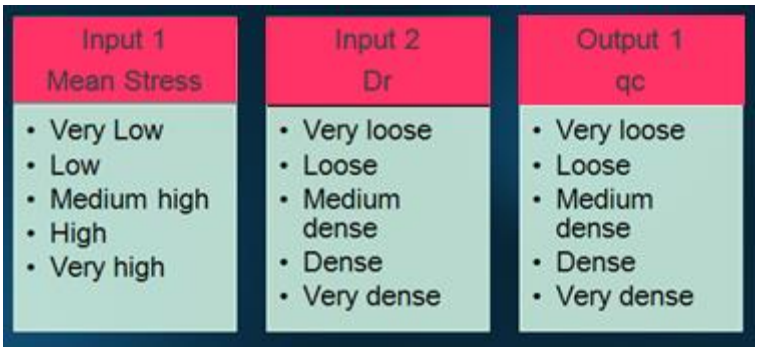

Figure 4. 12. A two-input single-output Mamdani fuzzy model for the FL CPT study.

Linguistic variables are used to represent an FL system's operating parameters (rules). The rule matrix is a simple graphical tool for mapping the FL control system rules. It accommodates two input variables and expresses their logical product (AND) as one output response variable. By intuition and experience, the system rules were decided. Based upon the inputs, appropriate output response conclusions were determined, and load these into the rule matrix (summarized in Table 4.8).

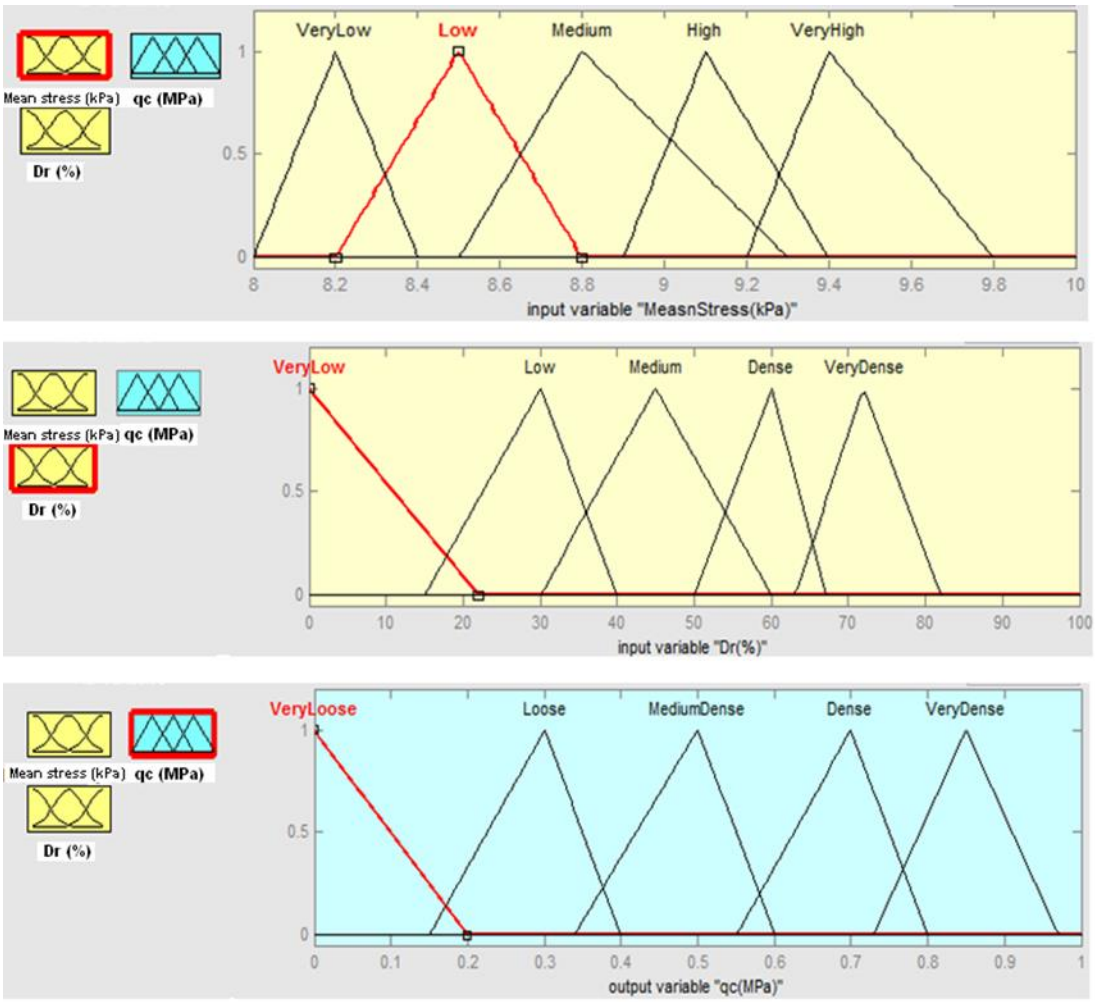

Figure 4. 13. Membership functions for the FL CPT study.

Table 4. 8. Fuzzy rules for the FL CPT study.

Fuzzy Rules			
	If AND	**if**	**then**
	Mean stress [kPa]	**D_r [%]**	**qc [MPa]**
1	Low	Very loose	Very loose
2	Low	Loose	Loose
3	Medium	Medium dense	Medium dense
4	Medium	Dense	Medium dense
5	High	Medium dense	Dense
6	High	Very dense	Very dense
7	Very high	Very dense	Very dense
8	not High	Loose	loose
9	not Low	Medium dense	Dense
10	not Low	Dense	Dense

Three-dimensional surface graph illustrates our model, governed by matrix of fuzzy rules, as shown in Figure 4.14.

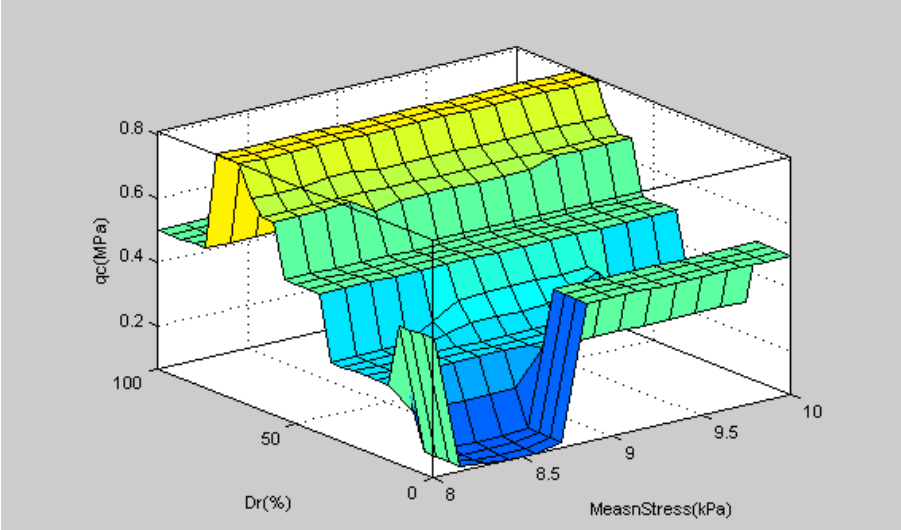

Figure 4. 14. 3D surface graph illustrates our model govern by matrix of fuzzy rules.

Based on the fuzzy rules, Figure 4.15. was obtained. The laboratory test results were compared to fuzzy outputs with two different deffuzzification methods: centroid and bisector. A very good match is observed. The closest approximation of the given set of data was a natural logarithmic function for both centroid and bisector defuzification methods. As a result, we have obtained an equation where D_r is dependent on lim q_c. It is presented below:

$$\text{For centroid: } D_r = 34.2 \ln(\lim q_c) + 69.561 \tag{4.6}$$

$$\text{For bisector: } D_r = 33.061 \ln(\lim q_c) + 68.808 \tag{4.7}$$

Results of approximation are very close to those obtained from the analytical analysis of the cone penetration resistance and the relative density, as in equation 4.5. At Figure 4.15 results from laboratory and fuzzy logic solution were compared. Bisector and centroid deffuzification methods were chosen. However there are more deffuzification methods, which are applied according to specific problem. Comparison of results by different deffuzzification methods for set: D_r = 47% and Stress = 8.94 kPa is showed in Table 4.9 and in Figure 4.16.

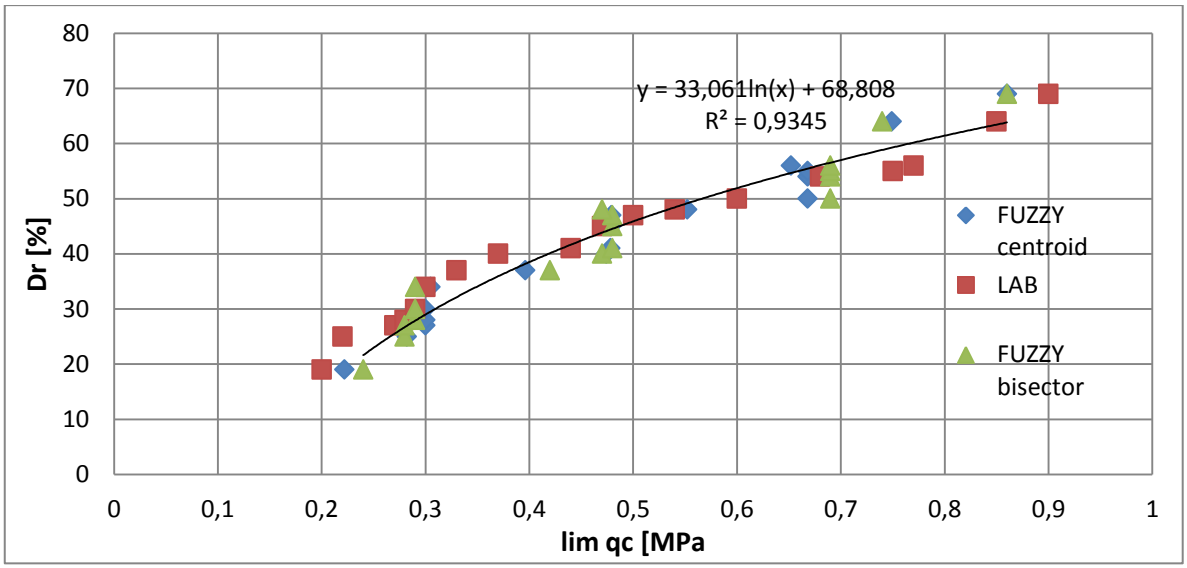

Figure 4. 15. Relationship between the relative density and the limit cone penetration resistance from the laboratory tests by the FL concept (trend line is shown for the bisector method).

Table 4. 9. Results of q_c with different deffuzzification methods.

Deffuzzification method	**q_c [MPa]**
CENTROID	0,48
BISECTOR	0,48
LOM	0,52
MOM	0,49
SOM	0,46
LABORATORY	0,50

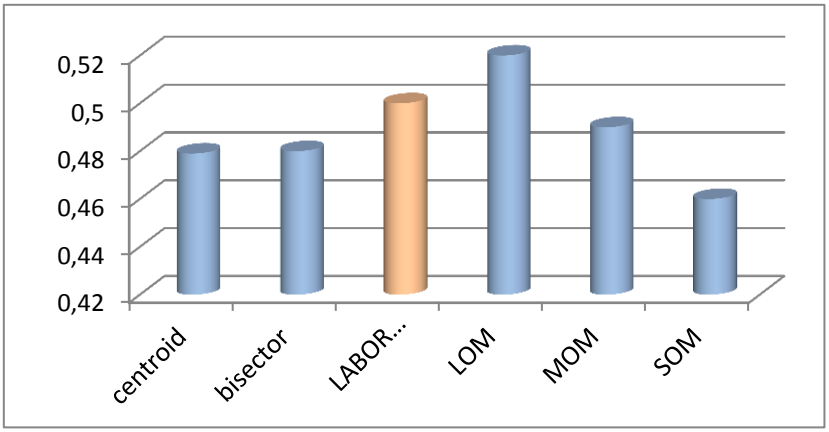

Figure 4. 16. Results of q_c with different deffuzzification methods, compared to the laboratory data.

FL was conceived as a better method for sorting and handling data, but also has proven to be a good choice for this geotechnical application, since it mimics human control logic. It uses an imprecise, but very descriptive language to deal with input data more like a human operator. It is very robust and forgiving of operator and data input and often works when first implemented with little or no tuning. It is also confirmed that logarithmic function approximating the relation between D_r and lim q_c was correct. Analytical and fuzzy logic solutions are very similar. It was proven by putting some random data (D_r, σ_{vo}) to program and obtaining lim q_c by Equation 4.6 or 4.7 that results are close to those assumed by equation 4.5.

CHAPTER 5

DISTINCT ELEMENT METHOD IN GEOMECHANICS

5.1. Introduction

In this chapter, numerical methods, that were implemented in this study, are explained. The special focus was put to description of:

1) Distinct Element Method

2) Particle flow code in two dimensions

3) Basic fluid analysis option

First, the distinct element method (DEM) is presented with special focus on the previous research done by the other scientists (e.g. Jang et al.,2006; Arrayo et al., 2011 and Bultanska et al., 2013) in the geomechanics field. Advantages and disadvantages of the DEM over the other numerical methods are expained. The software, which is based on the DEM is listed. Use of the DEM in geomechanics (O'Sullivan, 2011) is mentioned.

Second, the DEM sofware PFC2D, which is implemented in this study, is described briefely. The description contains practical aspects of the application of PFC2D in this thesis, including basic mechanics of PFC2D, selected particle generation, contact models and other parameters.

Finally, the basic principals and theoretical background of the basic fluid analysis option are described in brevity.

5.2. Distinct Element Method

The discrete element method (DEM), also called a distinct element method is a numerical method used to compute the stresses and displacements in a volume containing a large number of particles such as grains of sand. Modeling of the particles using the DEM is the approach towards the microscopic understanding of macroscopic particulate material behaviour (Herrmann, 1997; Kishino, 2001; Hinrichsen et al.,

2004). The DEM provides the possibility of investigating the mechanical behaviour of materials at both micro and macro levels. Methods like the distinct element method are generally considered as micro-macro transition (Kirkwood et al., 1949; Vermeer et al., 2001; Pöschel and Luding, 2001). Microscopic scale modeling of a sample of material (a representative volume) can be a valuable tool to derive macroscopic relations. There are needed to represent the material within the macroscopic continuum theory.

The DEM is currently used in various disciplines. However, it was pioneered by Cundall (1971) in geomechanics and mechanics of rock materials where we do not observe continuity between particles. The DEM can replicate the soil particulate nature, perform a large-scale deformation and failure of particles aggregate, incorporate various tests geometry and also mimic slip planes and separations form between groups of particles capturing failure mechanisms. The particle shapes and geometries are specified by the user. Spheres or ellipsoids are commonly used. In this study, Particle Flow in 2 dimensions (PFC2D) was implemented and the code which is a simplified DEM code because there is the restriction that particles can be only circular shaped. Because of this fact, overview over DEM will be focused on aspects, which are applicable to PFC2D software.

The DEM is gaining much popularity over the past two decades in the geomechanics field over the continuum methods like the finite element method (FEM). The use of the discrete element modeling is especially increasing among the researchers. However, the usage of DEM in industry is less commonplace. It is likely to change with increasing computing power. Reasons of preference of the DEM over the finite element method (FEM) or the finite difference method (FDM) are discussed below (Geng, 2010):

- In the DEM the evolution of material which is dependent on a scale during failure as well as large-scale deformation is preferably determined through particle-to-particle interaction mechanism.
- In the DEM continuum material behaviour specifications combine multiple physical processes into complex functions that are difficult to apply to natural, inhomogeneous materials like soil.
- DEM explicitly describes the dynamics of assemblies of particles and the micro-mechanical interaction processes between grains.

- The FEM is not able to replicate large displacements and rearrangements which are crucial characteristics of state changing processes of granular material.
- The DEM is better in modeling a discontinuous material than the other numerical tools such as the FEM, FDM and BEM (boundary element method).
- The DEM enable to monitor the interaction between discrete particles contact by contact.
- The DEM can be combined with other numerical methods, to solve various application problems (e.g. flow in ground, liquefaction etc.).
- Complex behaviour is captured by separately acting algorithms which mimics physical processes.
- DEM allows a more meticulous study of the micro-dynamics of powder flows than it is usually not even possible using physical experiments.

  Other strengths, which describe the DEM, but not distinguish it from other available techniques are:
- Results constitute a virtual laboratory.
- It contains explicit algorithms for the separate physical dynamic or quasi-static processes (e.g. earthquake analysis, machine foundation etc.).
- Used in analysis, testing, and research in various fields such as engineering, mechanics of materials, chemistry or agriculture.

DEM method also has some drawbacks. It is computationally expensive. For instance, typical real soil assembly contains billions of particles, but contemporary DEM assemblies must be usually scaled (magnification of particle diameter) in order to sustain the simulation for sufficiently long time. Also the DEM model need calibration phase which sometimes is complicated. Conducting experiments to define material properties and contact mechanics is a complex and difficult process too. This is the reason why constructing realistic DEM particle beds involve deep expertise, engineering intuition and proper analysis of physical tests results.

5.2.1. Key Problems in the 2-D DEM Modelling

All the DEM simulations performed in this thesis are carried out in two-dimensional (2D) environment. Besides there are limitations associated directly with the distinct element method, there are multiple problems related to 2D to mimic

physical phenomena by the distinct element method. The main restrictions of using two-dimensional DEM codes like PFC2D are:

(1) the concept of stress and strain,

(2) packing,

(3) porosity

(4) mass properties.

In details, these are presented in the user's guide of Itasca (2008). In this study, we focused on validation of porosity based on physical experiments calibration. The porosity computation in 2D codes is an area-based calculation which is in contrary to the volume based attitude, commonly applied in three-dimensional code.

In the real porous materials, porosity is observed to be higher than in 2D DEM simulations. It is due to the fact, that soil particles have a blockade, before reaching an optimal packing state. Bridging or arching of flowing solid particles is a serious hazard which is also easier to achieve in the 3D rather than the 2D simulations. Another clue problem of modeling in the two-dimensional codes is that, the centroids of all spheres are aligned in a single plane. This column like structure hardly occurs in reality. Moreover, the percolation which refers to the movement and filtering of fluids or small particles through porous materials can be conduct easily in the 3D simulations. It is proven that small particles are capable of percolating through the 3D assemblages, composed of larger particles. However, this process cannot happen in the 2D assemblies regardless of relative particle sizes.

5.2.2. Principles and Theory of Discrete Element Method

In the DEM, particles are interacting in a dynamic process. Whenever internal forces are in balance, state of equilibrium is developing. To find contact forces and displacements of an assembly under stressed conditions, tracing of movements of distinctive particles is used. Motions result from propagation through the grain system of disturbances. Disturbances are caused by a particular wall and particle movement and/or body forces.

In the DEM, the solution outline is the same as the one used in explicit finite difference method for any continuum analysis. The time-step chosen for the DEM simulation needs to be small enough so that during a single time-step, disturbances can

propagate just to neighbouring particles. The forces acting on any particle are established solely by its interaction with the particles in contact. The proper time-step can be chosen by the user or the DEM program, that can assign suitable time-step by means of a function of the physical properties of the discontinuum system. The advantage of usage explicit methods to solve geomechanics problems over implicit methods is that, the explicit DEM makes it possible to simulate a nonlinear interaction and behaviour of a great amount of particles with non-excessive computational power or the need for iterative procedure.

There are two basic law, upon which all DEM calculations are made. First one is the Newton's second low and the other is a force-displacement low at the contacts. Newton's second low has a function of law of motion of each particle which has to determine the motion of each discrete material from the contact and body forces acting upon it. Whereas, the force-displacement law is implemented to update the contact forces emerging from the relative motion at each contact.

5.2.3 Use of the DEM within Geomechanics

Use of the DEM in geomechanics is constantly rising and the subject was deeply investigated by O'Sullivan (2011). She pointed out the linear increase in the number of scientific papers, related to DEM after 1996 (Figure 5.1).

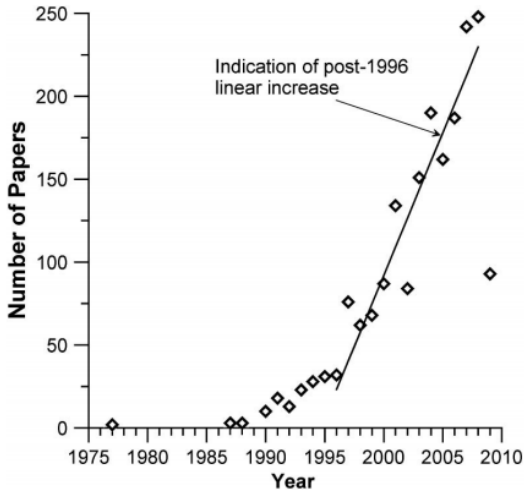

Figure 5. 1. Annual rate of discrete element modeling publications identified by using the approach of Zhu et al. (2007). (Source: O'Sullivan, 2011)

The basic assumption of the method is that the material consists of separate, discrete particles of different shapes and properties. Some examples are:

- liquids and solutions
- bulk materials in storage silos (cereal)
- granular matter (sand, gravel)
- powders
- Blocky or jointed rock masses

The distinct element method can be used to simulate behaviour of both cohesionless soil (Arrayo et al., 2011) and cemented granular material mass in which the material is represented by individual bonded particles (Potyondy and Cundall, 2004). The clay DEM simulations are less common because of the complexity of the surface interaction forces and the particle geometry however scientists like Anandarajah (2003) and Lu et al. (2007) successfully simulate the cohesive soil behaviour.

5.2.4. DEM Software

There is a wide variety of choice of software which is based on DEM. There are both open source and commercial numerical programs available nowadays.

Non-commercial software includes codes such as BALL and TRUBAL, dp3D (discrete powder 3D), ESyS-Particle, PASIMODO, LMGC90, LAMMPS, LIGGGHTS, Woo and the most popular YADE. Yade is modular and extensible code of DEM algorithms written in c++. Tight integration with Python gives flexibility to simulation description, real-time control and post-processing, and allows introspection of all the internal data. OpenMP enables to run in parallel on shared-memory machines.

Commercially available DEM software packages include: Bulk Flow Analyst, PASSAGE, LS-DYNA, StarCCM+ , UDEC, , SAMADII/DEM, DEMpack and the most popular software solving problems relating to geomechanics - PFC (2D and 3D).

5.3. Particle Flow Code in Two Dimensions

In this study, Particle Flow Code in 2D (PFC2D) was implemented to carry out all the discrete element method simulations. In this section, theoretical as well as

practical aspects of use of PFC2D will be discussed with particular attention given to subjects directly related to areas of interest of this study.

5.3.1. Basic Mechanics of PFC2D

A model in PFC2D is composed of elements like circular particles called also balls, clumps, cluster, joint sets and walls. Walls are used to define the boundary conditions as well as to help to generate an assembly of particles. The servo-controlled walls are useful tool, while calibration of stiffness parameters in the DEM (biaxial, brazilian tests). By means of walls compaction and the proper state of stress can be achieved too. Walls are built in PFC2D model in global coordinates as a line segments (straight or circular lines). Particles are generated in the space according to global coordinates too. Both balls and walls are identified by identity (ID) number.

There are few basic components of any problem, which need to be specified in PFC2D model. Firstly, an assembly of particles, contact behaviour, material properties, boundary and initial conditions need to be specified carefully. In order to construct a realistic model in the DEM, many parameters need to be taken into account. In Table 5.1, DEM parameters are listed and divided into 3 groups. Next step for problem solving with PFC2D is loading, solution and secondary modeling and last but not least, interpretation of results. The user needs to define location and size distribution. Usually scaling need to be applied, because of the limited computational power. We need to first understand the realistic response of the physical problem that we want to simulate by means of the DEM program like PFC2D. Based on that knowledge, the contact model and associate material properties can be assigned. Boundary and initial conditions are introduced to the model and they are defined for in-situ state. The sheme of general procedure for simple analyses is illustrated on the Figure 5.2.

Table 5. 1. Neccessary parameters to build a model in the DEM.

Physical	Mechanical	Other
Particlw size and shape	Normal/tangent stiffness	Gravity
Specific gravity	Contact friction coefficient	Porosity (derived quantity)
Contact area radius	Creep viscosity	Density (derived quantity)
Dilating sphere radius	Normal viscosity	Coordination number (derived quantity)

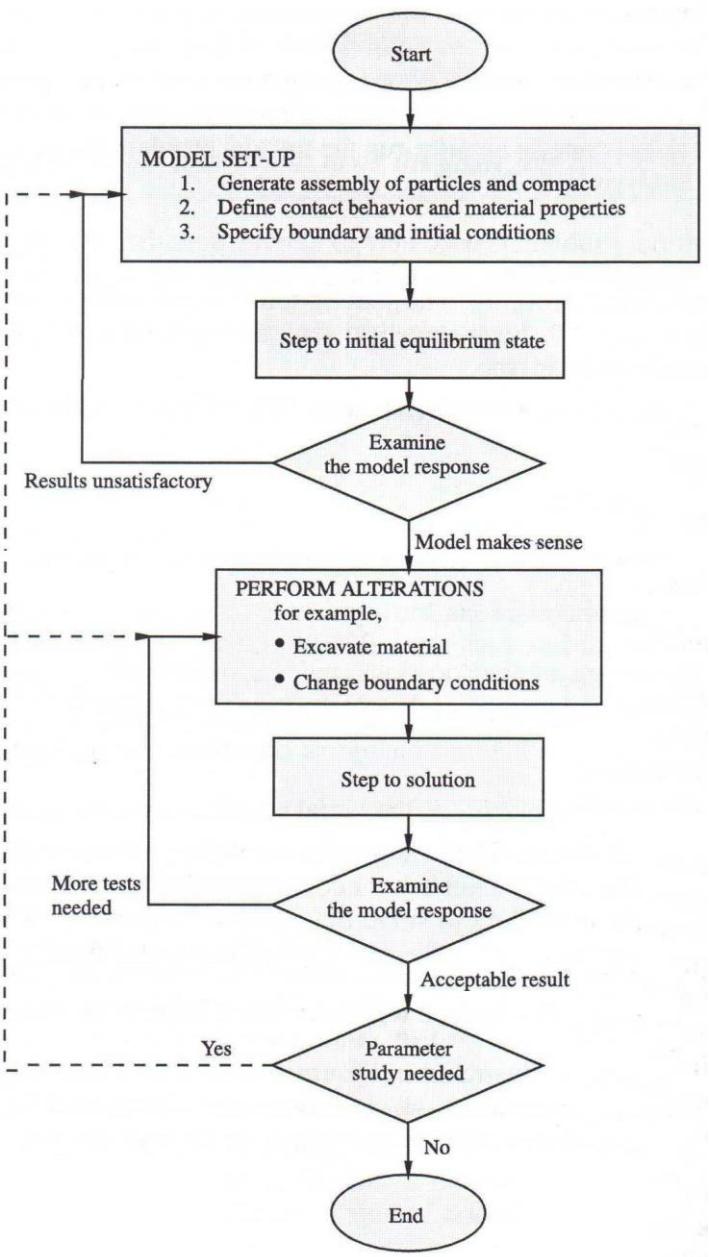

Figure 5. 2. Flow chart for the general solution procedure in PF2D.
(Source: Itasca, 2008)

5.3.2. Particle Generation

There are various methods to generate a particle assembly in PFC2D. Particles can be specified in exact location, independent of existing particles or can be placed by specifying larger number of particle (generate command). The second option is influenced by other objects and overlapping is impossible. There are regular and irregular assemblies. Regular one is the collection of particles that contains repeating

patterns in contrary to irregular assemblies which are chaotic. Usually, in geomechanics we use the second type because of nature is not regular. For instance, soil is highly anisotropic medium as farther of geotechnics, Karl von Terzaghi, said: *"Unfortunately, soils are made by nature and not by man, and the products of nature are always complex… As soon as we pass from steel and concrete to earth, the omnipotence of theory ceases to exist. Natural soil is never uniform. Its properties change from point to point while our knowledge of its properties are limited to those few spots at which the samples have been collected. In soil mechanics the accuracy of computed results never exceeds that of a crude estimate, and the principal function of theory consists in teaching us what and how to observe in the field."* The generation of irregular assembly is random; however, some structures like regular patterns can be assigned as well. Because in this study, the irregular assembly, which is to mimic the soil is implemented, the irregular particle assembly approach is presented thoroughly.

There is not the only proper way to create an irregular assembly of circular particles. The main objectives are to obtain a desired porosity and equilibrium state of particles. As the procedure to ensure if the assembly is in equilibrium is relatively straight forward though porosity in two-dimensional code is a huge unknown. Two methods of particle generation in enclosed area are the most common in use:

1. Radius expansion
2. Explosive repulsion

The boundaries remains fixed during a process in contrary to compaction methods, when walls are moving till assembly within them will reach desirable state. In both methods equilibrium is reached locally.

For the purposes of this work, radius expansion approach was chosen and applied to generate assembly for biaxial tests and CPT simulations in PFC2D. A population of particles (specified number) is created within a given area, bearing in mind that particles cannot overlap (smaller radius than desired one). Radius multiplayer, *m* is needed to be specified in order to obtain a specified porosity in the 2D DEM code. The porosity, *n* in PFC2D is defined by:

$$n = 1 - A_p/A \tag{5.1}$$

where,

A_p = sum of particle areas;

A=container area.

Hence the multiplayer for all particles m is expressed by:

$$m = \sqrt{\frac{1-n}{1-n_0}} \tag{5.2}$$

where,

n_0 = ‘old’ porosity (before radius expansion);

n = ’new’ porosity after radius expansion.

The derivation of m is explained step by step in Itasca User’s Manual (2008).

5.3.3. Contact Models

Particles are interacting with walls - Fig. 5.3(a) and with eachother – Fig. 5.3(b) and create contacts. Simply two entities are needed to create a contact, either ball-ball or ball-wall contact.

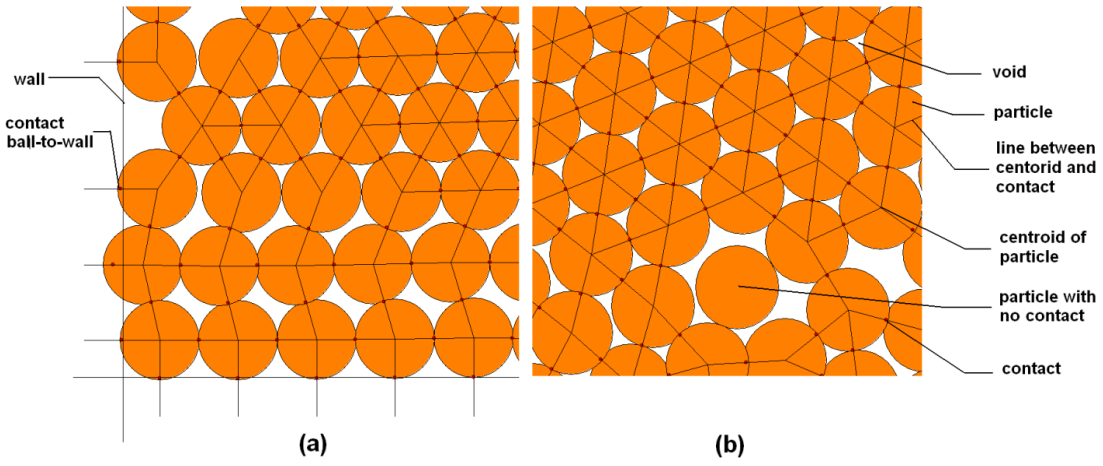

Figure 5. 3. Basic contact model in PFC2D for (a) walls, and (b) particles.

Each contact model can contain:

1. A contact-stiffness model
2. A slip separation model
3. A bonding model

In order to simulate a granular material, no bonding is needed. A contact-stiffness model provides an elastic relation between the contact force and relative displacement. The concept of contact forces and displacements is showed in Figure 5.4.

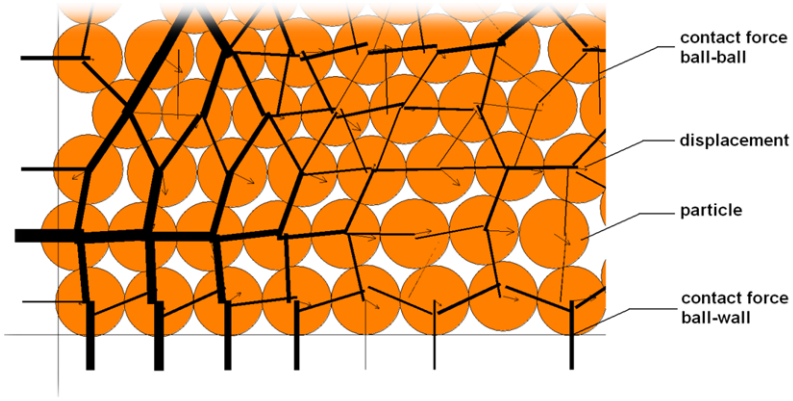

Figure 5. 4. Contact forces and displacements in PFC2D.

Normal and shear components of force and relative displacement relates directly to normal and shear stiffness. Shear components are related by tangent stiffness and normal components through normal (also called secant) stiffness. In general, normal contact force relates total component whilst shear contact force relates the increment of shear force to the increment of shear displacement. Normal contact force (F^n) can be explained by equation:

$$F^n = K^n U^n \tag{5.3}$$

where,

K^n = normal stiffness at the contact;

U^n = relative contact displacement.

Shear contact force (F^s) is described by:

$$\Delta F^s = -k^s \Delta U^s \tag{5.4}$$

where,

k^s = shear stiffness at the contact;

U^s = relative contact displacement.

However, the total shear component of contact force can be calculated by summing the old shear force, $F^{s\,old}$ at the start of the timestep with the shear elastic force increment, ΔF^s.

$$F^s \leftarrow F^{s\,old} + \Delta F^s \leq \mu F^n \tag{5.5}$$

where,

μ = friction coefficient.

5.4. Basic Fluid Analysis Option

In this study, the DEM sofware need to represent a saturated soil tested in laboratory. Therefore, coupling of fluid-particle is neccessary to implement. ITASCA optional feature called 'Basic fluid analysis option' was chosen to support coupled fluid-solid modeling. The sheme, which is based on well recognized SİMPLE sheme developed by Patankar (1980), solves the locally averaged two-phase mass and momentum equations for the liquid velocities and pressures. More information can be found in Boulliard et al. (1989). In general, the solutions can be considered as solving Navier-Stockes equation for a fluid, which affects a solid phase. It can be applicable in fully saturated, fixed, fluid domains. The internal discretization is regular (coarse-grids). Fluid cells are represent by rectangules. The essential formulation responsible for coupling with DEM code (in our case PFC2D) assumes that particle radius is minute compared to fluid grid. There are variety of options avaiable for boundary conditions. The scheme can be applied to a diversity of engineering problems, including sand sedimentation, sand transport (slurry flow), fluidized beds, pneumatic conveying or simulating saturated conditions, as required in this thesis. They will be mentioned in the following part. Details about all components of 'Basic fluid analysis option' are described in Optional Features PFC2D tutorial (Itasca, 2008).

5.4.1. Theoretical Considerations

As we are interested in average effects over many particles, Navier-Stokes equations need to be modified to include the effect of a particulate solid phase mixed

into the liquid. Following equations can characterize those effects in terms of porosity *n* and a coupling force, f_i (Itasca, 2008):

$$\rho f \frac{\partial \in v^{\rightarrow}}{\partial t} + \rho f v^{\rightarrow} \cdot \nabla(\in v^{\rightarrow}) = -\in \nabla p + \mu \nabla^2 (\in v^{\rightarrow}) + f \tag{5.6}$$

$$\frac{\partial \in}{\partial t} + \nabla \cdot (\in v^{\rightarrow}) = 0 \tag{5.7}$$

where,

ρf = density of the fluid;

$\in$ = porosity;

p = fluid pressure;

μ = dynamic viscosity;

$v^{\rightarrow}$=fluid velocity;

$f_b^{\rightarrow}$= body force per unit volume.

However in porous flow we observe two velocities. First one is the intersticial velocity $v^{\rightarrow}$ and the second one Darcy velocity called also macrosopic and denoted as $\in v^{\rightarrow}$. The first one is an actual velocity which a parcel of fluid hasas it moves through a pore space. The other, is the volumetric flow rate per unit of cross area (non-physical velocity). Porosity is another important part of a sheme as it is applied in porous medium. The porosity $\in$ is explained as:

$$\in = 1 - \frac{V_p}{V} \tag{5.8}$$

where,

V = volume of a fluid element;

Vp = total volume of particles within the considered element.

V_p can be defined as:

$$V_p = \frac{\pi}{6} \sum_{j=1}^{N} (d^j)^3 \tag{5.9}$$

where,

N = total numer of particles in an element;

d^j = diameter of the j-th particle.

As mentioned before, body force per unit volume, $f_b^{\rightarrow}$, called also a ‘drag force’ can be defined as:

$$f_b^{\rightarrow} = \beta U^{\rightarrow} \tag{5.10}$$

where,

β= coefficient;

$U^{\rightarrow}$=average relative velocity between particles and the fluid, written as:

$$U^{\rightarrow} = u^{\rightarrow} - v^{\rightarrow} \tag{5.11}$$

where,

$u^{\rightarrow}$= average velocityof all particles in a given fluid grid, defined as follow:

$$u^{\rightarrow} = \frac{1}{N}\sum_j u^{\rightarrow j} \tag{5.12}$$

The sum of average velocities covers all particles in a fluid element. Coefficient β depands on the porosity and the whole procedure of determining it, is described in literature (in detail by e.g. Tsuji, 1993 or summary of method in Itasca, 2008).

The equations of motion for discrete materia in PFC2D were mentioned in the previous paragraph. However while coupling with fluid they need to be complemented with the additional terms:

$$\frac{\partial u^{\rightarrow}}{\partial t} = \frac{f_{mech}^{\rightarrow} + f_{fluid}^{\rightarrow}}{m} + g \tag{5.13}$$

where,

$u^{\rightarrow}$=particle velocity;

m = particle mass,

$f_{mech}^{\rightarrow}$= sum of additional forces;

$f_{fluid}^{\rightarrow}$=total force applied by the fluid on the particle.

Figure 5.5 shows how calculation is done, within the fluid sheme look like in entire PFC2D (Itasca, 2008).

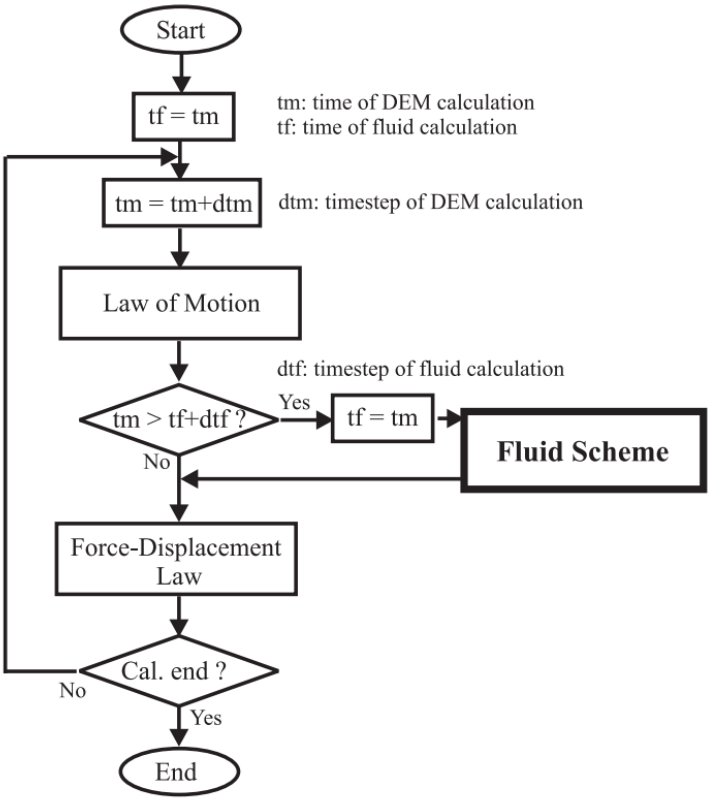

Figure 5. 5. Flow chart in PFC2D.
(Source: Itasca, 2008)

As we can notice from the chart, the sheme is invoked at each fluid time step, t_f, betwixt mechanical DEM calculation including law of motion and force-displacement law. Usually mechanical time step for the DEM, t_m is bigger than that for the fluid. If t_m equals or exceeds the predicted t_f+dt_f, then the fluid sheme is accomplished. The convergence and calculation process of the fluid calculation is showed clearly in Figure 5.6 (Itasca, 2008).

Boundary conditions are obligatory to be specified along all the boundary of the fluid region. The boundary can be just orthogonal in shape, as well as in fluid grids. For each boundary, different boundary conditions can be specified:

(1) pressure,

(2) velocity,

(3) slip or nonslip.

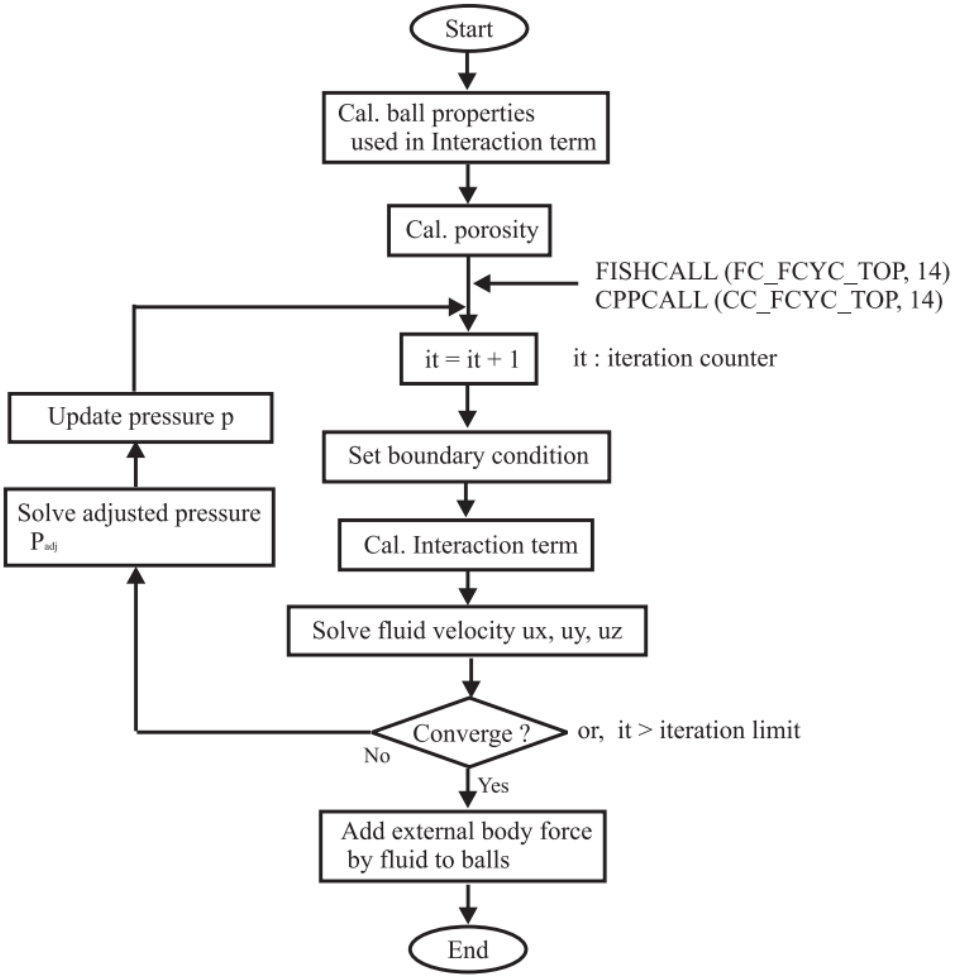

Figure 5.6. Flow chart of the fluid sheme.
(Source: Itasca, 2008)

CHAPTER 6

CALIBRATION OF PHYSICAL PROPERTIES OF THE DISCRETE MATERIAL USING BIAXIAL TESTS

6.1. Introduction

In this chapter, the calibration of the properties of the discrete material to the properties of the tested soil was conveniently done by comparing real and simulated triaxial with the DEM biaxial tests. The material properties that required calibration were normal and tangential stiffness and interparticle friction. The trial and error procedure was used.

In first part, the background of calibration procedure is presented. The numerical analyses were undertaken using the Particle Flow Code in 2D (Itasca, 2008). The laboratory data, which was used for the numerical simulations is presented in Chapter 4.

In the second part, the results of comparison of experimental and numerical tests are shown. A good match between the experimental data and the two-dimensional DEM results is observed.

Finally, further numerical tests were run to determine the peak friction angle (ϕ) of the material assembly in order to verify the validity of the input variables. The set of parameters is estabilished for furher DEM modelling.

6.2. Calibration Procedure

The inverse modeling with unknown micro-properties was implemented in this study (Itasca, 2008). It is a very suitable method to match the given laboratory results of the soil investigated in this research, The detailed information about the method is given in Chapter 4.

In the laboratory we first performed drained triaxial tests. The results of the drained triaxial tests are given in Chapter 4. Afterwards we have done numerical

biaxial tests in PFC2D environment. Trial and error procedure was used after deciding on geometry of chamber and discrete material.

This procedure allowed us to estimate the three microscopic parameters given below:

1. normal stiffness (k_n),
2. tangent stiffness (k_s),
3. friction coefficient (μ).

These parameters led us to reproduce the macroscopic behaviour, characterized by elasticity modulus (E) and Poisson's ratio (ν). The stress-strain curve was obtained from the laboratory drained triaxial tests and the numerical biaxial tests, respectively with a constant confining stress of 100 kPa.

In order to verify the validity of the model's input variables, further numerical tests were run to determine the peak friction angle (ϕ) of the assembly, which is designed to simulate sand.

Calibration technique consists of two steps. These steps are biaxial tests and simple slope tests. Basically in this study, numerical biaxial tests were performed. Afterwards, it was validated by simple numerical test for slope angle. Biaxial test procedure by the DEM is composed of:

1. Sample preparation
2. Computing and controlling the stress state
3. Monitoring the test during the loading proccess
4. Analysis of the numerical test results.

6.2.1. Sample Preparation for DEM Biaxial Tests

The tested sand in laboratory is represented by the discrete circular particles in PFC2D. The sand is modeled as a group of uniformly sized spheres and considered theoretically. Radius expansion method, which is explained in Chapter 5, is employed to generate an assembly with a specified particle size, porosity and sample size. The sufficient number of particles, suggested by many researchers (e.g. Kruyt, 1993) to obtain meaningful biaxial tests results, is known to be higher than thousand elements. Following the chosen particle-generation approach, assembly of 5283 spheres of 1mm diameter was created. This is shown in Figure 6.2(a).

Porosity is a crucial factor affecting the initial stress state (σ_{vo}) of the assembly. Initial porosity of the specimen in triaxial tests was set as 0.16. It was based on the limit value of the porosity for the specimens, such that if a higher value of the porosity is taken, particles do not exchange contact forces (Utili and Nova, 2008) as shown in Figure 6.1. From Figure 6.1, we can conclude that porosity of 0.17 is a limit value for triaxial tests in 2D simulations. At the level of porosity of 0.17, the relative density is close to 100%. Initial dimensions of a rectangular cell, constructed of four rigid frictionless walls in which biaxial tests were conducted are 100 mm by 50 mm. Sample size depicted the actual cross-sectional area of the triaxial cell; though the discrete material was scaled and simplified. The sample is shown in Figure 6.2(a) which reproduces the actual triaxial sample shown in Figure 6.2(b). The actual triaxial apparatus is depicted in Fig. 6.2(c).

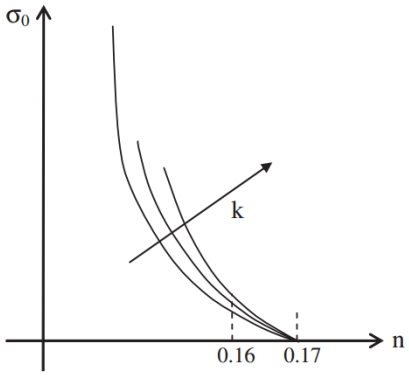

Figure 6. 1. Qualitative relationship between porosity and initial stress for various contact stiffnesses. n = 0.16 is the porosity value adopted for all the calibration simulations. (Source: Utili and Nova, 2008)

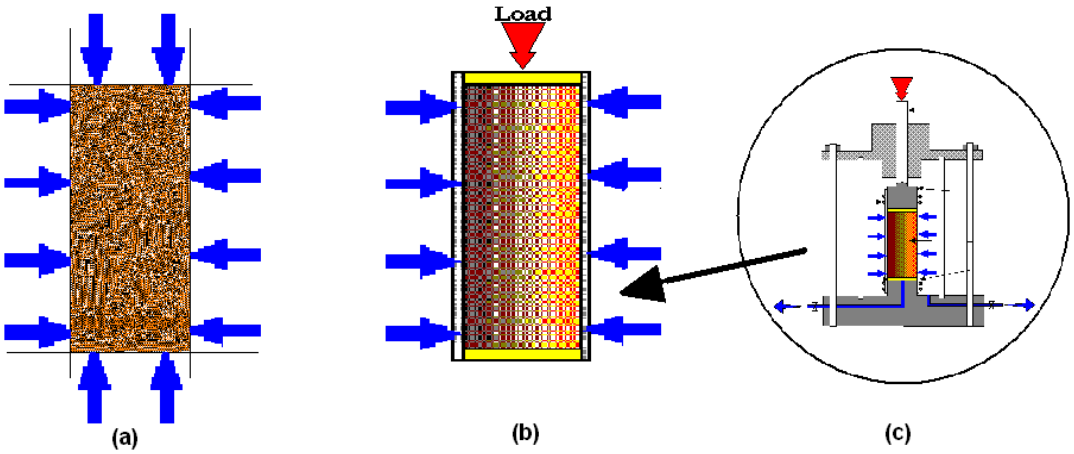

Figure 6. 2. (a) Biaxial sample, (b) triaxial sample, (c) triaxial apparatus.

6.2.2. Computing and Controlling the Stress State

Throughout the loading process, the confining stress of 100 kPa was maintained constant by adjusting the lateral-wall velocities using a numerical servomechanism, as explained in ITASCA, 2008. The stresses are calculated by taking the average wall forces divided by appropriate areas ($\sigma=F_i/A_i$). The strains (ε) in both x- and y-directions are computed using the equation given below:

$$\varepsilon = \frac{L-Lo}{0.5(Lo+L)} \tag{6.1}$$

where,

L = current specimen length in corresponding direction;

L_o = initial sample length in that direction.

The mean confining (σ_c) and axial deviatoric stress (σ_d) along with axial (ε_a) and volumetric strain (ε_v) were monitored and recorded during the test.

6.2.3. Monitoring the Test during the Loading Proccess

Throughout the loading process of the model, the confinig stress was held constant by means of adjusting the velocities of lateral walls. The numerical servomechanism was implemented. The function was called once in every step of calculation. The algorithm is explained in Section 3.10.5 in thr FISH in PFC2D volume of Itasca manual (2008).

6.3. Results of the Biaxial Tests

The stress-strain curve obtained from the DEM triaxial simulation was compared with the laboratory tests with an identical confining stress of 100 kPa, as shown in Figure 6.3. A good match was observed between the experimental data and the two-dimensional DEM results. The DEM stress-strain curve has its peak at the same axial strain as laboratory experiments (7.7%). Nevertheless, the PFC simulations could not reflect the change of the elastic modulus in the actual testing. At initial axial strain, the

deviatoric stress is higher for the DEM than for the laboratory results. From 4.5 to 9.5%, the results are the same for both.

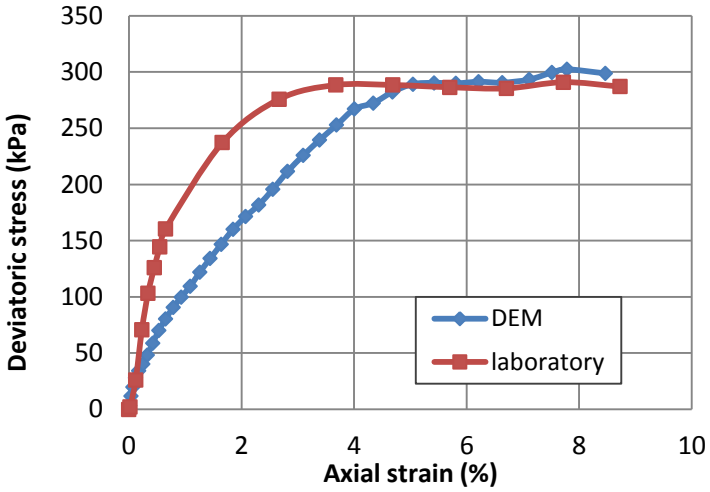

Figure 6. 3. Stress-strain curves of a laboratory triaxial and DEM biaxial tests for confining stress of 100 kPa.

The results of volume change versus axial strain are shown in Figure 6.4.

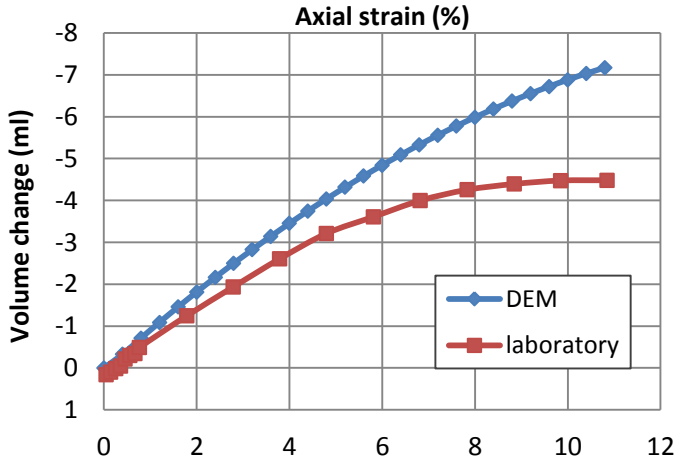

Figure 6. 4. Volume change vs axial strain of laboratory triaxial and DEM biaxial tests for confining stress of 100 kPa.

The volume change for the DEM is higher than that of the laboratory experiments. It needs to be taken into account that biaxial tests were performed in two-dimensional environment, in contary to the 3D real conditions during laboraory triaxial tests. Both numerical and experimental tests indicated that sample was loose sand. The loose sand

decreases in volume, while shearing. Stress-strain curve and volume change behaviour have confirmed that argument. However the topic of volume change is much more complex and requires multiple triaxial and biaxial tests, in order to determine a critical void ratio for the tested soil. For the 2D simulation there are more limitations, which were listed in Chapter 5 which cause ambiguity in interpreation of the test results.

In Section 4.2, elasticity modulus was calculated, based on the triaxial test results under drained loading conditions. The same procedure was used to calculated modulus of elasticity from the DEM results. The DEM and the laboratory results are compared and summarized in Table 6.1. The secant modulus from zero deviator stress up to ½ ($E'_{1/2}$) or 1/3 ($E'_{1/3}$) of peak deviatoric stress are in better agreement than the initial elasticity modulus obtained through tangent method. The errors according to laboratory values are 8, 27 and 40%, respectively.

Table 6.1. Calculation of elasticity modulus from stress-strain curve for initial confining pressure of 100 kPa using laboratory and DEM results.

Initial confining pressure of 100 kPa	E'_{init}	ε_a at ½ of peak σ_d	½ of peak σ_d	$E'_{1/2}$	ε_a at 1/3 of peak σ_d	1/3 of peak σ_d	$E'_{1/3}$
[kPa]	[MPa]	[%]	[kPa]	[MPa]	[%]	[kPa]	[MPa]
Laboratory	**18.19**	3.99	288.40	**7.23**	2.66	275.8	**10.37**
DEM	**25.30**	4.01	267.09	**6.67**	2.67	201.7	**7.55**
$\Delta E'_i = E'_{lab.} - E'_{DEM}$	**-7.11**			**0.56**			**2.82**
$\Delta E'_{\%} = \frac{\Delta E'_i}{\Delta E'_{lab.}} 100$	**-39.1%**			**7.7%**			**27.2%**

6.4. Verification of Peak Friction Angle

In order to verify the validity of the input variables, further numerical tests were run to determine the peak friction angle (ϕ) of the material assembly. Generally peak friction angle for dry, loose material is considered as the angle of repose (Lambe and Whitman, 1969). Laboratory tests by Skinners (1969) revealed that the peak friction angle does not increase linearly as a function of friction coeefficient (μ). Therefore a great deal of numerical simulations must to be done to establish the proper angle of repose of a slope. Particular attention must be paid to the problems related to usage of angle of repose of a material to estimate macroscopic soil parameter like friction angle.

The main uncertainty and difficulties that one can encounter during an investigation are:

(1) failure mechanism,

(2) uncertain porosity,

(3) particle angularity,

4) uncertain confining stress.

Numerical model consisted of the discrete material defined during biaxial tests and was formed by dropping the balls in the corner of a box under the gravity. The Mohr-Coulomb friction angle based on laboratory triaxial test chamber results of the soil for initial vertical stress of 100 kPa and 200 kPa of 36^0 was compared with the numerical model. As shown in Figure 6.5, an excellent match is found between experimental and numerical results.

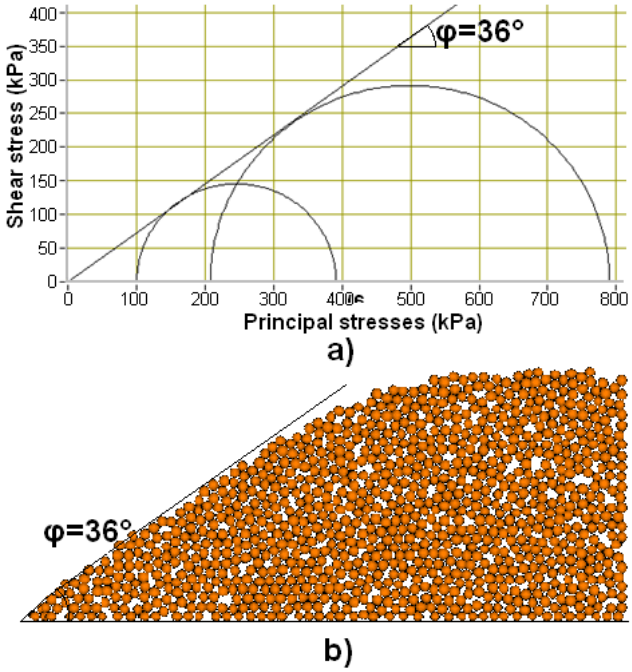

Figure 6. 5. Comparison of friction angle from (a) Mohr-Coulomb envelope (b) DEM simulation.

Nevertheless, the PFC simulations could not reflect the change of the elastic modulus in the actual testing. However, by a trial and error procedure, the best set of parameters were determined to match the laboratory results. Moreover, the calibration stage exposed that different combinations of parametric values may result in a

compatible discrete material behavior. Accordingly, there is no unrepeatable set of values that best matched the laboratory data. For the CPT simulations, a set of parameters is listed in Table 6.2.

Table 6. 2. Granular deposit simulation data.

Particles	
Diameter (d)	10 mm
Friction coefficient (μ_p)	1.0
Density (ρ)	2650 kg/m^3
Normal stiffness (k_n)	$6 \cdot 10^6$ N/m
Tangent stiffness (k_s)	$1 \cdot 10^6$N/m
Ratio $\alpha = k_s/k_n$	1/6

CHAPTER 7

CALIBRATION OF DEM CPT MODEL

7.1. Introduction

Once the prediction of the drained triaxial tests was verified, series of calibration attempts were extracted in order to evaluate any further prediction capabilities of the DEM model.

In this chapter, we primarily focused on the calibration of the model parameters in simplified conditions. The basic equation to detemine the cone penetration resistance ($q_{c)}$ values was implemented. Morover, particles had bigger size as well the velocity of cone was icreased significantly. The analysis given in this chapter enabled us to select timestep history interval, the boundary conditions, the fluid grid size and the boundary conditions for fluid. The preeliminary study on the grain size was performed.

Next, the scaling factor was implemented into the equation to determine the cone penetration resistance. The scaling factor was a crucial element for the purpose of this study, due to limitations of two-dimensional software. Therefore, it enabled us to compare the results obtained from the laboratory CPTs (3D) and numerical DEM simulations (2D).

Multiple attempts of the CPT simualtions were performed in order to find suitable grain size and to validate the porosity in two-dimensional media. Scaling factor was implemented in this stage of the analysis and other assumptions were necessary to make a suitable correlation between laboratory and numerical analysis.

7.2 Calibration of the CPT Model

Below, we have listed the calibration of:

1. Calculation steps
2. Wall on top of the soil
3. Boundary conditions

4. Computational fluid grids
5. Prticle size

7.2.1. Calculation Steps

A simplified CPT model was created to determine the history recording of forces accumulated on the cone pushed downwards into the discrete assembly. In the laboratory, we obtained the q_c values recorded at every 2 cm to a depth of 1.1 - 1.3 m . The goal is to check, whereas the forces recorded on the cone surface at every 2 cm are enough in PFC2D. We have to bear in mind that q_c in the DEM program has a pluviating nature and need to be smoothed.

Box dimensions were set to be 1.7x1.44 m which were the same as in the laboartory. Cone diameter was set as 10 cm and the cone velocity was kept constant as 1m/s. Cone and box were built with the aid of wall logic in PFC2D. The stiffness and friction of the cone were assigned as for the steel. Majority of the researchers prefer to use a frictional cone with the part of sleeve 30 cm above cone frictionless (e.g Arrayo et al., 2011). It is depicted in Figure 7.1(a). In this study fricional cone and sleeve were implemented as illustrated in Fig. 7.1(b). It took 2000 steps to penetrate the cone into the sand till the depth of 1m. The particles had properties founded by the calibration of micro properties of discrete material derived in Chapter 6.

To obtain the cone penetration resistance, the force in the Y-direction was measured during the whole penetration process. For the simple calibration steps, the cone penetration resistance was calculated as an average force accumulated at cone in Y-direction (F_y) divided by area of cone (A_c) . It is very simplified procedure to investigate other factors, such as boundary conditions affecting simulations. Assumption is fair enough because for some steps of calibration the formula was implemented to all cases. Scaling factor, S will be introduced to analysis, after estabilishment of:

(1) history steps,
(2) boundary conditions,
(3) wall on the top,
(4) particle diameter.

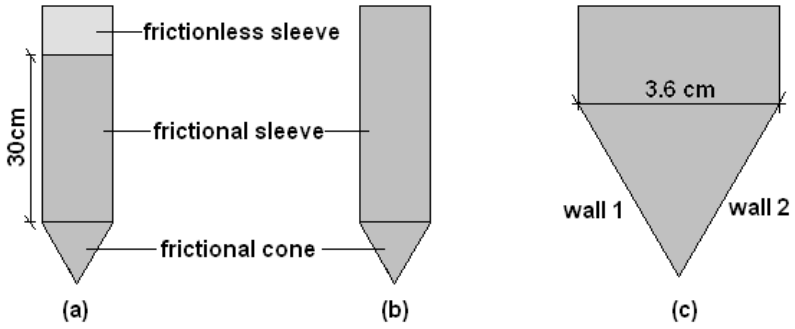

Figure 7. 1. (a) Simplified CPT model by Arrayo et al., 2011, (b) simplified CPT model by Bakunowicz and Ecemis, 2014, (c) notation of walls.

Results of timesteps history intervals are shown in Figure 7.2 and 7.3. The notation of walls 1 and 2 is shown in Figure 7.1(c). The results were gathered for different history intervals. Based on the amount of timesteps and velocity of cone we concluded that following intervals of history recording were obtaind for each command:

Skip 0 – 0.5 cm

Skip 2 – 1.0 cm

Skip 4 – 2.0 cm

Skip 8 – 4.0 cm

It means that after using, for instance, command ‘Skip 2’ force will be recorded every 1 cm. The ‘Skip’ command was used to make the calculations more compuationally efficient. A complete describtion of the commands that control PFC2D are gathered in Itasca - Command Reference, 2008.

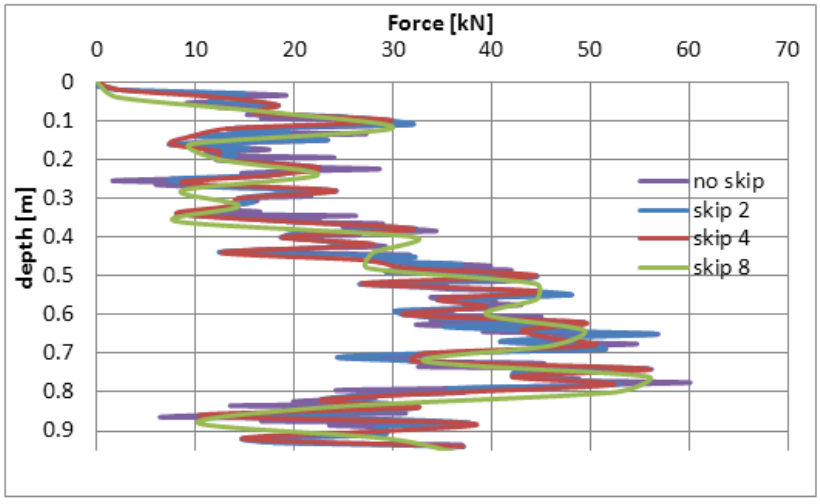

Figure 7. 2. Influence of timesteps of history on wall 1.

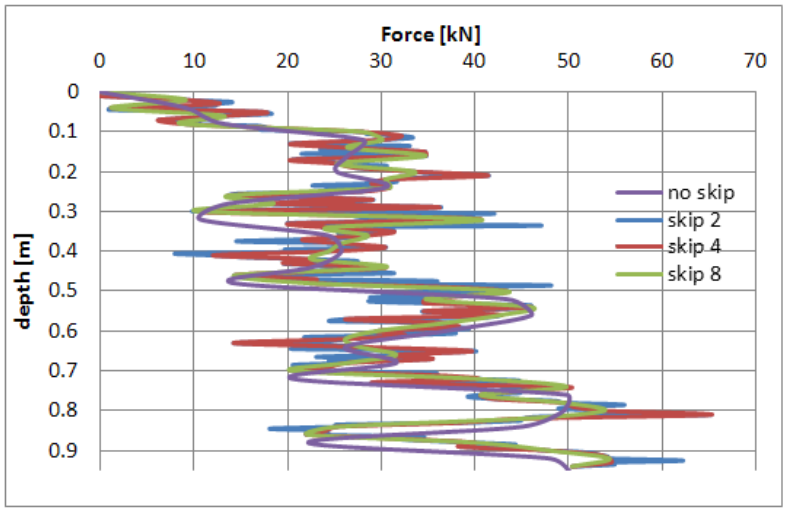

Figure 7. 3. Influence of timesteps of history on wall 2.

From Figures 7.2 and 7.3, we can conclude that at every 2 cm recording of forces accumulated on the walls, which are simulating the cone, is fairly enough. To obtain history recording in each 2 cm, the command 'skip 4' was used in PFC2D program. In the further CPT DEM simulations, 2 cm interval was chosen. Another conclusion reached from this analysis is that the forces accumulated on right and left wall are much different at the same time. For chosen history interval of 2 cm, forces on wall 1 and 2 are shown in Figure 7.4. One reason of this situation is that, it is much simplified case and the cone is not in contact with the stable amount of particles at every moment. Therefore after comparing the results from Figure 7.4 for wall 1 and 2, we have concluded that a sum of Y-forces as an average of forces acting on the cone is obligatory.

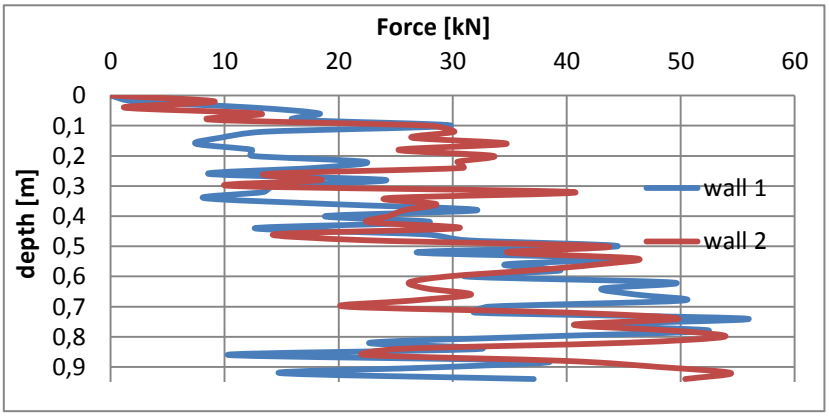

Figure 7. 4. Forces accumulated on cone with 2cm history interval for wall 1 and 2.

7.2.2 Wall on Top of the Soil

The assembly of discrete particles is unbonded. While performing a cone penetration simulations, the particles after touching the cone surface are getting scattered and their direction changes randomly. The wall on top of the soil would stop this mechanism, though there are other cirsumstences like the porosity in the 2D, which needs to be taken into account.

In this study, we have decided to use a moving wall on the top of the soil. Afterwards, it will be called “wall on top” . The schematic view of the cone, box and wall on top is shown in Figure 7.5. The simple wall logic to create walls and cone was used in PFC2D. Due to the fact that in the 2D medium while penetrating the cone into the soil, the porosity is decreasing drastically. In our case, the laminar box simulated in the 2D has the area of 2.7 m^2 and in 3D the volume of 1.35 m^3. The cone used in experiments has a area of 0.462 m^2 and the volume of 0.111 m^3 at the penetration depth of 1.4 m. The area of the cone compared to the total area of the box at the penetration depth of 1.4 m was 17.1% in 2D. However, the volume of cone compared to the total volume of the box at the same penetration depth was just 8 % in the 3D case. Therefore the wall on the top is moving upwards, while the cone is moving downwards into the desrete material. Four colors were used in the assembly to observe the displacement patterns while insertion of the cone penetrometer.

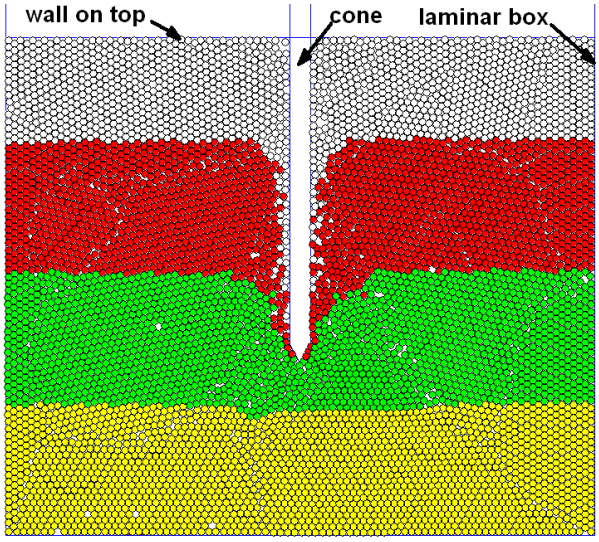

Figure 7. 5. The schematic view of the cone, box and wall on top in PFC2D.

The calibration tests were performed in the simplified conditions. The soil assembly was consisted of balls of 2cm diameter. To make computations faster, the velocity was assigned as 1m/s. The assembly was created by creating a box of bigger dimensions and larger amount of random balls. Next, the assembly was settled under the gravity. The porosity was observed in PFC2D, by means of measurement circle (MC) built in the middle of the box, was 0.10. This circle had a radius of 0.7m. The measurement circle created inside the box is shown in Figure 7.6.

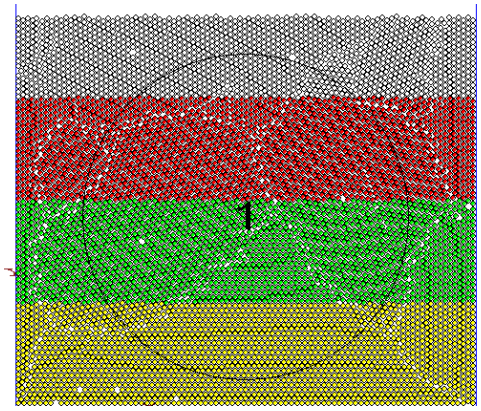

Figure 7. 6. Measurement circle location.

In the same assembly of particles (diameter 2 cm) different cones were implemented. The diameters of cones varied between 3 -10 cm. The cones used in this part of the calibration are shown in Fig. 7.7. Results of this analysis are depicted in Figures 7.8 and 7.9. Summary of the results from cone penetration tests with constant wall on top of the soil are presented in Figure 7.8. In Figure 7.9, there are depicted results from CPT done with the moving wall on top. The results obtained from the analysis, show that results with moving wall on top are more stable. The limit cone resistance, lim q_c at depth of 0.90 m for different cones are very simmilar for the case of moving wall on top. The greatest difference was 0.50 MPa. Contrary results were obtained for the case with stable wall on top, where limit q_c values are much more different (up to the difference of 1.50 MPa). Moreover, in simulations without the moving wall on top, cone resistance is rising more significantly with depth, rather than in the simulations with moving wall on top. In this study we focused on limit values of q_c. Therefore the boundary wall on top of the asssembly had a great adventage in this particular case.

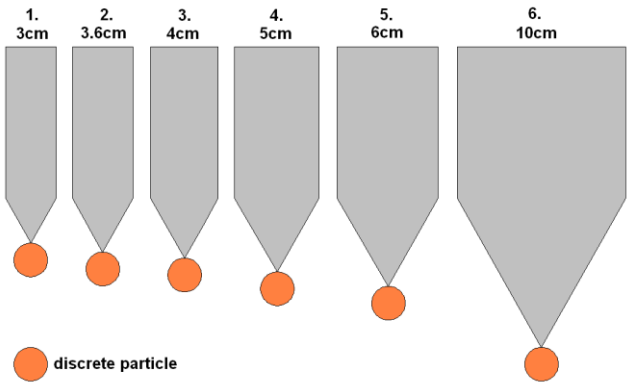

Figure 7. 7. Cones used during calibration phase.

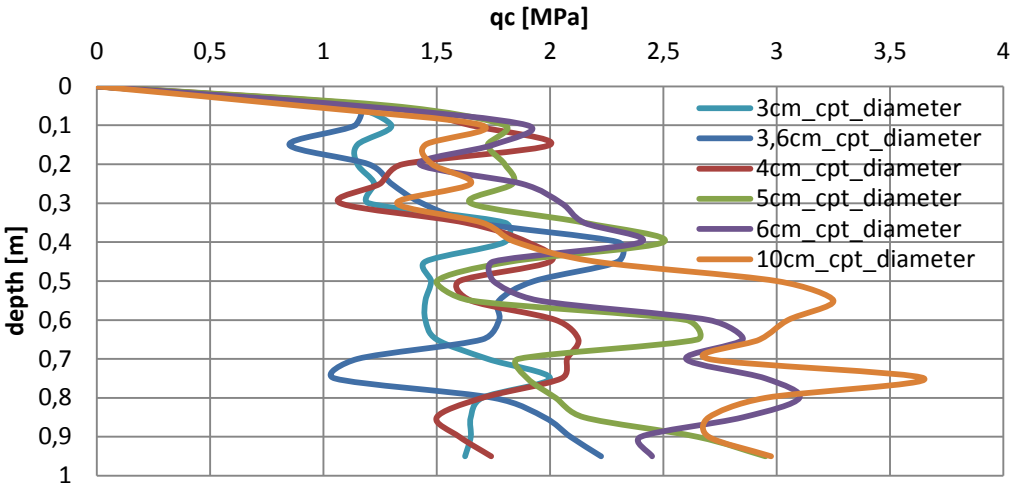

Figure 7. 8. Summary of results of the CPT simulations without moving wall on top.

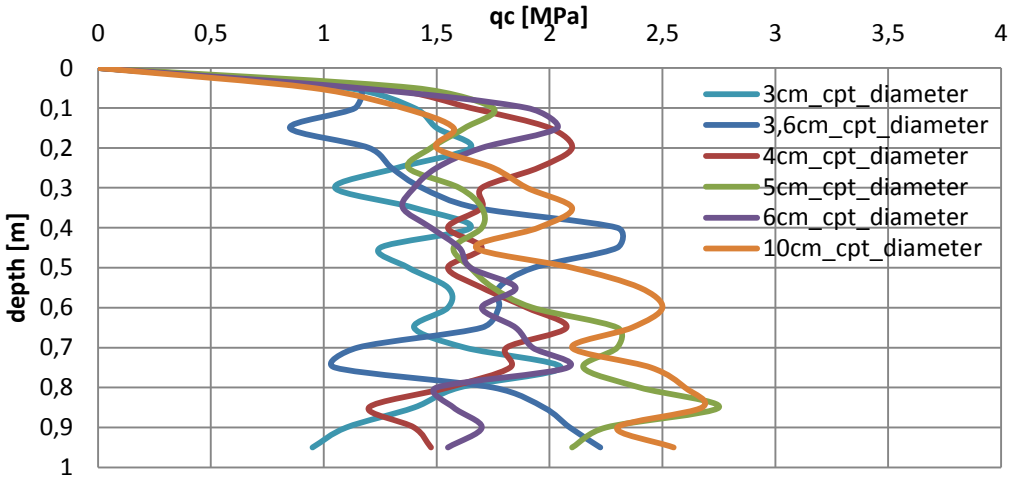

Figure 7. 9. Summary of results of the CPT simulations with moving wall on top.

Figure 7.10 presents the change in porosity, compared to the initial state of the assembly. We can observe that the average decrease in the porosity after penetration up to 0.95 m is equal to 0.01, as shown in Fig. 7.10. It is more expected value then the average porosity change, which was obtained from the simulations with a constant wall on top of the soil – 0.02.

Analysis was a first stage of the investigation of the boundary conditions. In general, results appeared to be slightly influenced by the boundary effects in the analyses considering various cone diameters. Rotations of the particles cause an unstable force measurement to occur, though the results showed that this influence of boundary conditions at the depth 0.95 m are not crucial for ther analysis after implementation of moving wall on top.

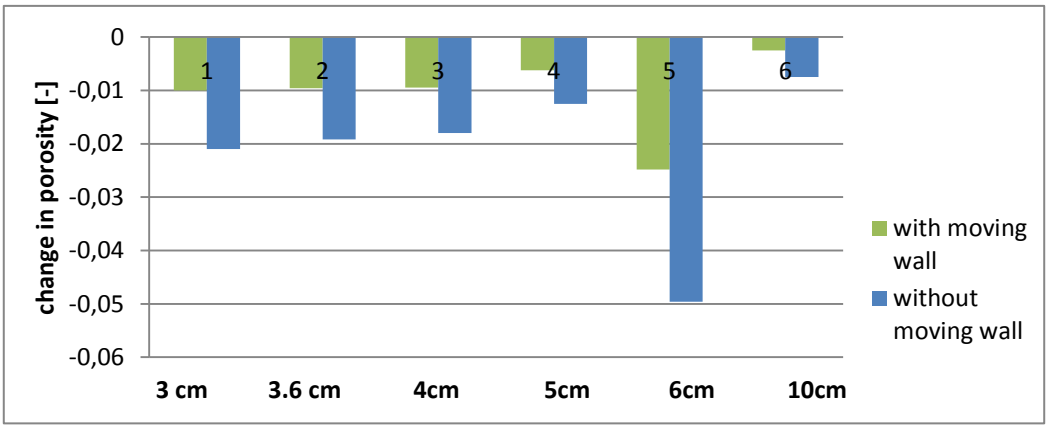

Figure 7. 10. Porosity change after the CPTs.

7.2.3 Boundary Conditions

It is very important to consider the proper boundary conditions for the DEM simulations. It is crucial to balance the computation limitations with the realistic solutions. Hence, multiple tests were run in this study. We investigated to find about what is the size of affected zone within the walls in PFC2D by insertion of the CPT probe. Even, we have taken into account the location of the cone penetration system in the laboratory. As shown in Figure 7.11, the cone penetration in the laboratory was conducted very close to the boundaries, especially in the N-S plane. It was convincing evidence to reduce the dimensions of the laminar box used in the DEM simulations.

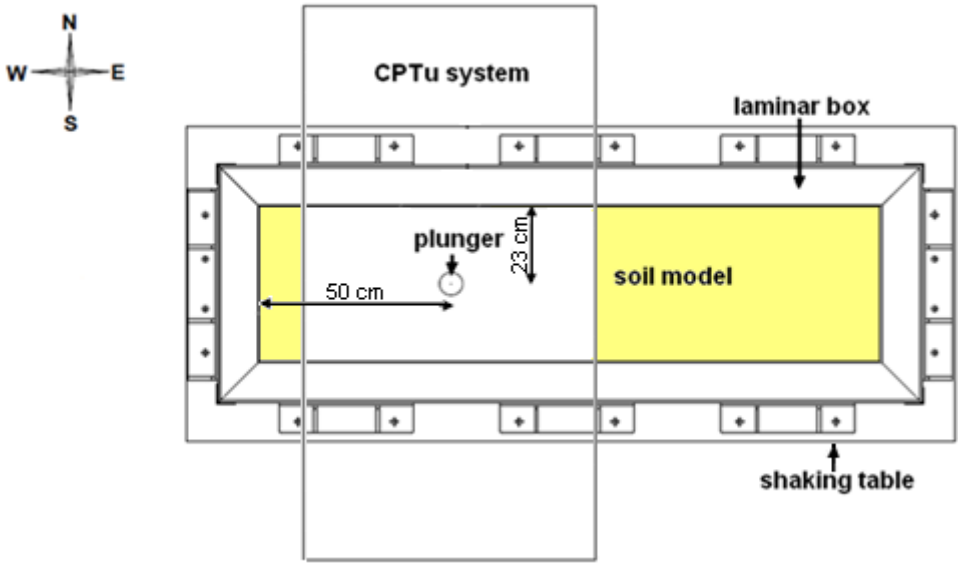

Figure 7. 11. Location of the CPT in the laboratory – top view.

In the literature, many attempts were made to simulate the CPTs by the DEM (Bultanska et al., 2013; Arrayo et al., 2011; Jiang et al., 2006). The dimensions were reduced with increase in diameter of particles. Bultanska et al. (2010) made a study to find the effect of chamber dimensions on calibration chamber testing. The ratio, R_d of chamber diameter, D_c to cone diameter, d_c is created as as follows (Figure 7.12):

$$R_d = \frac{D_c}{d_c} \tag{7.1}$$

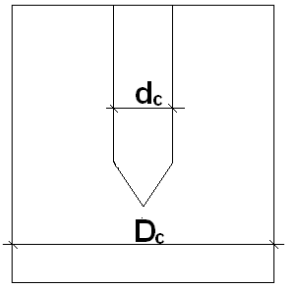

Figure 7. 12. Ratio of chamber diameter, R_d.

In Table 7.1, we listed the summary of geometric parameters of the 2D DEM studies related to penetration tests.

Table 7. 1. Literature on geometric parameters of 2D DEM studies related to CPTs.

Investigator	Diameter of chamber D_c [m]	Diameter of cone d_c[m]	Diameter of particle D_{50} [mm]	$R_d = \frac{D_c}{d_c}$
Ma (1994)	0.16	0.01	0.80	16.0
Calvetti & Nova (2005)	1.20	0.10	13.50	12.0
Yiang et al. (2006)	0.63	0.36	2.92	17.5

The multiple tests were run and it was found out that the rectangular area of 0.7m wide and 1.2m long is enough to give realistic results. The aim is to make a CPT simualations up to 0.95-1m. It is due to the nature of laboratory CPT results which are succesfully made till this depth. In this study, the ratio of chamber diameter (R_d) is 19.44, which is a higher value than those mentioned in previous studies, listed in Table 7.1.

7.2.4. Computational Fluid Grids

The sand was fully saturated during the laboratory experiments. Therefore, the fixed coarse-grid fluid flow concept (called sheme) was implemented in the DEM modelling to support coupled fluid-particles. SIMPLE sheme, developed by Patankar (1980) was used in this study. Basic Fluid Analysis Option sheme was explained in Chapter 5.

The Basic Fluid Analysis Option by Itasca has an option to record the fluid pressure. However there are specific circumstances in which this option cannot be used properly. Due to large strains occuring during penetration mechanism, the approach cannot be applied to investigate the pore water pressure (u) change during penetration of the cone into the soil . The measurements of u in the DEM-SIMPLE analysis lead to extremely high values of the pore water pressure, while penetrating a discrete material and it confirmed the work of Tsuji et al. (1992) and Kawaguchi et al. (1993) who claimed that particle-fluid interaction by coupling of PFC2D and SIMPLE sheme cannot be applicable to the study of liquefaction (large strains and change in pore water pressure). However, fluid can affect the forces on the cone tip. These forces are different than the ones gathered from the dry assembly. In this study, we decided to

reproduce ideal saturated conditions of the soil by imposition of the grids. The covergence of the fluid model needs to be done, while performing final simulations,because it depends on the number and size of the particles. Specification of criterion for the covergence of the SIMLE scheme, as well as selecting the fluid time-step (usually smaller than for the DEM) needs to be done simultaneously with the DEM calculations. It needs to be detected at what time-step we can obtain the best covergence and the fastest calculation.

7.2.4.1 Grid Size

Calibration of the fixed coarse grids was the next stage of the calibration process. The dimensions of the grids cannot be too big. However, the amount of grid should not be excessive to not make the computations slower. The model dimensions were 0.7 m width and 1.2m height, surrounded by bottom, top and side walls. Extra fluid cells were created outside the model walls. Their function is to reflect the boundary conditions. The total number of finite grids was chosen to be 1200, including 40 grids in the x-direction and 30 grids in the y-direction. As seen in Figure 7.13(a), the grids were exceeding the boundary of the box. Each cell size was in rectagular shape of x_f = 1.75cm by y_f = 4cm as shown in Figure 7.13(b).

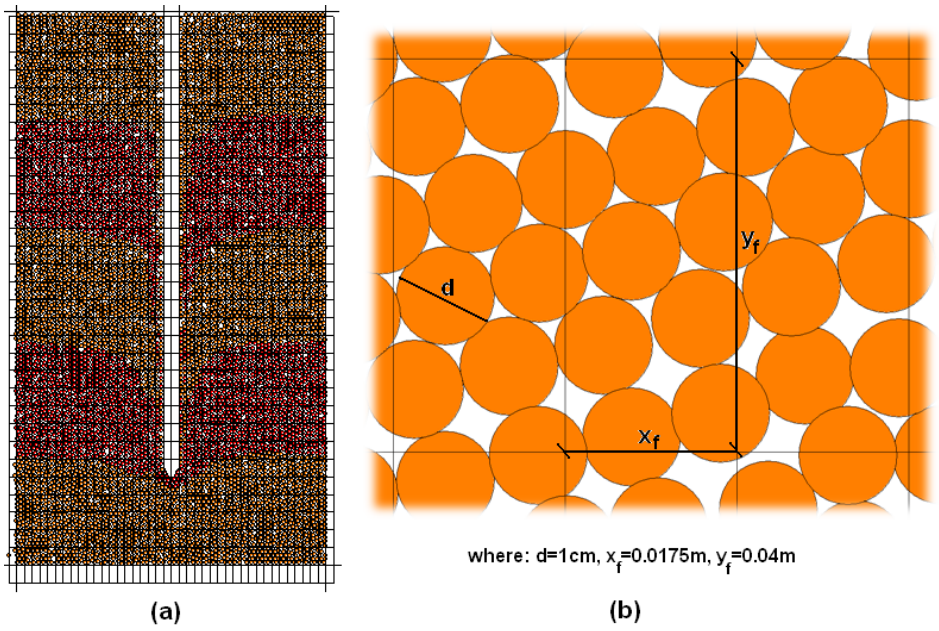

Figure 7. 13. (a) DEM-SIMPLE model of CPT, (b) computational fluid grids.

7.2.4.2. Boundary Conditions of the Fluid

One of the principles of the basic fluid analysis option states that the boundary conditions must be specified along whole boundary of the fluid area (Itasca - Optional Features, 2008). In order to depict the conditions observed in the laboratory, the following boundaries are assigned to the DEM model:

- Bottom = slip-wall boundary
- Sides = slip-wall boundary
- Top = zero-pressure wall boundary

A zero-pressure boundary was selected at top of the model box. Because the fluid pressure was equal to zero, according to the basic fluid mechanics equation:

$$\Delta P = \rho g z \tag{7.2}$$

where,

ΔP = change in pressure;

ρ = density of fluid;

g = gravity of earth;

z = depth.

7.2.4.3. Fluid Properties

Basic two fluid properties were selected for the model. Density of water at 20°C was 1000 kg/m^3 and viscosity was 1.1 mPa·s. The geometry of combined DEM and SIMPLE model is depicted in Figure 7.14. In Fgure 7.14(a) the coupled DEM-SİMPLE model of the CPT is shown with specified boundary conditions, properties and pressure of the fluid. On the picture, yellow color resesent the pressure of 0 kPa and apricot color is approximately 11.8 kPa at initial state. It was noticed, that while conducting CPT, the pressure values are incorrect due to large strains limitation. In Figure 7.14(b) we can observe another capability of PFC2D which is porosity measurement in the continuity. However, still instability problem occurs (Itasca – Optional Features, 2008). In Figure 7.14(b), we can observe that the program detects the recessed cone in the soil (yellow color- lack of of particles, which means the biggest porosity). The orange color

repersents the porosity with particles. We expected it to be similar in whole stratum, due to the particle packing method, which enable us to create almost uniform porosity in whole assembly.

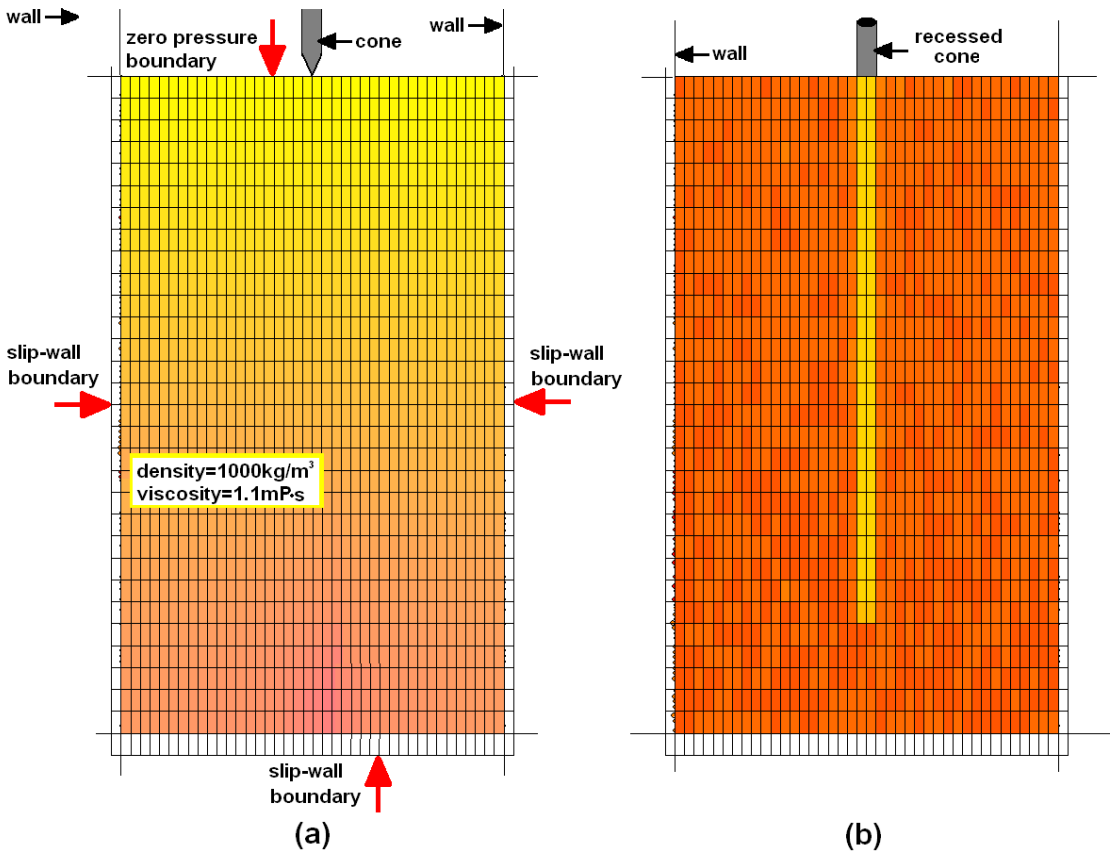

Figure 7. 14. Fluid model of (a) boundary conditions, properties and pressure of fluid before the CPT, (b) porosity of fluid with recessed cone.

7.2.5. Particle Diameter

In order to compare the results with the real problems, the proper scaling in numerical simulations is very important (Bultanska et al., 2010). After calibration of the boundary walls which are simulating a boundary conditions, it is neccessary to chose the proper diameter of particles. The appropriate diameter of discete material is crucial, in order to mimic the soil in laboratory. Cone which is consisted of stiff walls needs to be always in contact with at least few particles at each size of the cone. Unfortunately the computational limitation did not allow us to perform multiple simulations without decreasing the number of particles as well as the box dimensions.

PFC2D software allows us to observe the contact forces' chains in the assembly. Figure 7.15(a) shows the particles with diameter of 2cm while Figure 7.15(b) presents the particles with diameter of 1 cm (twice smaller than (a) case). At each analysis, the cone diameter was 3.6 cm and the cone velocity was set to 1 m/s, porosity was 0.10 in PFC2D. Although the porosity, diameter of the cone and the penetration velocity was the same in each figure, we observed different patterns of contact force chains.

The influance of the diameter of the cone on number of contacts is shown in Figure 7.15. Arragement of the contact forces in the assembly with smaller particles (b) is more symetric than the (a) arrangement. If the cone has contacts with more particles, the measurement of force Y (F_y) on the cone surface is more stable and accurate.

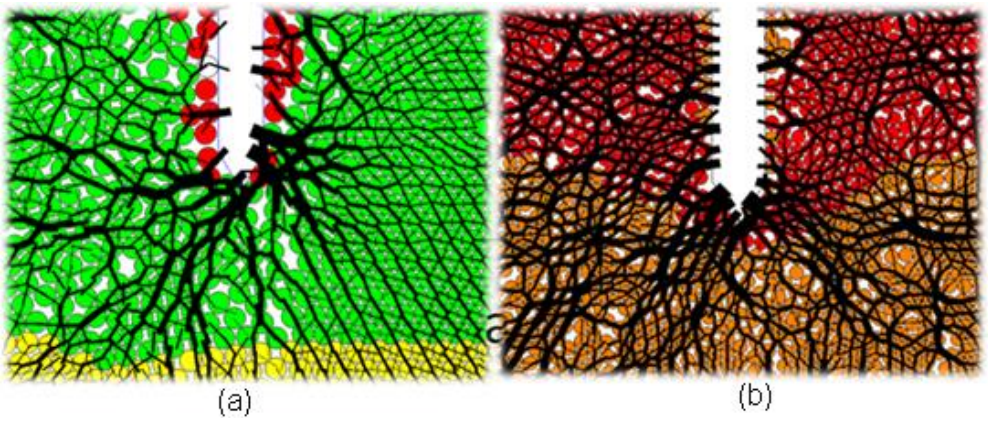

Figure 7. 15. Contact forces' chains in the assembly of the particle diameter of (a) 2cm; and (b) 1cm.

Figure 7.16 shows the effects of cone diameter on contacts between cone and particles. Data was obtained from the results of calibration of wall on top of the box mentioned in Section 7.2.2. CPT simulations were performed in the same assembly of particles (the same porosity, particle diameter etc.) by means of different cones (diameters varied from 3.6 to 10 cm) for this purpose. At the same depth of 0.95 m, we counted the number of particles in contact with the cone surface (wall 1 and 2). We were able to produce general trend, which is shown in Figure 7.16. Relationship between the number of cone-particles' contacts (Nr_c) and the diameter of the cone (d_c) is:

$$Nr_c = 1.3215 d_c - 0.0903 \quad (7.3)$$

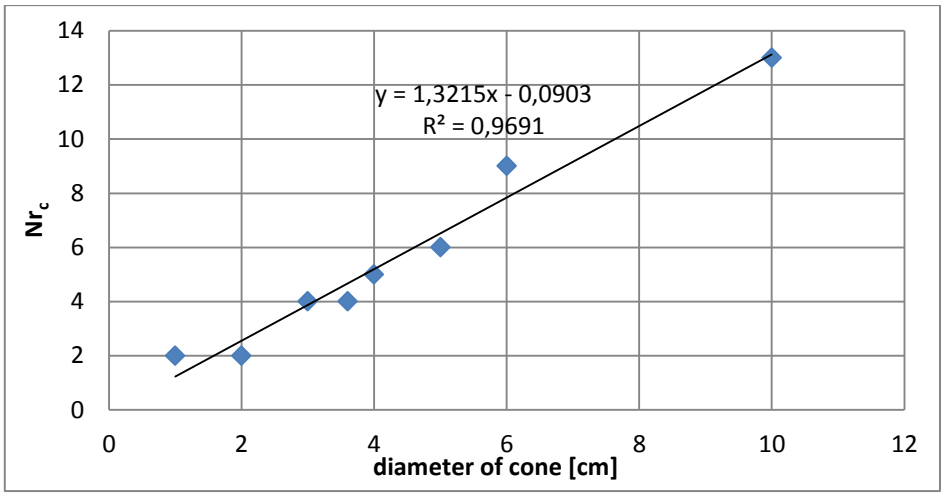

Figure 7. 16. Influence of the cone diam. on the number of cone-particles contacts.

In Table 7.2, the results are gathered and the ratio of the number of contacts to the diameter of cone was calculated. In this study, the diameter of particle was 2 cm and the best results we have obtained for the cone of 6 cm diameter. At this diameter, number of contacts found to be relatively the highest ultimately. The particle diameter should be at least 3 times smaller than that for the cone diameter. In presented studies, we have decided to keep diameter of the cone 3.6 cm and its velocity 2 cm/s similar to real test. It leads to conclusion that particles diameter should be smaller than 1.2 cm. Whereas we have decided to make more tests, in order to determine the diameter of particles in this study. This will be descibed in the following paragraphs.

Table 7. 2. The results of the cone diameter effects on the number of cone-particles conatcts with their ratio.

a	**b**	**b/a**
Diameter of cone [cm]	**number of contacts**	**ratio**
3	4	1.33
3.6	4	1.11
4	5	1.25
5	6	1.20
6	9	**1.50**
10	13	1.30

7.3. Scaling Factor

In the previous steps of analysis, a basic calculation of cone penetration resistance was employed. The goal of the previous calibration steps was to detect which factors are influencing the q_c. However in order to determine the final size of grain and to validate the porosity in 2D DEM model, a scaling factor, S was applied. Force accumulated on cone in Y direction (F_y) was collected to obtain a limit q_c value. The limit q_c was obtained by an equation given below:

$$\lim q_c = F_Y/(A_c \cdot S) \tag{7.4}$$

where,

A_c = area of cone in 3D (10 cm^2);

S = scaling factor which can be described by:

$$S = [\ 2\pi\ (\ D / 2 + d)\ ]\ /\ d \tag{7.5}$$

where,

D = diameter of cone;

d = diameter of discrete particle as shown in Fig. 7.17.

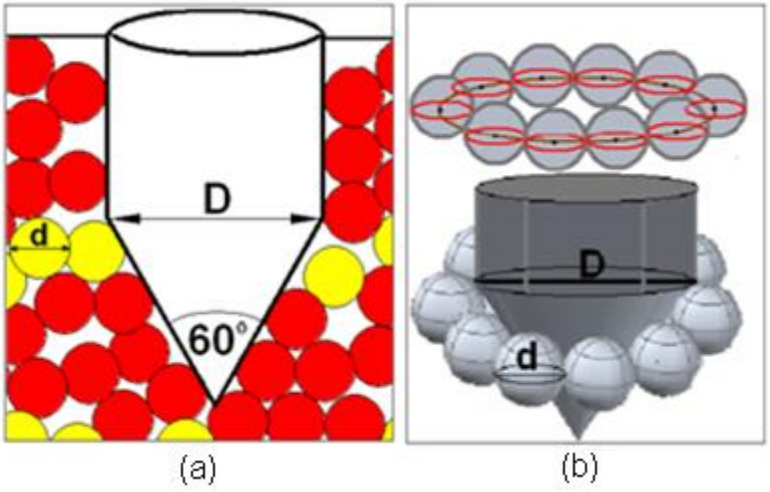

Figure 7. 17. Scaling logic for (a) 2D and (b) 3D simulations.

The scaling factor is assumed to be a maximum number of particles in contact with the cone in the middle plane (illustrated in Fig. 7.17). The circumference shown in Figure 7.17(b) is divided by the diameter of discrete particle. Scaling logic is very important in this study, because as it is 2D environment we need to assume the z-component, as we want to simulate the phenomenon which occurs in real 3D environment.

7.4. Validation of the Particle Size

As mentioned before, to achieve suitable number of contacts between the cone and the particles at each step of CPT tests, the diameter of particle cannot be larger than 1.2 cm. In this part of analysis, multiple tests were performed, in order to find satisfying size of grain with affordable computation time.

In this study, numerous tests were also performed, in order to find satisfying size of grain with affordable computation time. The range of porosity, which has been investigated, was from 0.11 to 0.16. A total of 24 CPT simulations up to 1 m depth were done. The particle diameters were selected as 0.8cm, 1.0 cm, 1.5 cm and 2.0 cm. The data from the numerical program was smoothened due to the unstable character of force detected on the cone surface. In Figure 7.18, the q_c results from assembly of 1.0cm particle diameter are shown with the smoothing curve method. It was done intuitively. The key element in this study was to find the value of the cone peneteration resistance at the depth of 1m. The limit value was assigned to each DEM-CPT simulation. In Figure 7.18 we can observe the mechanism of smoothing procedure. The limit q_c was chosen intuitively. In this example the limit value for the presented DEM-CPT results is 0.5 MPa. In this study, limit q_c is abbreviated as "lim q_c".

The numerical experiment results are demonstrated in Figure 7.19. The lim q_c values were determined by means of scaling factor and the lim q_c was selected as mentioned above. As shown in the figure for particle diameter of 0.8 cm and 1.0 cm, the lim q_c values are almost similar. As we concluded before the diameter should not be bigger than 1.2 cm. Based on the previous investigation and as a result of validation of particle size, it was decided to prefer 1.0 cm particle diameter in CPT simulations.

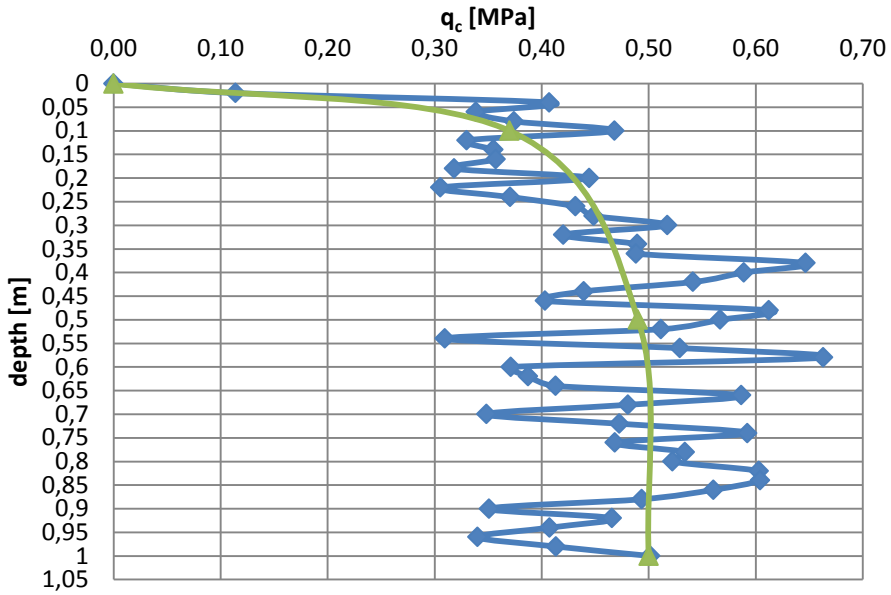

Figure 7. 18. Smoothing procedure and determination of limit qc for data obtained from DEM CPT simulations.

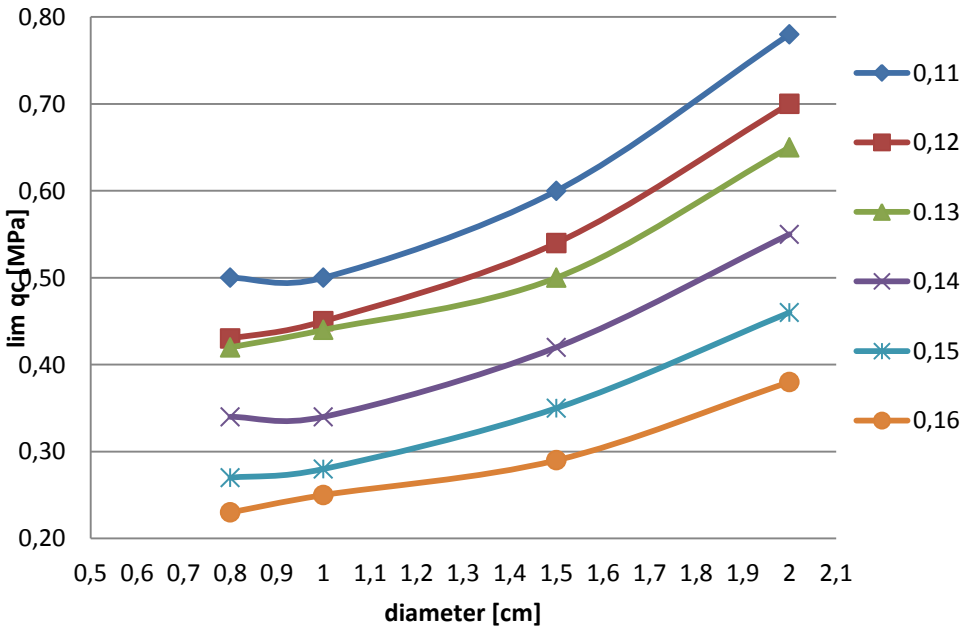

Figure 7. 19. Numerical experiment results from validation of particle size by DEM (Legend: scope of porosity from 0.11 to 0.16).

CHAPTER 8

VALIDATION OF POROSITY IN THE 2D DEM CPT MODEL

8.1 Introduction

As it was mentioned before, porosity is crucial limitation of the two-dimensional modelling. Therefore 3D packing from laboratory test results were compared with data obtained from the numerical analysis in 2D. Assumptions were obligatory to make a correlation between laboratory and numerical analysis. Therefore, in this chapter multiple simulations were presented to investigate the porosity relationship between 3D laboratory tests and the 2D DEM model.

Firstly, the CPT model was defined, based on findings from Chapter 6 and 7. Seven assemblies of spherical particles were tested. The range of porosity, which has been investigated, was from 0.09 to 0.16 in regard to the previous findings of Utili and Nova (2008). In this part, all the main DEM parameters are given.

In the second part, the focus was to make a suitable correlation between the laboratory tests and numerical analysis. Hence, multiple simulations were run to investigate the porosity relationship between the 3D laboratory tests and the 2D DEM model. The data from the laminar box shaking table tests is used to validate porosity in two-dimensional environment. Observations of the behavior of soil in the laminar box and discrete material in 2D DEM enabled us to make a correlation between porosity from the large scale experiment and the PFC2D model.

In this chapter, moreover, we investigated the porosity and the coordination number change after the cone penetration. Contact forces and displacement vectors were observed in the scope of porosity at the penetration at 1 m deepth. Number of particles, which were checked at different porosity levels are briefly presented in this chapter. Finally, the results from the cone penetration DEM simulations were compared with the laboratory results. Good covergence was achieved.

8.2. CPT Model

The CPT mechanism was built by means of wall-logic algorithm with normal and tangent stiffness. Beforehand, multiple simulation tests were performed in order to examine the effects of boundary conditions, porosity, particle size and fluid grid dimensions on the cone tip resistance.

The model box dimensions of 1.2 m (height) and 0.7 m (width) are sufficient to represent the boundary conditions in the laminar box. Walls were chosen to simulate boundary conditions which occur in the laminar box. Normal stiffness of the walls of the box is set to be the same as normal stiffness of particles. Tangent stiffness of walls was neglected as well as walls were considered to be frictionless.

Seven assemblies of spherical particles were tested. The assembly representing the micro-mechanical model of saturated sand consisted of 9702 particles for n = 0.09 and 8960 particles for n = 0.16 radii of 0.01 m. The assembly had a height of 1.2m and was divided into 5 regions with different colors in order to observe the particles position alternation. Fig. 8.1(a) and (b) shows before and after CPT penetration, respectively.

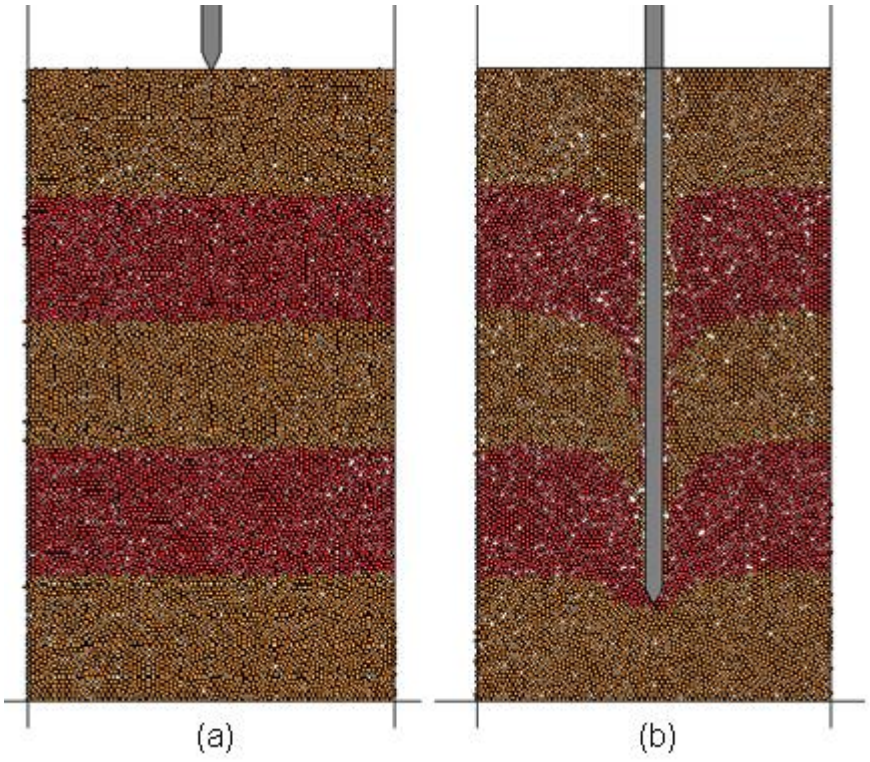

Figure 8. 1. Final CPT model (a) before and (b) after cone penetration.

Stiffness k_n and k_s, and particle friction, μ_p were determined in the biaxial tests. There k_n was found as $6 \cdot 10^6$ N/m, k_s as$1 \cdot 10^6$ N/m and μ_p as 1.0. Density was chosen to be 2650 kg/m^3, as it is common value of matrix density, ρ_{matrix} for the quartz sand. Matrix density is often used for inferring porosity from the bulk density. Afterwards, fluid cells were created. The parameters which described water behaviour were density and viscosity of value of 1000 kg/m^3 and $1.1 \cdot 10^{-3}$ Pa·s, respectively.

After creating an assembly filled with particles, the cone was built by means of four walls. Tangent and normal stiffness were assigned as $1 \cdot 10^{18}$ N/m and friction as 1.0. The velocity was assigned for each wall in y-direction as 2 cm/s. Forces accumulated on the two walls creating the 60° angle with each other were recorded during whole penetration process up to depth of 1 m.

Before starting the cone penetration test simulations, the mechanical time-step was determined. The critical time-step, t_{crit} for the mass – spring system was given by Bathe and Wilson (1976):

$$t_{crit} = \sqrt{m/k} \tag{8.1}$$

where,

m = total mass of the particle;

k_1 = stiffness of the spring.

Mass of particle is 0.205 kg and stiffness of spring (we assume just the normal stiffness) is $6 \cdot 10^6$ N/m. We have obtained t_{crit} $1.825 \cdot 10^{-4}$ s for the particles. However we need to take into account time-step calculation for the fluid. Convergence is extremely important to obtain a stable solution. Howeevr, PFC2D may choose the time-step for fluid by itself by selecting the minimum value of:

1. 100 times of mechanical step,
2. Courant–Friedrichs–Lewy condition (CFL),
3. Half of minimum value over all fluid cells defined by the size of the cell divided by average particle velocity in each direction (Basic fluid Analysis Option - Itasca, 2008).

Another method is to select the time-step by the user. We have decided to choose both time-steps mechanically. We have chosen the timestep for discrete material as $5 \cdot 10^{-4}$s and $2 \cdot 10^{-3}$s for fluid. We have achieved these values by observing program

response - speed of simulations. Critical timestep for the fluid was chosen as $1 \cdot 10^{-4}$s. It was chosen so as corresponding to the critical timestep value for a single DEM particle, as $1.825 \cdot 10^{-4}$ s. To penetrate 1 m of soil we need 1000000 steps. All simulations achieved good convergence, although the average time of simulation of 1000000 steps took approximately 24h which also depends on the processor. Input parameters for the discrete material, cone, walls and the fluid are listed in Table 8.1.

Table 8. 1. Input parameters for the discrete material, cone, walls and fluid.

Particles	
Diameter (d)	10 mm
Friction coefficient (μ_p)	1.0
Density (ρ)	2650 kg/m^3
Normal stiffness (k_n)	$6 \cdot 10^6$ N/m
Tangent stiffness (k_s)	$1 \cdot 10^6$N/m
Ratio $\alpha=k_s/k_n$	1/6
Cone	
Diameter (D)	36 mm
Friction coefficient (μ_c)	1.0
Normal stiffness	$1 \cdot 10^{18}$ N/m
Tangent stiffness	$1 \cdot 10^{18}$ N/m
Walls	
Friction coefficient (μ_w)	0.0
Normal stiffness	$6 \cdot 10^6$ N/m
Tangent stiffness	$6 \cdot 10^6$ N/m
Width	0.7 m
Length	1.2 m
Fluid (water at 20°C)	
Density	1000 kg/m3
Viscosity	$1.1 \cdot 10^{-3}$ Pa·s
Computation parameters	
Time step for DEM	5·10-5 s
Time step for SAMPLE	2·10-3 s
Finite volume dimension	0.0175·0.0400 m

8.3. Calibration of Porosity in the 2D DEM CPT Model

After the DEM simulations, the cone penetration resistance for various porosities was obtained along with its limit value at the depth of 1 m. Consequently, the

data of the CPT performed in the laminar box at the same depth and the rate of penetration was used to validate the porosity in two-dimensional environment.

The correlation is based on the Equation 4.5, which was derived in Chapter 4. Then, we determined the relationship between D_r and lim q_c. Obtained from numerical analysis limit q_c values allowed us to find a correlation between porosity detected in PFC2D assembly corresponding to the real porosity for investigated soil in this study. We compared the lim q_c from laboratory and numerical CPT tests. The unknown parameter was porosity of the discrete material in PFC2D simulations. The lim q_c from the DEM simulations was substituted in Eq. 4.5 and the relative density in each assembly was calculated. Afterwards the formula derived from basic soil mechanis equation was used to obtain the void ratio in each DEM assembly:

$$e = e_{max} - \frac{D_r(e_{max} - e_{min})}{100} \tag{8.2}$$

where,

e = void ratio;

e_{max} = maximum void ratio (for our soil e_{max} = 0.8);

e_{min} = minimum viod ratio (for our soil e_{min} = 0.6);

D_r= relative density.

Porosity was calculated by means of equation:

$$n = \frac{e}{e+1} \tag{8.3}$$

where,

n =porosity;

e = void ratio.

The results are gathered in Table 8.2. Figures 8.2-8.4 demonstate multiple relations based on above calculations. Fig. 8.2 presents relationship between the limit q_c and the D_r, Fig. 8.3 shows the limit q_c values corresponding to void ratio while Fig. 8.4 depict the relationship of limit q_c and porosity.

Table 8. 2. Relationship of porosity from the DEM with the relative density, porosity and void ratio in the tested soil.

n in PFC2D [-]	lim q_c [Mpa]	Relative density (D_r)[%]	Void ratio (e)	Porosity (n)
0.09	1.20	71.78	0.654	0.395
0.1	1.07	68.48	0.660	0.398
0.11	1.00	66.53	0.664	0.399
0.12	0.90	63.49	0.669	0.401
0.13	0.82	60.81	0.674	0.403
0.14	0.68	55.42	0.685	0.406
0.15	0.56	49.83	0.695	0.410
0.16	0.50	46.56	0.702	0.412

Observations of the behavior of soil in the laminar box and discrete material in the 2D DEM enabled us to make a correlation between the porosity obtained from the large scale experiment and PFC2D model. Figure 8.5 depicts the relationship between the porosity in two-dimensional DEM model with related to its real porosity. The correlated data lied down very close to a parabolic curve (Fig. 8.5), which can be described by the following equation:

$$n_{lab} = 1.5394 n_{DEM} 2 - 0.1389 n_{DEM} + 0.3955 \quad (8.4)$$

where,

n_{lab} = porosity in the laboratory;

n_{DEM} = porosity in the DEM simulations.

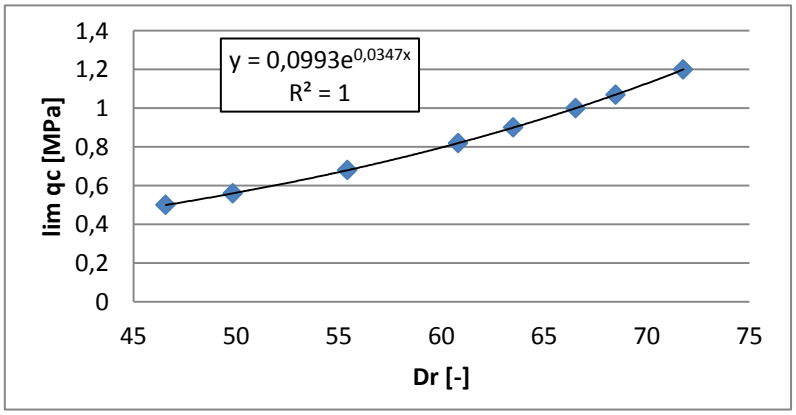

Figure 8. 2. Relationship between the limit cone penetration resistance and the relative density from the CPT DEM simulations.

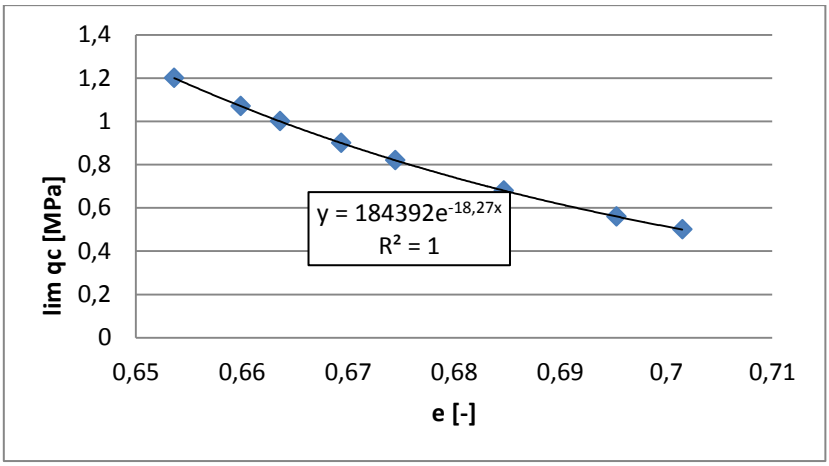

Figure 8. 3. Relationship between the limit cone penetration resistance and the void ratio from the CPT DEM simulations.

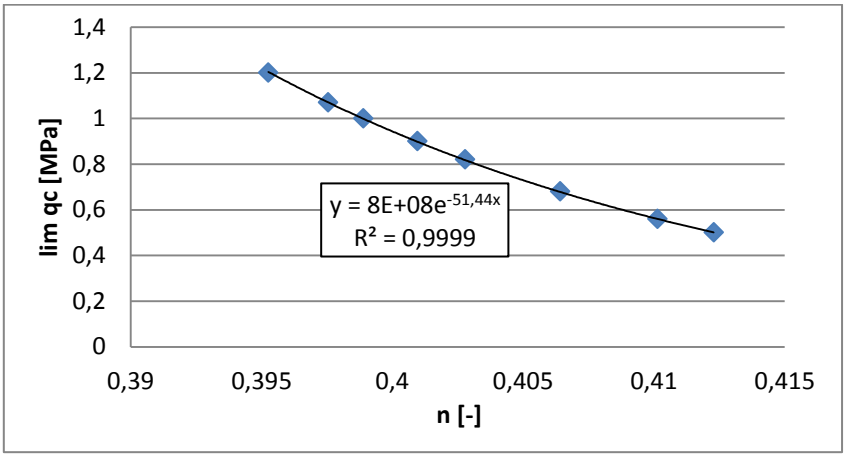

Figure 8. 4. Relationship between the limit cone penetration resistance and the porosity from the CPT DEM simulations.

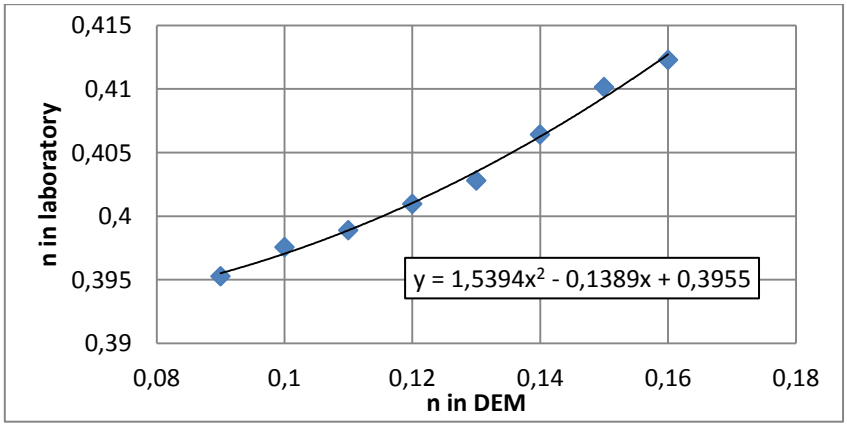

Figure 8. 5. Relationship between the porosity in laboratory and in the DEM.

There is a noticeable difference between the uniform circles packing in PFC2D and in the laboratory experiments for this particular soil. Dereszewiecz (1958) calculated that the closest of regular packings of uniform spheres in the 3D has porosity of 0.2595 whilst the same assembly in the 2D has a porosity of 0.0931. Simulations performed by means of PFC2D in this study also showed significant difference between two and three-dimensional packing of discrete particles with a decreased porosity in the DEM with respect to the laboratory porosity measurements.

8.4. The Other DEM CPT Simulations' Results

8.4.1. Measurement Circles

Multiple quantities, such as porosity, stress and strain rate, coordination number and sliding fraction are defined on the specific area – measurement circle. Theoretical considerations with about measurement logic in PFC2D with its limitations and assumptions are described in 3-7 Section of Theory and Background, Itasca (2008).

During all the CPT tests performed in order to validate porosity in the 2D DEM model, measurement circle (MC) logic was used. Three measurement circles were created in the sample as shown in Fig. 8.6. Location and radius of each circle are specified and shown in the Fig. 8.6.

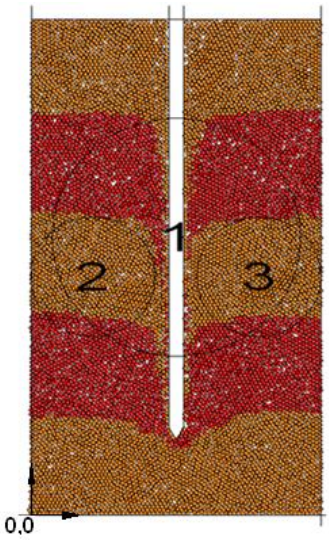

No. of MC	Location		Radius
	X	Y	R
1	0.35	0.7	0.3
2	0.15	0.6	0.15
3	0.55	0.6	0.15

Figure 8. 6. Locationof measurement circles in the box.

For preparing sphere packing, the radii expansion method was applied. It enabled to prepare the close to uniform packing and porosity in the whole assembly. The measurement circles were chosen in this specific location, because the first MC - gives wiser observation prospective before the CPT test however second and third MC enabled us to observe changes which occured in the assembly after the CPT tests. To obtain average values before and after the CPT, second and third MC were considered.

8.4.2. Porosity Before and After the CPTs

The porosity is very important quantity in the 2D DEM simulations due to the fact that primarily assigned porosity in the program does not reflect the posoity of real phenomenon in nature (three-dimensional environment).

After validation of porosity for sand (described in Chapter 7), the porosity before and after CPT was compared.

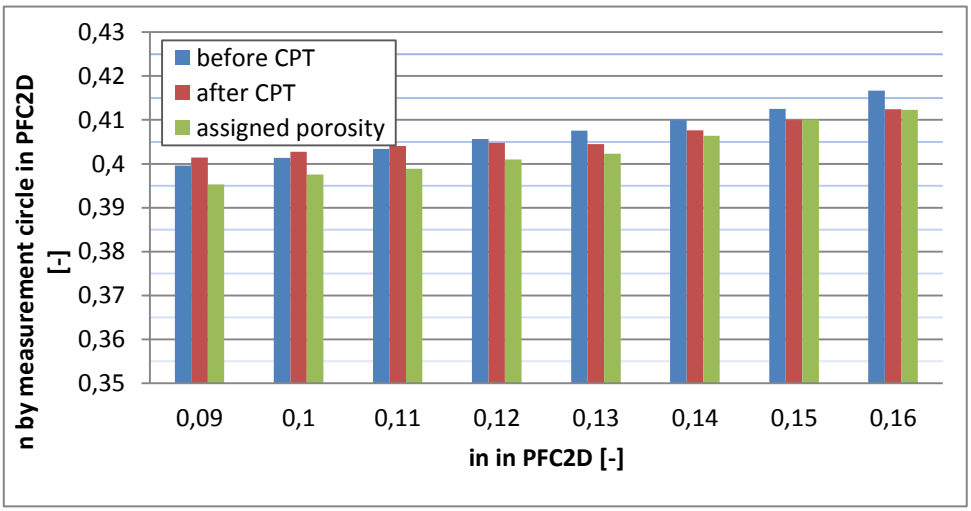

Figure 8. 7. Porosity in the box before and after the cone penetration tests.

In Figure 8.7, results of before and after cone penetration porosity are presented. X-axis shows the initial porosity assigned to the discrete assembly. Y-axis shows the porosity detected by the measurement circles. The green column represents the initial porosity assigned to the whole sample and the calibrated value of it is shown on the y-axix. The blue column shows the porosity before the cone penetration. The red column

presents the porosity after the cone peentration measured by the measurement circles (average of MC 2 and MC 3).

Porosity from 0.09 to 0.12 (in PFC2D) is slightly greater after CPTs. It was expected to decrease, eventhough a wall on the top was moving upwards. The reason behind this response can be explained by the results from the following analysis. In order to gain deeper insight into the porosity in the 2D DEM environment, an assembly of very small particles (d=0.1cm) and tight packing (n = 0.09 in PFC2D) within (0.2 x 0.435)m was created. Figure 8.8 (a) and (b) present the modelled case. The cone had real dimensions and stiffness. In more tightly packing – smaller porosity, some particles under big strains are getting out from the model cell. It is illustrated in Fig. 8.8(c). The stiffness of the walls, which represented the borders of assembly, were the same as particles' stiffness. Consequently under great strains particles may leave the boundary area. While conducting the CPT, PFC2D program cannot find suitable location for many moving particles. Thanks to this application, another limitation of the DEM modelling in the 2D was detected. Wall on the top and the same stiffness of box walls as particles prevent particles to get inside the cone - Fig. 8.8(b); while some particles are forced to leave the boundary conditions limited by box walls - Fig. 8.8(c). Thus, this simple test showed that so small particles cannot be implemented to reproduce realistic results of CPT simulations.

At looser assemblies (porosity higher than 0.12 in PFC2D) we have observed the decreasing porosity while penetrating the assembly. Particles were not forced to leave the bondary conditions as there was a free space they could find accomodation after each time step of calculation.

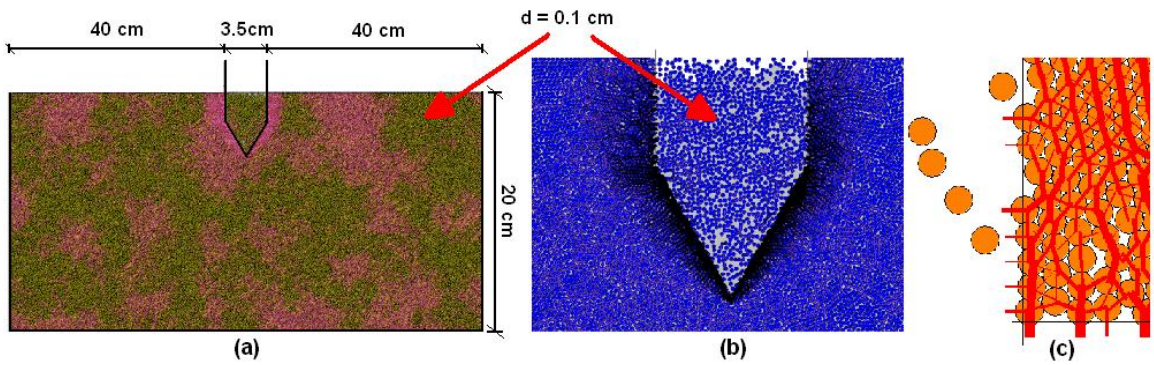

Figure 8. 8. (a) Model of the CPT in dense assembly (n = 0.09 in PFC2D); particles occur to penetrate (b) inside the cone, (c) outside the boundary conditions, due to penetration process.

8.4.3. Coordination Number Before and After CPTs

Coordination number (CN) is described as the average number of active contacts per particle (Theory and Background – Itasca, 2008). Coordination number was measured before and after the cone penetration. Therefore we can observe how the average amount of contacts per particle have been changed due to penetration. In Fig. 8.9, it is demonstated that in one assembly there are different number of contacts. Just uniform packing of spheres has mostly the same number of particles. We are unlikely to find any particles with no contacts. The scope of the porosity and the implemented procedure to obtain initial desired porosity prevents from occurance of suspended particles with zero contacts.

Figure 8. 9. Discrete particles with diffrent amount of contacts.

Results from the three measurements circles (MC 1, MC 2 and MC 3) are presented. Figure 8.10 (a) shows the results of the CN before (MC1, MC 2 and MC 3) and Figure 8.10 (b) after (MC 2 and MC 3) CPTs. The porosity is already calibrated and validated for the tested soil. We can observe that with increasing porosity, the coordination number is getting smaller nevertheless before or after the penetrometer tests. However, the results from the analysis for MC 2 and MC 3 for the case before the CPTs are more stable, less scattered. MC 2 and MC 3 are situated symmetrically on both sides on cone. Therefore, the results of the CN are expected to be similar, but not the same as it measurement logic has many approximations and assumptions. In Figure 8.10(a), there are almost identical in contrary to the results after the CPTs which are much more scattered, as shown in Figure 8.10(b).

The average results of the CN analyses before and after the CPTs are presented in Figure 8.11. MC 2 and MC 3 were taken into account while calculating process. We can observe similar situation as with porosity before and after CPTs. Firstly, in low porosities (up to n = 0.398), the coordination number is decreasing after the penetration and after increasing significantly. It can be explained by the fact that in tight packing

some particles are leaving the specified boundary conditions. In looser assemblies, particles can find accommodation within the sample borders and the porosity more significantly decreases due to cone pushed downwards. It can be concluded that DEM CPT modelling is more accuarate for loose and medium assemblies.

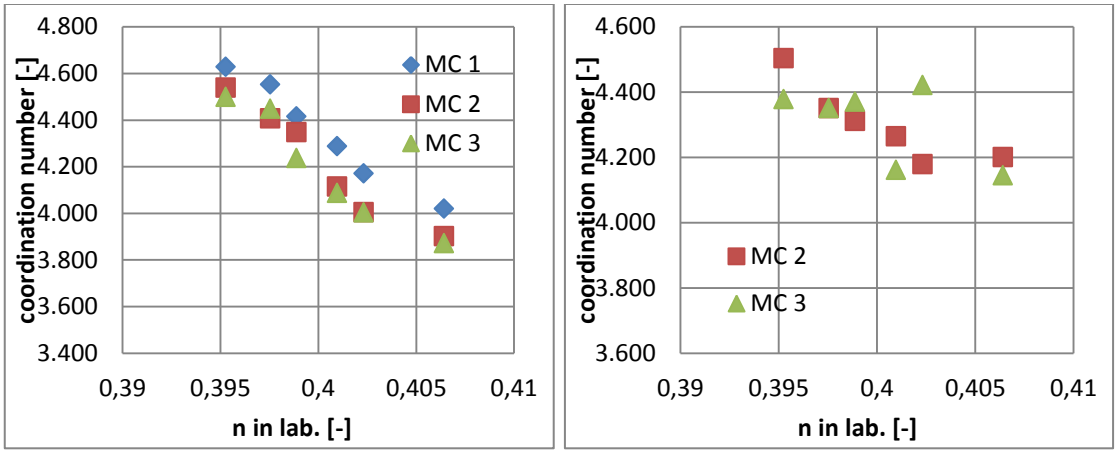

(a) (b)

Figure 8. 10. CN results (a) before and (b) after the CPTs.

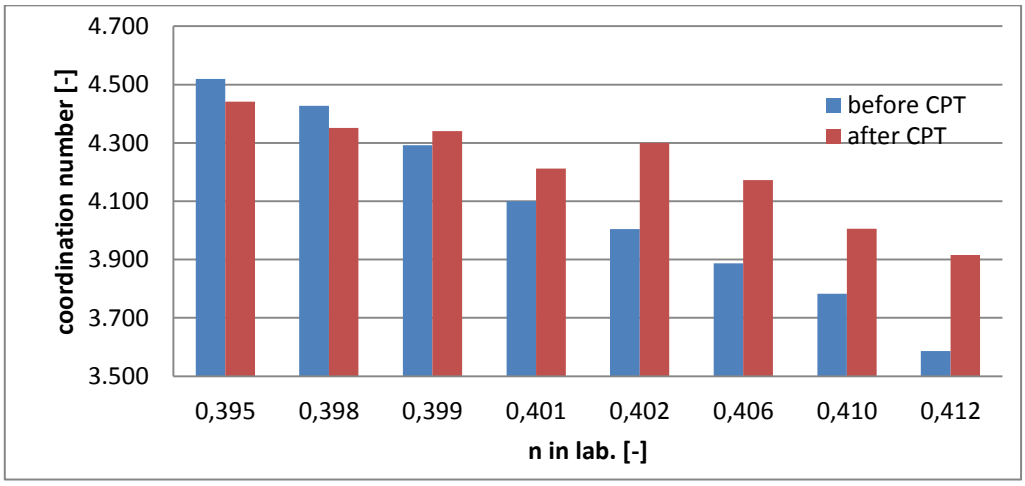

Figure 8. 11. Average CN results before and after the cone penetration.

8.4.4. Effects of Cone Penetration on Contact Forces and Displacement Vectors

Cone insertion into the granural material results in a complex behaviour, including change in contact forces chains and displacement patterns. The contacts

forces and dispalcement vectors in initially the most loose and dense assemblies are shown in Figure 8.12 and 8.13, respectively. Results from the validation of particle diameter were used. It needs to be noted that the location of the particles after the cone penetration may be arbitrary. We can observe that in the assemblies with smaller particles (for instance 0.8 cm) the chains of contact forces are more complex, though the magnitude of force is smaller than in assemblies consisted of bigger particles. Grafics from PFC2D program are able to reproduce the contact forces without given magnitude of each chain, though we can compare them by visual observation. The thicker contact forces chains have greater magnitude then more fine lines. In smaller particles assemblies, we detected more contacts on the cone (both wall 1 and 2) however their magnitude is smaller compared to assemblies consisted of bigger particles, where even there were less contacts between cone and particles, the magnitude was significantly higher. It was thus concluded both from the analysis of graphical illustrations from PFC2D program, as well from the analysis results of the validation of the particle size presented in Section 7.4.

The displacement of each particle is drawn as an arrow with length proportional to the magnitude, and orientation equal to that of the displacement vector (Itasca, 2008). However displacements cannot be compared with eachother, because of limitations and assumtions explained in 'Theory and Background' PFC2D manual (2008). The main limitation is due to 2D simualtions of 3D phenomenon. PFC2D takes into account a two in-plane components of the displacement, negletting the third one.

Displacement vectors show more significant displacement of particles near the cone. In assemblies with bigger size of particles magnitude of displacement vector was greater. Because of different amount of particles in the box, as well as particle size, they cannot be compared qualitatively. However it was possible to detect the affected by cone penetration area. Region in short distance from cone was inconsiderably afflictedby insertion of penetrometer. Displacement vectors in those regions were very small. Observations have lead us to conclusion that boundary conditions were chosen properly. Thus from Figures 8.12 and 8.13 we can conclude that in denser assemblies (Figure 8.12) displacement vectors are smaller then in looser assemblies (Figure 8.13). It is due to the fact that particles in tight packing have smaller freedom to move than those in the looser assemblies.

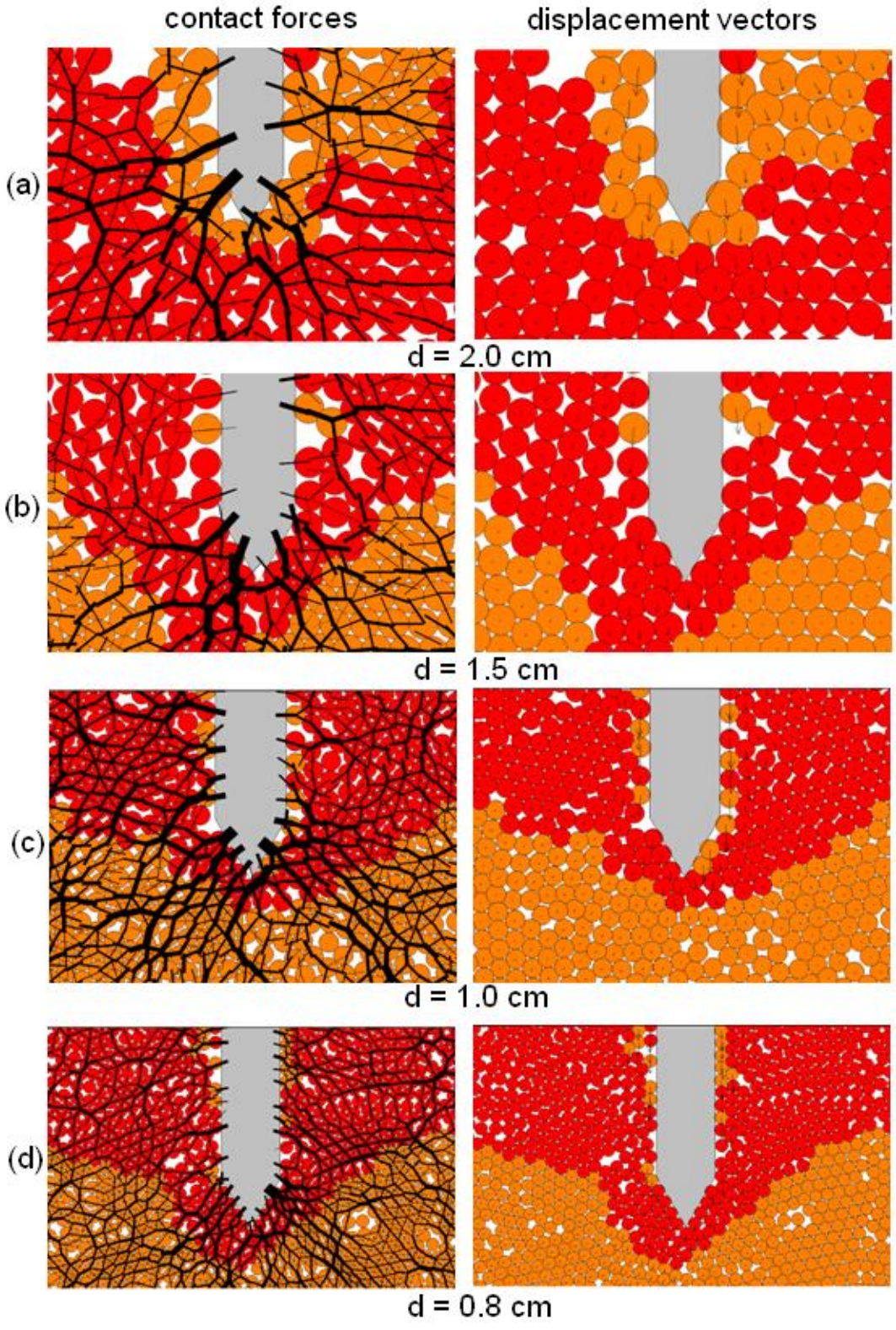

Figure 8. 12. Contact forces and dissplacement vectors near the cone at 1 m depth from assembly of porosity of 0.39 and particle diameter of (a) 2.0 cm, (b) 1.5 cm, (c) 1.0 cm and (d) 0.8cm.

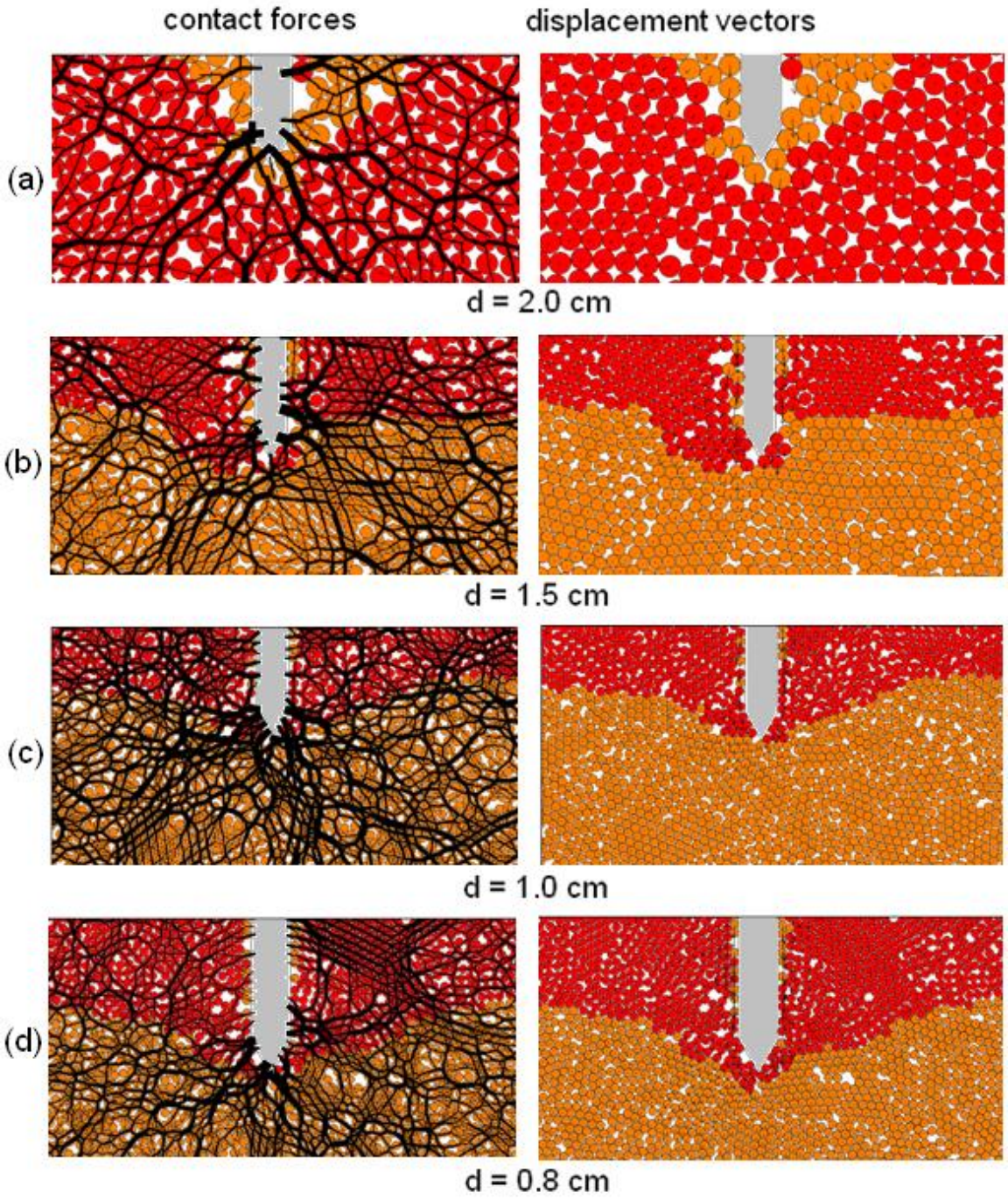

Figure 8. 13. Contact forces and dissplacement vectors near the cone at 1 m depth from assembly of porosity of 0.41 and particle diameter of (a) 2.0 cm, (b) 1.5 cm, (c) 1.0 cm and (d) 0.8cm.

We can conclude that DEM modelling in two-dimensional environment gives better results for loose and dense assemblies. This conclusion is based on results of porosity, coordination number, contact forces and dissplacement vectors investigation.

8.4.5. Number of Particles in Model Assembly at Different Porosities

Number of particles at different porosities were investigated. Due to the same sample preparation procedure (radii expansion method), the relationship between porosity and number of particles is linear. Figure 8.14 shows the relationship between number of particles in the box and porosity from the laboratory experiments, validated in this chapter.

The equation obtained from the analysis results for the tested soil in laboratory is described as:

$$number_{of\ particles} = -105.96 \cdot n_{lab} + 9807 \tag{8.4}$$

where,

$number_{of\ particles}$ = total number of particles created in the model for CPTs

n_{lab} = porosity in the laboratory.

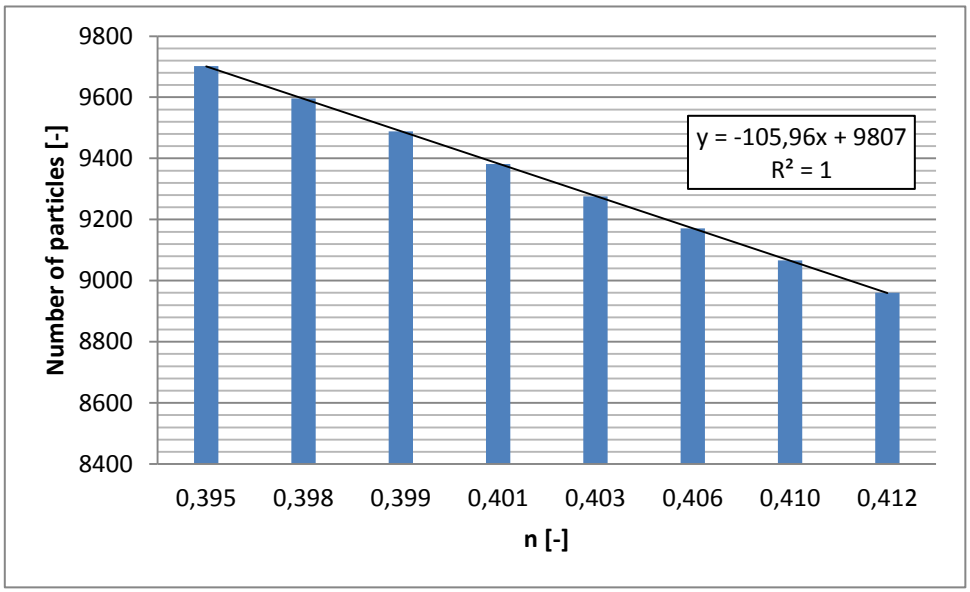

Figure 8. 14. Contact forces and dissplacement vectors near the cone at 1 m depth from assembly of porosity of 0.41 and particle diameter of (a) 2.0 cm, (b) 1.5 cm, (c) 1.0 cm and (d) 0.8cm.

The assembly representing the micro-mechanical model of sand consisted of 8960 to 9702 particles with different radii of 0.005 m and sample size of (0.7x 1.2) m. Investigated porosity range was 0.395 to 0.412, which corresponds to the relative density of 51 to 26%, respectively. Results of the initial number of particles shows that implemented algorythm for particle generation created an uniform assembly. R-squared value is equaled to 1 from Fig. 8.14. However, after penetration particles are penetrating through the boundary conditions with different degree. In looser assembles it was not observed, but in more tight packing, many particles are leaving the bouddary conditions. It slightly affects the porosity within the walls. Moreover, given investigation supports the thesis introduced in Section 8.4.2

8.5. Validation of the CPT model

The results of the DEM simulations were compared with the CPT results from laboratory experiments. In Figure 8.3, the comparison of the DEM and the laboratory results is shown for different relative density. We can observe that for looser assemblies a very good much was obtained. For more dense assemblies (D_r higher than 65%). The reason of that it can be that limit values were assigned with knowledge of q_c results up to 1.3-1.4 m. After reaching the depth of 1 m, the q_c drastically rise, which was especially visible in dense assemblies.

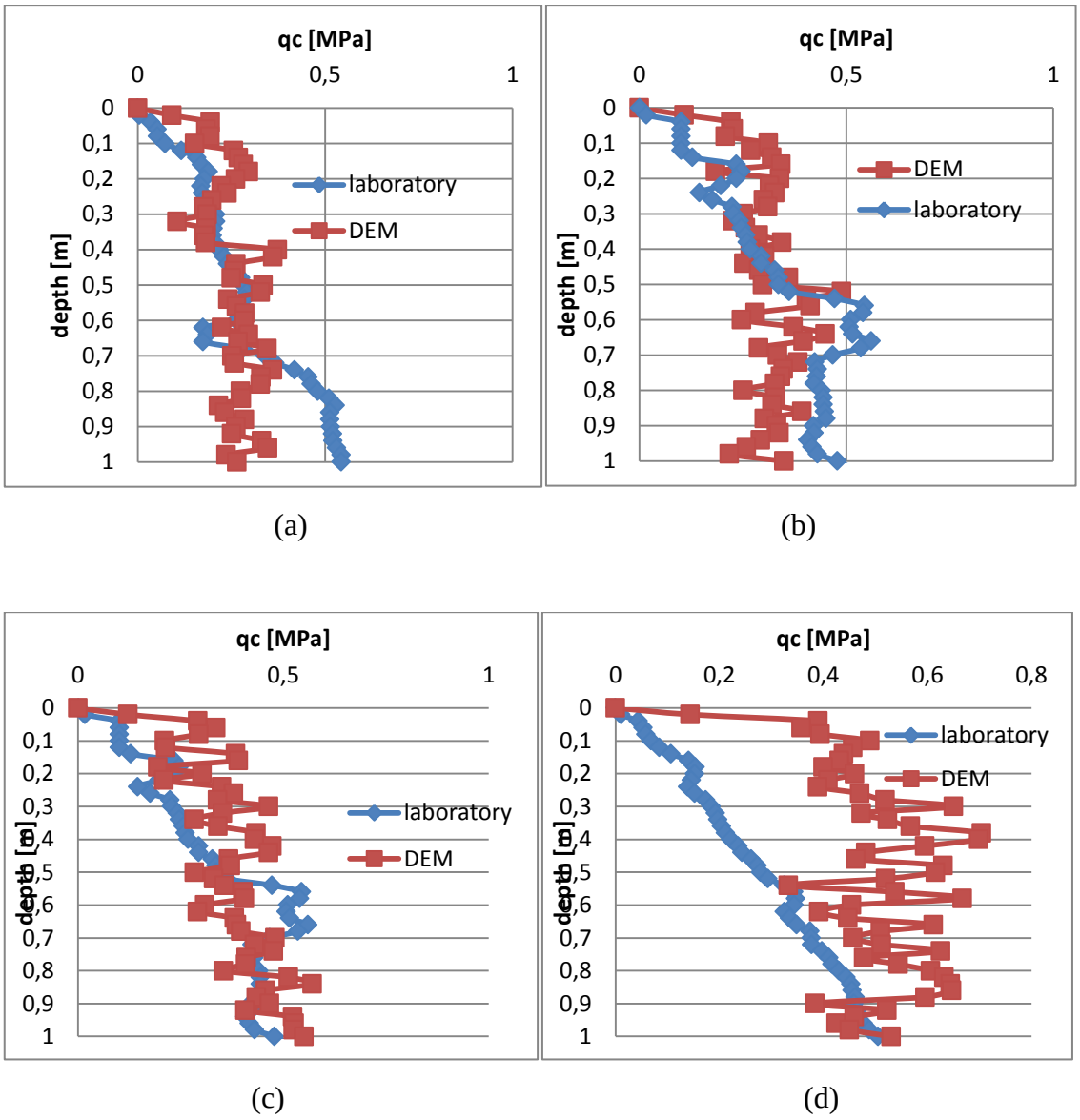

Figure 8. 15. Comparison of DEM and lab. results after validation of porosity (a) D_r=45%, (b) D_r=50%, (c) D_r=60% and (d) D_r=65%.

CHAPTER 9

CONCLUSIONS

9.1 Summary of Findings

In this thesis, the physical models are used in order to calibrate a distinct element model. Calibrated mechanical DEM parameters are normal stiffness, tangent stiffness, and friction coefficient. They were successfully determined from the consolidated drained triaxial experiments conducted in the laboratory. Calibration stage exposed that there is no unrepeatable set of values that best matched the laboratory data. Calibrated stiffness parameters along with the physical parameters enabled us to reflect the real behavior of tested soil in the DEM modeling.

Several CPT tests are used to validate porosity in the two-dimensional DEM model. Results obtained from physical experiments are compared with the numerical simulations by PFC2D. For the tested saturated soil, we have achieved a relationship which can be used to compute a real porosity in the 2D model. Real porosity represents the void fraction, which would occur in the 3D real assembly. We need to bear in mind the fact that scaling and calibration performed in this study is valid just for the tested soil. On the other hand, the numerical simulations and experiments show that validation of porosity for a particular soil is a valuable tool for the parametric studies or investigation of behavior of soil under different range of porosity. DEM analysis of cone penetration revealed that simulations' results are more successful for loose and medium dense soils, rather than dense soils. Capability of DEM program enabled to investigate porosity, coordination number, contact forces and dissplacement vectors successfully.

From the results, we can deduce that two-dimensional DEM CPT model can be a powerful tool to enrich the conventional physical calibration tests. In this thesis it is also proven that CPT laminar box based correlations facilitate to overcome limitations of 2D simulation. This outcome can be widely and successfully applied both in scientific research and engineering practice.

9.2. Suggestions for Future Research

Penetration mechanism into the soil is a complex phenomenon and much research can be done based on findings and ideas acquired from this study. As DEM was used in geomechanics problems relatively recently (Cundall, 1971), there is still a great ambiguity related to cone penetration tests. Following problems can be investigated by means of ITASCA software, PFC2D:

1) Parametric study for the particular tested soil after validation of porosity
   - Stiffness of particles
   - Stiffness of cone
   - Friction of particles
   - Friction of cone
   - Boundary conditions
2) Investigation of velocity fields and displacements
3) Different method of particles generation for instance consolidation in an amplified gravity field after generation of particles
4) Implementation of clump logic into the particle generation

Unfortunately, parametric studies which were conducted to examine the effects of permeability and compressibility on liquefaction screening by DEM simulations revealed that due to limitation of Basic Fluid Analysis Option, the results of analysis are not realistic. Undrained conditions in real soil cause that at a greater penetration rate, q_c results are smaller. However, in discrete assembly we had observed an opposite situation as qc was increasing with the higher velocity of CPT. Due to large strains during penetration mechanism, the approach cannot be applicable to investigate pore water pressure (u) change during CPT. The measurements of pore water pressure in the DEM-SIMPLE analysis lead to extremely high values of pore water pressure while penetrating a discrete material and it confirmed the work of Tsuji et al. (1992) and Kawaguchi et al. (1993) who claimed that particle-fluid interaction by coupling of PFC2D and SIMPLE cannot be applicable to the study of liquefaction (large strains and change in pore water pressure). It is believed that examination of those effects related to CPTs can be successfully simulated by PFC3D. The following topics can be handled by PFC3D and CCFD:

1) Simulations of CPTs in three-dimensional environment by PFC3D
2) Comparison of CPT results by PFC2D and PFC3D
3) Parametric studies

REFERENCES

Ahmadi, M.M, Byrne, P.M. and Campanella, R.G. 2005. Cone tip resistance in sand: modeling, verification and applications. *Canadian Geotechnical Journal*, 42: 977-993.

Anandarajah, A. (2003). Discrete Element Modeling of Leaching Induced Apparent Overconsolidation in Kaolite. *Soils and Foundations*. 43(6): 1-12.

Arrayo, M., Bultanska, J., Gens, J, Calvetti, F. and Jamiolkowski, M. 2011. Cone penetration tests in a virtual calibration chamber. *Géotechnique*, 51(6): 525-531.

Amin, H.K., El Zahaby, K.M, Taha, M.A. and Bazaraa, A.S. 2001. Using fuzzy set theory (FST) in selecting a suitable foundation type. *Proceedings of the 6th international conference on Application of artificial intelligence to civil and structural engineering.*

ASTM D3441- 05. Standard Test Method for Mechanical Cone Penetration Tests of Soil.

ASTM D7181- 11 05. Standard Test Method for Consolidated Drained Triaxial Compression Test for Soils.

ASTM D422 – 63. Standard Test Method for Particle-Size Analysis of Soils.

ASTM D 854-00. Standard Test Method for S"pecific Gravity of Soil Solids by Water. Pycnometer.

ASTM D 4253. Standard Test Method for Maximum Index Density of Soils Using a Vibratory Table.

ASTM D 4254. Standard Test Method for Minimum Index Density.

ASTM D2434 – 68. Standard Test Method for Permeability of Granular Soils (Constant Head).

Bakunowicz, P Ecemis, N. 2014. Validation of porosity in 2D-DEM CPT model using large scale shaking table tests in saturated sands. *Procc. of 14th International Conference of the International Association for Computer Methods and Advances in Geomechanics.* September 22-25, 2014 Kyoto, Japan. (accepted)

Baligh, M.M. 1985. Strain Path Method. *Journal of Geotechnical Engineering,* 111: 1108-1136.

Bishop, R.F., Hill, R. and Mott, N.F. 1945. The theory of indentation and hardness tests. *Proc. Physics Society,* 57: 147-159.

Bishop, A.W. and Henkel, D.J. 1962. *Measurement of soil properties in the triaxial test*. London : E. Arnold.

Bolton, M.D. and Gui, M.W. 1993. The study of relative density and boundary effects for cone penetration tests in centrifuge. *Research report: CUED/D-SOILS/TR256*, Department of Engineering, Cambridge University.

Bouillard, J.X., Lyczkowski, R.W. and Gidaspow, D. 1989. Porosity distributions in a fluized bed with an immersed obstacle. *AIChE Journal*, 35(6): 908-922.

Bowles, J. E. 1996. Foundation Analysis and Design, Fifth edition, The McGraw-Hill Companies, Inc. Bowles, *J. E.: Foundation Analysis and Design*, Fifth edition, The McGraw-Hill Companies, Inc.

Butlanska, J., Arroyo, M. and Gens, A. 2013. Homogeneity and Symmetry in DEM Models of Cone Penetration. POWDERS AND GRAINS 2009, *Proceedings of The 6th International Conference On Micromechanics Of Granular Media, Colorado, 13-17 July 2009.*

Bultanska, J., Arrayo, M and Gens, A. 2010 Size effects on a virtual chamber. *In Numerical methods in geotechnical engineering: NUMGE*. 225-230.

Cee-Ing, T.1987. *An analytical study of the cone penetration test*. PhD Thesis, Oxford University.

Chesworth, W. 2008. *Encyclopedia of Soil Science*. Dordrecht: Springer.

Cundall, P.A. 1971 A computer model for simulating progressive large scale movements in blocky rock systems. *IRSM Symp., Nancy, France, Proc*. 2: 129-136.

Cundall, P.A. and Strack, O.D.L. 1979. The distinct numerical model for granular assemblies. *Géotechnique*, 29(1): 47-65.

De Borst, R. and Vermeer, P. A. 1984. Possibilites and limitations of finite elements for limit analysis. *Géotechnique*, 34(2): 199-210.

DeGregorio, V.B. 1990. Loading systems, sample preparation and liquefaction. *Journal of Geotechnical Engineering Division*, 116(5): 805- 821.

Dereszewicz, H. 1958. Mechanics of granular matter. *Advances in applied mechanics*. 5: 233- 306.

Durgunoglu, H.T. and Mitchell, J.K. 1975. Static penetration resistance of soils. *Proc. of the ASCE Specialty Conference on In-Situ Measurements of Soil Properties*, 1: 151-189.

Ecemis, N. 2013. Simulation of seismic liquefaction: 1-g model testing system and shaking table tests. *European Journal of Environmental and Civil Eng*. 17(10): 899-919.

Esworth, D., Mattioli, G., Taron, J., Voight, B. and Herd, R. 2008 Implications of magma transfer between multiple reservois on eruption cycling. *Science*. 322:246-248.

Frost, J.D., and Park, J. Y. 2003. A critical assessment of the moist tamping technique. *Geotechnical Testing Journal*, 26(1): 57-70.

Geng, J. 2010. *Discrete element modelling of cavity expansion in granural materials*. PhD Thesis, University of Nottingham.

Haythornthwaite, R.M. 1970. The mechanics of the triaxial test for soils. *Report No. 9, LL 63*, Brown University.

Herrmann, H. J. 1997. Intermittency and self-similarity in granular media. *Powders and Grains 97*. Rotterdam: Balkema.

Hinrichsen, H. and Wolf, D. E. 2004. *The Physics of Granular Media*. Weinheim: Wiley VCH.

Houlsby, G.T and Hitchman, R. 1988. Calibration chamber tests of a cone penetrometer in sand. *Géotechnique,* 38: 575-587.

http://www.ce.washington.edu /~liquefaction/html/what/what1.html. (Accessed April, 2014)

http://www.intranet.cee.lsu.edu/grad/Lists/resfac/AllItems.aspxwww.envi.se (Accessed April, 2014).

http://www.gauda-geo.com (Accessed April, 2014).

http://www.gdsinstruments.com/__assets__/pagepdf/000037/Part%201%20Introduction%20to%20triaxial%20testing.pdfwww.geomil.com (Accessed April, 2014).

http://www.seattlerobotics.org/encoder/mar98/fuz/flindex.html (Accessed April, 2014).

http://www.wikipedia.org/wiki/Discrete_element_method (Accessed May, 2014).

http://www.wikipedia.org /wiki/Leaning_Tower_of_Pisa (Accessed March, 2014).

Huang, W., Sheng, D., Sloan, S.W. and Yu, H.S. 2004. Finite element analysis of cone penetration in cohesionless soil. *Comput. Geotech*. 31(7): 517-528.

Huang, A.B. and Huang, Y.T. 2007. Undisturbed sampling and laboratory shearing tests on sand with various fines contents. *Soils and Foundations*, 47(4): 771-781.

Ishihara, K. 1993. Liquefaction and flow failure during earthquakes. *Géotechnique,* 43(3): 351–415.

ISSMFE . 1989. International Reference Test Procedure for cone penetration test (CPT). *Report of the ISSMFE Technical Committee on Penetration Testing of Soils – TC* 16 7:6-16.

Itasca Consulting Group. 2009. *FLAC, Fast Lagrangian Analysis of Continua*, version 6.0, Itasca Consulting Group, Minneapolis, Minnesota, USA.

Itasca Consulting Group, Inc. 2008. *PFC2D Version 4.0 Manual (4th edn) – Command Reference.* Minneapolis, Minesota.

Itasca Consulting Group, Inc. 2008. *PFC2D Version 4.0 Manual (4th edn) – FISH in PFC2D.* Minneapolis, Minesota.

Itasca Consulting Group, Inc. 2008. *PFC2D Version 4.0 Manual (4th edn) – Optional Features*. Minneapolis, Minesota.

Itasca Consulting Group, Inc. 2008. *PFC2D Version 4.0 Manual (4th edn) – Theory and Background.* Minneapolis, Minesota.

Itasca Consulting Group, Inc. 2008. *PFC2D Version 4.0 Manual (4th edn) – User's Guide.* Minneapolis, Minesota.

Jiang, M.J, Yu, H.S. and Harris, D. 2006. Discrete element modeling of deep penetration in granural soils. *International Journal of Numerical and Analytical Methods in Geomechanics*, 30: 335-361.

Juneja, A. and Raghunandan, M.E. 2010. Effect of Sample Preparation on Strength of Sands. *Indian Geotechnical Conference, Bombay, 16–18 December 2010.*

Kaehler, S. D. *An Introduction to Fuzzy Logic*. www.seattlerobotics.org.

Kahraman, I. 2013. *Seismic Liquefaction: 1-G Model Testing System And Shake Table Tests*. Master Thesis, Izmir Institut of Technology.

Kawaguchi, T., Tanata, T. and Tsuji, Y. 1992. Numerical simu-lation of fluized bed using the discrete element method. *JSME (B),* 58(551): 79-85

Kirkwood, J.G., Buff, F.P. and Green, M.S. 1949. The statistical mechanical theory of transport processes. *J. Chem. Phys*., 17(10): 988.

Kishino, Y. 2001. *Powders and Grains.* Rotterdam: Balkema.

Koloski, J.W., Schwarz, S.D. and Tubbs, D.W. 1989. Geotechnical Properties of Geologic Materials, *Engineering Geology in Washington*, 1(78).

Kruyt, N. P. 1993. Towards micro-mechanical constitutive re-lations for granular materials. *Proc. Modern approaches to Plasticity*. Balkema, 147-178.

Kuerbis, R., and Vaid, Y. P. 1988. Sand sample preparation-the slurry deposition method. *Soils and Foundations*, 28(4): 107-118.

Kuhlawy, F.H. and Mayne, P.H. 1990. Manual on estimating soil properties for foundation design. *Report EL-6800 Electric Power Research Institute.*

Kumar, N.S., Kumar, V., Deb, A. and Roy, D. 2010. Finite element analysis of cone penetration in sand. *Proc. of 2nd International Symp. On Cone Penetration Testing, California, 9-11 May 2010.*

Ladd, R.S. 1978. Preparing test specimens using undercompaction. *Geotechnical Testing Journal*, 1(1): 16-23.

Lade, P. V. and Yamamuro, J. A. 1997. Effects of nonplastic fines on static liquefaction of sands. *Canadian Geotechnical Journal*, 34(6): 918-928.

Lambe, T.W. 1969. *Soil Mechanics*. John Wiley and Sons, Inc.

Lu, X., Lapusta, N. and Rosakic, A.J. 2007. Pulse-like and crack-like ruptures in experiments mimicking crustal earthquakes. *Proc. Of National Academy of Sciences of the USA.* 104(18): 931-936.

Lunne, T, Robertson P.K and Powell, J.J.M. 1997. *Cone penetration testing in geotechnical practice*. New York: Blackie Academic, FF Spon/Routledge Publishers.

Meyerhof, G.G. 1951. The ultlmate bearing capacity of foundations. *Géotechnique*, 2: 301-332.

Mitchell J.E. 1988. Densification and improvement of hydraulic fills. *Proc. Specialty Conf. on Hydraulc Fill Structures*, 21: 606–633.

Monkul, M.M. 2010. *Influence of Silt Size and Content on Static Liquefaction Potential of Sand.* PhD thesis, Oregon State University.

Monkul, M. M. and Yamamuro, J.A. 2010. The effect of nonplastic silt gradation on the liquefaction behavior of sand. *Proceedings of the 5th International Conference on Recent Advances in Geotechnical Earthquake Engineering and Soil Dynamics, San Diego, California.*

Murthy, T. G., Loukidis, D., Carraro, J. A. H., Prezzi, M. and Salgado, R. 2007. Undrained monotonic response of clean and silty sands. *Geotechnique*, 57(3): 273–288.

O'Sullivan, C. 2011. Particle-Based Discrete Element Modeling: Geomechanics Perspective. *International Journal of Geomechanics*, 11: 449-464.

Palla, N., Gudavalli, S., Chao, L., Jao, M. and Wang, M. C. 2012. Numerical Analysis of Texas Cone Penetration Test. *International Journal of Applied Science and Technology*, 2(3): 1-6.

Parkin, A.K and Lunne, T. 1982 Boudary effects in the laboratory calibration of a cone penetrometer for sand. *Proc. 2nd European Symp. Penetration Testing, Amsterdam*, 2: 761 -768.

Patankar, S.V. 1980. *Numerical Heat Transfer and Fluid Flow.* Hemisphere Publishing.

Phillips, R. and Valsangkar, A.J. 1987. An experimental investigation of factors affecting penetration resistance in granular soils in centrifuge modeling. *Technical Report No CUED/D-Soils TR210*, Cambridge University, UK.

Polito, C. P., and Martin II, J. R. 2003. A reconciliation of the effects of non-plastic fines on the liquefaction resistance of sands reported in the literature. *Earthquake Spectra, EERI*, 19(3): 635–651.

Pöschel, T. and Luding, S. 2001. *Granural gases*. Berlin: Springer.

Potyondy, D.O. and Cundall, P.A., 2004. A bonded-particle model for rock, *Int. J. Rock Mech. Min. Sci.* 41: 1329-1364.

Prandtl, L. 1921. *Über die Eindringungsfestigkeit (Härte) plastischer Baustoffe und die Festigkeit von Schneiden (On the penetrating strengths (hardness) of plastic construction materials and the strength of cutting edges).* Zeit. Angew. Math. Mech., 1(1): 15-20.

Randolph, M.F., Carter, J.P. and Wroth, C.P. 1979. Driven piles in clay the effects of installation and subsequent consolidation. *Géotechnique*, 29(4): 361-393.

Renzi, R., Corte, J.F., Bagge, G., Gui, M. and Laue, J. 1994. Cone Penetration Tests in the Centrifuge: Experience of Five Laboratories, Proc. of International Conference Centrifuge 94, Singapore, 31 August-2 September, 77-82.

Roache, P.J. 1976. *Computational Fluid Dynamics*. Hermosa Publishers.

Sagaseta, C., Whittle, A. and Santagata, M. 1995 Deformation analysis of shallow penetration in saturated clay. *Research Report R94-09, Dept. of Civil and Environmental Engineering,* MIT, Cambridge Mass.

Salgado, R. 1993. *Analysis of penetration resistance in sands.* PhD Thesis, University of California, Berkley.

Salgado, R., Mitchell, J.K. and Jamiolkowski, M. 1997. Cavity expansion and penetration resistance in sand. *J. Geotech. Geoenviron Eng*., 123(4), 344-354.

Santamarina, J.C. 1987. *Fuzzy sets and knowledge systems in geotechnical engineering*. PhD Thesis, Purdue University.

Sharp MK, Dobry R and Phillips, R. 2010. CPT-based evaluation of liquefaction and lateral spreading in centrifuge. .*J Geotech. and Geoenviron. Eng.* 136(10).

Sitharam, T.G., Dash, H. K. (2008). Effect of non-plastic fines on cyclic behavior of sandy soils. *GeoCongress 2008: Geosustainability and Geohazard Mitigation,* 178:381-385.

Skinner, A.E 1969. A note on the influence of interparticle fric-tion on the shearing strength of a random assembly of spherical particles. *Géotechnique*, 19(1): 150-157.

Teh, C.I. and Houlsby, G.T. 1991. An Analytical Study of the Cone Penetrometer Test in Clay. *Géotechnique,* 41(1): 17-34.

Terzaghi, K. 1943. *Theoretical Soil Mechanics.* New York: Wiley.

Thevanayagam, S. 1998. Effect of fines and confining stress on undrained shear strength of silty sands. *Journal of Geotechnical and Geoenvironmental Engineering*, 124(6): 479-491.

Tsuji, Y., Kawaguchi, T. and Tanata, T. 1993. Discrete particle simulation of two-dimensional fluized bed. *Powder Tech*. 77: 79- 85.

Utili S. and Nova R. 2008. DEM analysis of bonded granular geomaterials, *Int. J. Numer. Anal. Meth. Geomech.*, 32: 1997-2031.

Vaid, Y. P., Sivathayalan, S., and Stedman, D. 1999. Influence of specimen reconstituting method on the undrained response of sands. *Geotechnical Testing Journal*, 22(3): 187–195.

Vaid, Y.P. and Sivathayalan, S. 2000. Fundamental Factors Affecting Liquefaction Susceptibility Sands. *Canadian Geotechnical Journal*, 37(3): 592- 606.

Vermeer, P.A., Diebes, S., Ehlers, W., Herrmann, H.J., Luding, S. and Ramm, E. 2001. *Continuous and discontinuous modelling of cohesive frictional materials*. Berlin: Springer.

Vesic, A.S. 1975. Bearing capacity of shallow foundations. *Foundation Engineering Handbook,* New York: Van Nostrad: 121-147.

Whitman, R.V. 1985. Liquefaction of soils during earthquakes. *Committee on Earthquake Eng., National Research Council*, Washington, D.C: National Academy Press.

Wood, F. M., Yamamuro, J.A. and Lade, P.V. 2008. Effect of depositional method on the undrained response of silty sand. Canadian Geotechnical Journal, 45: 1525-1537.

Yamamuro, J.A. and Wood, F.M. 2004. Effect of depositional method on the undrained behavior and microstructure of sand with silt. Soil Dynamics and Earthquake Engineering 24: 751–760.

Yu, H.S. and Houlsby, G.T. 1991. Finite cavity expansion in dilatant soils: loading analysis. Géotechnique 41(2): 173-183.

Zhu, H. P., Zhou, Z. Y., Yang, R. Y., and Yu, A. B. 2007. Discrete particle simulation of particulate systems: Theoretical developments. Chem.Eng. Sci., 62(13): 3378–3396.